VOLUME 102 | SUPPLEMENT 1 | MARCH 2022

LI

LABORATORY INVESTIGATION

THE BASIC AND TRANSLATIONAL PATHOLOGY RESEARCH JOURNAL

ABSTRACTS (24-73)

BONE AND SOFT TISSUE PATHOLOGY

2022

USCAP 111TH ANNUAL MEETING

REAL INTELLIGENCE

MARCH 19-24, 2022 LOS ANGELES, CALIFORNIA

Published by SPRINGER NATURE
www.ModernPathology.org

USCAP Creating a Better Pathologist
AN OFFICIAL JOURNAL OF THE UNITED STATES AND CANADIAN ACADEMY OF PATHOLOGY

EDUCATION COMMITTEE

Rhonda K. Yantiss
Chair

Kristin C. Jensen
Chair, CME Subcommittee

Laura C. Collins
Chair, Interactive Microscopy Subcommittee

Yuri Fedoriw
Short Course Coordinator

Ilan Weinreb
Chair, Subcommittee for Unique Live Course Offerings

Carla L. Ellis
Chair, DEI Subcommittee

Adebowale J. Adeniran
Kimberly H. Allison
Sarah M. Dry
William C. Faquin
Karen J. Fritchie
Jennifer B. Gordetsky
Levon Katsakhyan, Pathologist-in-Training
Melinda J. Lerwill
M. Beatriz S. Lopes
Julia R. Naso, Pathologist-in-Training
Liron Pantanowitz
Carlos Parra-Herran
Rajiv M. Patel
Charles "Matt" Quick
David F. Schaeffer
Lynette M. Sholl
Olga K. Weinberg
Maria Westerhoff

ABSTRACT REVIEW BOARD

Benjamin Adam
Oyedele Adeyi
Mariam Priya Alexander
Daniela Allende
Catalina Amador
Vijayalakshmi Ananthanarayanan
Tatjana Antic
Manju Aron
Roberto Barrios
Gregory R. Bean
Govind Bhagat
Luis Zabala Blanco
Michael Bonert
Alain C. Borczuk
Tamar C. Brandler
Eric Jason Burks
Kelly J. Butnor
Sarah M. Calkins
Weibiao Cao
Wenqing (Wendy) Cao
Barbara Ann Centeno
Joanna SY Chan
Kung-Chao Chang
Hao Chen
Wei Chen
Yunn-Yi Chen
Sarah Chiang
Soo-Jin Cho
Shefali Chopra
Nicole A. Cipriani
Cecilia Clement
Claudiu Cotta
Jennifer A. Cotter
Sonika M. Dahiya
Elizabeth G. Demicco
Katie Dennis
Jasreman Dhillon
Anand S. Dighe
Bojana Djordjevic
Michelle R. Downes
Charles G. Eberhart
Andrew G. Evans
Fang Fan
Julie C. Fanburg-Smith
Gelareh Farshid
Michael Feely
Susan A. Fineberg
Dennis J. Firchau
Gregory A. Fishbein
Agnes B. Fogo
Andrew L. Folpe
Danielle Fortuna
Billie Fyfe-Kirschner
Zeina Ghorab
Giovanna A. Giannico
Anthony J. Gill
Tamar A. Giorgadze
Alessio Giubellino
Carolyn Glass
Carmen R. Gomez-Fernandez
Shunyou Gong
Purva Gopal
Abha Goyal
Christopher C. Griffith
Ian S. Hagemann
Gillian Leigh Hale
Suntrea TG Hammer
Malini Harigopal
Kammi J. Henriksen
Jonas J. Heymann
Carlo Vincent Hojilla
Aaron R. Huber
Jabed Iqbal
Shilpa Jain
Vickie Y. Jo
Ivy John
Dan Jones
Ridas Juskevicius
Meghan E. Kapp
Nora Katabi
Francesca Khani
Joseph D. Khoury
Benjamin Kipp
Veronica E. Klepeis
Christian A. Kunder
Stefano La Rosa
Stephen M. Lagana
Keith K. Lai
Goo Lee
Michael Lee
Vasiliki Leventaki
Madelyn Lew
Faqian Li
Ying Li
Chieh-Yu Lin
Mikhail Lisovsky
Lesley C. Lomo
Fang-I Lu
aDeqin Ma
Varsha Manucha
Rachel Angelica Mariani
Brock Aaron Martin
David S. McClintock
Anne M. Mills
Richard N. Mitchell
Hiroshi Miyamoto
Kristen E. Muller
Priya Nagarajan
Navneet Narula
Michiya Nishino
Maura O'Neil
Scott Roland Owens
Burcin Pehlivanoglu
Deniz Peker Barclift
Avani Anil Pendse
Andre Pinto
Susan Prendeville
Carlos N. Prieto Granada
Peter Pytel
Stephen S. Raab
Emilian V. Racila
Stanley J. Radio
Santiago Ramon Y Cajal
Kaaren K Reichard
Jordan P. Reynolds
Lisa M. Rooper
Andrew Eric Rosenberg
Ozlen Saglam
Ankur R. Sangoi
Kurt B. Schaberg
Qiuying (Judy) Shi
Wonwoo Shon
Pratibha S. Shukla
Gabriel Sica
Alexa Siddon
Anthony Sisk
Kalliopi P. Siziopikou
Stephanie Lynn Skala
Maxwell L. Smith
Isaac H. Solomon
Wei Song
Simona Stolnicu
Adrian Suarez
Paul E. Swanson
Benjamin Jack Swanson
Sara Szabo
Gary H. Tozbikian
Gulisa Turashvili
Andrew T. Turk
Efsevia Vakiani
Paul VanderLaan
Hanlin L. Wang
Stephen C. Ward
Kevin M. Waters
Jaclyn C. Watkins
Shi Wei
Hannah Y. Wen
Kwun Wah Wen
Kristy Wolniak
Deyin Xing
Ya Xu
Shaofeng N. Yan
Zhaohai Yang
Yunshin Albert Yeh
Huina Zhang
Xuchen Zhang
Bihong Zhao
Lei Zhao

To cite abstracts in this publication, please use the following format: **Author A, Author B, Author C, et al. Abstract title (abs#). In "File Title."** ***Laboratory Investigation*** **2022; 102 (suppl 1): page#**

24 NF1 Mutant Spindle Cell Neoplasms: A Selected Series Diagnosed at a Cancer Center

Oluwadamilare Ajayi[1], Marilyn Bui[1], Jane Messina[1], Daryoush Saeed-Vafa[1]
[1]H. Lee Moffitt Cancer Center & Research Institute, Tampa, FL

Disclosures: Oluwadamilare Ajayi: None; Marilyn Bui: *Consultant*, AstraZeneca; *Consultant*, Visiopharm; *Consultant*, ContextVision; *Speaker*, Physicians' Education Resources; *Speaker*, Gather-Ed; Jane Messina: None; Daryoush Saeed-Vafa: None

Background: Spindle cell neoplasms are a diagnostically challenging entity, and often morphology and immunohistochemistry (IHC) are insufficient to definitively classify them. Next generation sequencing (NGS) offers the potential to refine diagnoses as well as therapeutic options. Somatic NF1 mutations have been reported in numerous spindle cell malignancies. We present our institutional experience with diagnostically challenging spindle cell neoplasms in which NF1 mutations were identified.

Design: An IRB-approved retrospective review of our institutional database from 2018-2021 was performed, identifying all cases submitted with a potential diagnosis of sarcoma in which an NF1 truncating mutation was detected via Foundation One testing or a DNA/RNA based NGS assay. Clinical and pathologic features of each case were collected.

Results: Of a total of 248 cases tested, 18 (7.2%) were identified as having NF1 truncating mutations. Final integrated diagnoses included 4 malignant peripheral nerve sheath tumor (22%), 3 pleomorphic undifferentiated sarcoma (22%), 3 desmoplastic melanoma (DM) (16.7%), 2 malignant phyllodes tumor (11%), 2 pleomorphic dermal sarcoma (11%), 1 neurofibroma, 1 high-grade myxofibrosarcoma, 1 pleomorphic rhabdomyosarcoma, and 1 unclassified. In 3 cases, the NGS data changed the final diagnosis compared to the original diagnosis of high-grade sarcoma. All 3 cases were ultimately classified as DM; each possessed >1 somatic NF1 truncating mutation along with an ultraviolet (UV) signature, suggestive of desmoplastic melanoma. Two of these three cases were negative for S-100, Sox10 and BRAF by IHC.

Conclusions: NGS is an extremely powerful and potentially underused tool in the pathologist's toolbox. When conventional methods of IHC and morphologic analysis fail to render a diagnosis, NGS may provide the final piece of the diagnostic puzzle. Here we identified three cases for which the NGS results significantly altered the primary pathologic diagnosis leading to a more accurate diagnosis, treatment plan, and ultimately the most optimal patient care possible.

25 ATM Loss in High-Grade Sarcomas

Doaa Alqaidy[1], Ingram Ingram[2], Jeffrey Cloutier[2], Khalida Wani[2], Alexander Lazar[2], John Livingston[2], Wei-Lien (Billy) Wang[2]
[1]University of California San Francisco, San Francisco, CA, [2]The University of Texas MD Anderson Cancer Center, Houston, TX

Disclosures: Doaa Alqaidy: None; Ingram Ingram: None; Jeffrey Cloutier: None; Khalida Wani: None; Alexander Lazar: None; John Livingston: *Grant or Research Support*, REPARE Therapeutics; Wei-Lien (Billy) Wang: None

Background: Sarcomas are a heterogeneous group of rare tumors that are challenging to manage, particularly when widely metastatic. Several studies including The Cancer Genome Atlas (TCGA) Sarcoma project have identified *ATM*, Ataxia Telangiectasia Mutated, mutated in some aggressive sarcomas. ATM is a protein kinase that plays a critical role in DNA damage repair during cell replication and tumors which have loss maybe more sensitive to DNA damaging chemotherapy. As such, several trials are underway to identify ATM deficient tumors. One way to detect tumors with inactivating *ATM* mutations is by examining for complete protein loss by immunohistochemistry. We assessed the prevalence of ATM loss in various aggressive sarcomas by using protein loss as an indicator for *ATM* mutation.

Design: Unstained slides prepared from tissue microarrays covering common aggressive sarcoma subtypes including leiomyosarcoma(uterine(UtLMS) and soft tissue(StLMS)),undifferentiated pleomorphic sarcoma(UPS) and angiosarcoma(AS) of various stages(primary, recurrent and metastatic). Immunohistochemical studies performed using an anti-ATM monoclonal antibody (Y170,1:250, Abcam) and was previously validated on tumors with known deleterious *ATM* mutations. Nuclear staining extent was assessed as follows: complete loss (0%), low ATM loss (1-10%), heterogeneous loss (10%-50%) and diffusely retained (>50%). Staining intensity was recorded as high, medium, and weak.

Results: Complete loss was seen in 17%(N=93/535) of sarcomas and was most frequent in LMS(StLMS N=50/191, 26%, UtLMS N=27/122,22%), followed by UPS(N=13/130, 10%) and AS(N=3/92,3%). Low loss(weak intensity) was seen in 10%(N=55/535) of

samples(St-LMS N=27/191,14%;UtLMS,N=11/122,9%;UPS,N=13/130,10%;AS,N=4/92,4%). Heterogenous loss(weak moderate intensity) was seen in 22%(N=116/535) of cases (StLMS N=39/191,20%;UtLMS N=25/122,21%;UPS,N=44/130,34%;AS,N=8/92,9%). The remaining cases (N=271/535,50%) exhibited moderate strong diffuse labeling. Amongst stage, loss trended lower with higher stage in StLMS (28%,primary vs 25%,recurrent vs.23%, metastasis) and UtLMS(33%vs.26%vs. 17%),while increasing prevalence of loss higher with stage in UPS(8%vs. 11%vs.17%) and in AS(2%vs.0%vs.13%).

Conclusions: ATM loss can be detected in aggressive sarcomas by immunohistochemistry, suggesting some patients maybe amendable to targeted therapies. Loss of ATM varied by subtype with LMS having the highest loss and may vary by stage. Heterogenous patterns can be seen and needs further investigation.

26 Osteoid Osteoma of the Short Tubular and Small Bones of Hands and Feet: A Series of 33 Cases

Fatimah Alruwaii[1], Scott Kilpatrick[1], John Reith[1], Karen Fritchie[1]
[1]Cleveland Clinic, Cleveland, OH

Disclosures: Fatimah Alruwaii: None; Scott Kilpatrick: None; John Reith: None; Karen Fritchie: None

Background: Osteoid osteoma typically arises in the long bones of extremities or the spine. Patients often report pain relieved by NSAIDS, and radiographic findings are usually sufficient for diagnosis. The clinicopathologic features of these tumors involving the short tubular and small bones of the hands and feet have been less well clarified.

Design: Our institutional and consultation archives were searched for all cases of pathologically confirmed osteoid osteoma over the past 30 years. Clinical presentation, radiographic and morphologic features, and follow-up data were recorded.

Results: A total of 220 cases (83 females, 137 males) were retrieved. 33 (15%) arose in the bones of the hands (n= 15) and feet (n=18). Age ranged from 6-64 years (median 29 years). Specific anatomic sites were distal phalanx (n=13, 40%; including 8 in the fingers and 5 in the toes) , talus (n=6, 8%), proximal phalanx (n=4,12%; all in the fingers), metatarsal (n=4,12%), metacarpal (n=2,6%), cuneiform (n=2,6%), calcaneus (n=1,3%) and middle phalanx (n=1, 3%; finger). All cases with available clinical data (31 of 33) presented with pain and significant swelling. The clinical and radiographic impressions were available for 31 (of 33) cases and included: osteoid osteoma (n=10, 30%), osteomyelitis (n=9, 27%), fracture (n=3, 9%), enchondroma (n=3; 9%), glomus tumor (n=2, 6%), post-traumatic (n=1; 3%), avascular necrosis (n=1, 3%), ligament tear (n=1, 3%) and ankle instability (n=1, 3%). Histologically, all cases showed characteristic histologic features including anastomosing woven bony trabeculae lined by osteoblasts with intervening fibrovascular stroma with no aggressive features seen. Follow-up was available in 13 cases (2-216 months, median 60 months); 5 cases presented with clinically local recurrence/residual disease within a year; all were initially thought to have osteomyelitis and were treated by debridement.

Conclusions: Osteoid osteoma involving the small and short tubular bones of the hands and feet is rare. These lesions often present with a broad differential diagnosis and frequently are initially confused with osteomyelitis clinically. Although follow-up was limited, morphology and behavior seems to parallel osteoid osteomas arising at more conventional sites. Awareness that this entity may present in the hands and feet will help pathologists and clinicians accurately classify these tumors.

27 Molecular Characterization of Dedifferentiated Solitary Fibrous Tumor

William Anderson[1], Adrián Mariño Enríquez[2], Christopher Fletcher[2]
[1]Brigham and Women's Hospital, Harvard Medical School, Boston, MA, [2]Brigham and Women's Hospital, Boston, MA

Disclosures: William Anderson: None; Adrián Mariño Enríquez: None; Christopher Fletcher: None

Background: Solitary fibrous tumor (SFT) is a fibroblastic tumor with distinctive histologic features, molecularly defined by the presence of *NAB2-STAT6* fusions. Most cases are biologically low-grade, and the overall recurrence rate is 10-30%. However, very rare examples show transition to a high-grade morphologically non-distinctive sarcoma (dedifferentiated SFT, DDSFT) and are associated with a very poor prognosis. Such cases are genomically unstable and harbor more frequent alterations of *TP53* and *TERT*, although the full spectrum of molecular alterations in DDSFT is unknown. We studied the genetics of DDSFT to identify clinically actionable molecular alterations.

Design: DDSFT (n=12) were retrieved from departmental and consultation files. Immunohistochemistry was performed for STAT6. Targeted next-generation sequencing, using a clinically validated platform (Oncopanel) covering the coding regions of 447 cancer-associated genes and 191 frequently rearranged genomic regions, was performed in each case in the region of dedifferentiation.

Results: Our cohort comprised 12 patients (8 females, 4 males), with a median age of 59 years (range 31-80). Tumors had a median size of 10.0 cm (range 3.0-23.8) and involved the abdominal cavity (5/12), thorax (3/12), vertebrae (2/12), thigh (1/12) and trunk (1/12). For each tumor, separate areas of well-differentiated SFT were verified in the same (n=11) or a prior (n=1) specimen. Dedifferentiated areas were histologically diverse, with epithelioid, spindled, pleomorphic, or round cell morphology, and occasional heterologous components. STAT6 expression was lost or reduced in 50% (6/12) of cases. Molecular findings are summarized in Figure 1. All tumors harbored *NAB2-STAT6* fusions, predominantly truncating *STAT6* (75%; 9/12). Median tumor mutational burden was 4.2 mutations/Mb. Frequently altered genes were *TP53* (67%; 8/12), *TERT* (58%; 7/12), *RB1* (17%; 2/12), and *PTEN* (17%; 2/12). One case that lacked these alterations showed *IGF2* amplification.

Figure 1 - 27

Case	1	2	3	4	5	6	7	8	9	10	11	12
TMB	3.8	4.6	3.0	4.6	1.5	3.8	2.3	5.3	5.3	7.6	4.6	3.8
Age	79	61	54	73	50	68	45	80	31	51	42	75
Sex	F	M	F	F	F	F	M	M	F	F	M	F

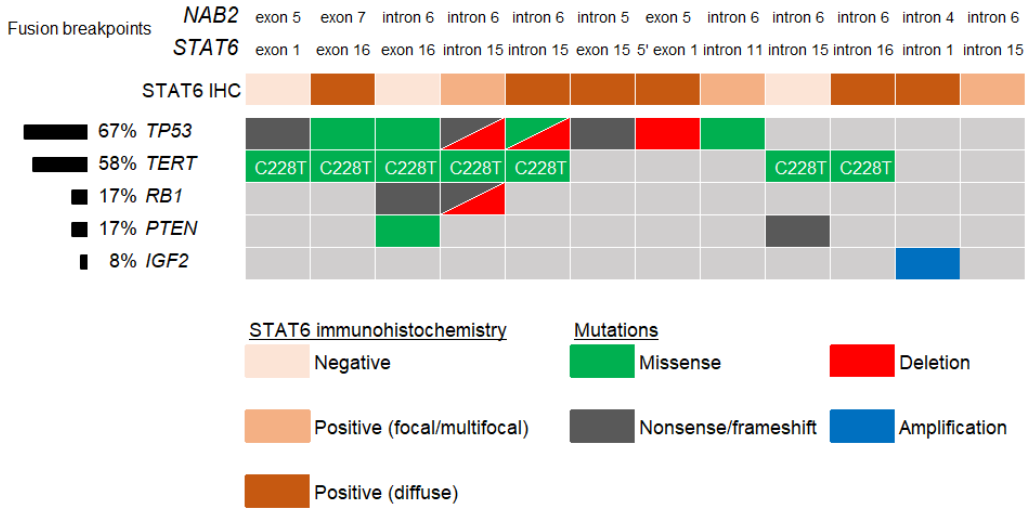

Conclusions: The diagnosis of DDSFT may be challenging due to reduced or absent STAT6 expression and requires extensive sampling to identify a concurrent or previous well-differentiated component. DDSFT is enriched for fusions truncating *STAT6* and *TERT* promoter mutations, and shows frequent inactivation of tumor suppressor genes, most commonly *TP53*, as well as *RB1* and *PTEN.*

28 Superficial CD34-Positive Fibroblastic Tumor: A Clinicopathologic Analysis of 52 Cases

William Anderson[1], Fredrik Mertens[2], Jason Hornick[1], Christopher Fletcher[3]
[1]Brigham and Women's Hospital, Harvard Medical School, Boston, MA, [2]University Hospital Lund, Lund, Sweden, [3]Brigham and Women's Hospital, Boston, MA

Disclosures: William Anderson: None; Fredrik Mertens: None; Jason Hornick: None; Christopher Fletcher: None

Background: Superficial CD34-positive fibroblastic tumor (SCD34PFT) is a rare mesenchymal neoplasm that was recently established as a distinct entity in the 2020 World Health Organization Classification. Around 60 cases have now been described and although it appears to have a very good prognosis, with only one reported metastasis, long-term follow-up data are limited. In addition, SCD34PFT shows considerable clinical and morphologic overlap with soft tissue tumors harboring *PRDM10* rearrangement, which are known to overexpress CADM3; this relationship is incompletely understood. We

present a large series of SCD34PFT to further characterize its clinicopathologic features and clinical behavior. We also evaluate the diagnostic utility of CADM3 immunohistochemistry in our cohort.

Design: Fifty-two SCD34PFTs were retrieved from departmental and consultation archives. Immunohistochemistry for CD34 and CADM3 was performed; AE1/AE3 and desmin were performed in a subset of cases. Clinical follow-up data were obtained.

Results: Our cohort comprised 52 patients (27 males, 25 females), with a median age of 40 yrs (range: 14-85). SCD34PFT most commonly arose in the lower limbs (71%) followed by the trunk (13%), upper limbs (10%), and head and neck (6%). The median tumor size was 2.9 cm (range 1.0-9.0 cm). Tumors were composed of sheets of spindled, polygonal or epithelioid tumor cells with abundant often glassy eosinophilic cytoplasm, including many cells showing striking nuclear pleomorphism (Figure 1). Mitoses were very rare. Prominent stromal histiocytes were often present. All tumors expressed CD34. CADM3 was also frequently positive (96%; 49/51). There was more limited AE1/AE3 (76%; 13/17) and desmin (38%; 18/48) expression. Follow-up in 13 patients so far (median duration: 21 months) revealed that all patients are currently alive with no evidence of disease. However, one patient had suffered both a local recurrence and regional lymph node metastasis, which were completely excised.

Table 1. Clinical characteristics of 52 superficial CD34-positive fibroblastic tumors.

Age	
Median (range)	40 (14 - 85) years
Sex	
Male	27
Female	25
Male-to-female ratio	1.1:1
Anatomic site [%]	
Lower limb	37 (71%)
Thigh	23 (44%)
Leg	14 (27%)
Upper limb	5 (10%)
Arm	4 (8%)
Forearm	1 (2%)
Trunk	7 (13%)
Head / neck	3 (6%)
Depth (n=41) [%]	
Subcutis only	28 (69%)
Subcutis and dermis	12 (29%)
Dermis only	1 (2%)
Deep/subfascial	0
Tumor size (cm)	
Median (range)	2.9 (1.0 - 9.0)

Figure 1 - 28

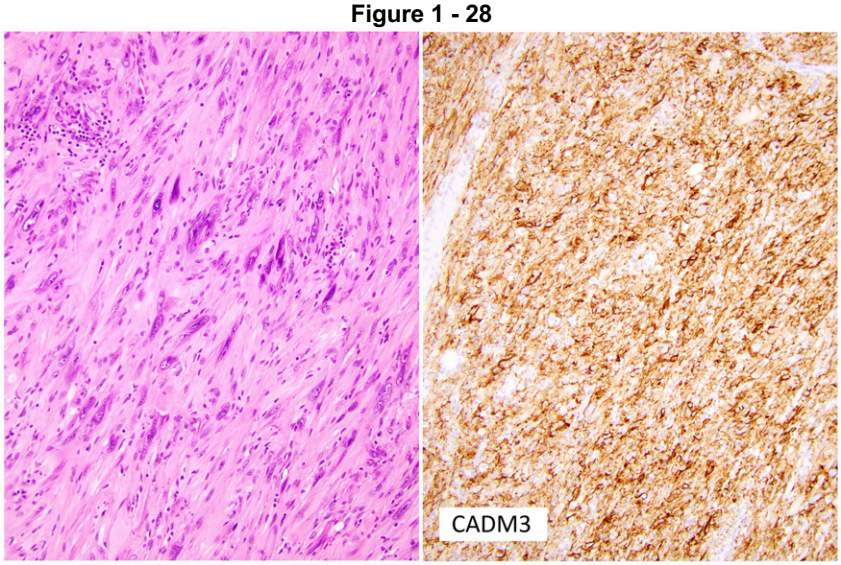

Conclusions: Our series contributes further understanding to the clinicopathologic spectrum of SCD34PFT. Follow up data obtained thus far corroborate that the majority are indolent, but that rare cases have the potential to metastasize to regional lymph nodes. Finally, our initial results indicate that CADM3 is a highly sensitive marker, which may be used to support the diagnosis.

29 Myxofibrosarcoma in Adolescents and Young Adults: A Clinicopathologic Study of 34 Cases

Karen Arispe Angulo[1], Steven Billings[2], Shruti Agrawal[1], Karen Fritchie[3]
[1]Cleveland Clinic Foundation, Cleveland, OH, [2]Cleveland Clinic, Lerner College of Medicine, Cleveland, OH, [3]Cleveland Clinic, Cleveland, OH

Disclosures: Karen Arispe Angulo: None; Steven Billings: None; Shruti Agrawal: None; Karen Fritchie: None

Background: Myxofibrosarcoma (MFS) is a locally aggressive fibroblastic malignancy that characteristically arises in the proximal extremity of patients in the sixth and seventh decade of life. Cases arising in adolescence and young adulthood are rare, potentially leading to diagnostic challenges.

Design: Our institutional and consultation archives were searched for 'myxofibrosarcoma' and 'myxoid malignant fibrous histiocytoma' arising in patients 40 years or younger over the last 29 years. Clinicopathologic data was collected.

Results: 34 cases of myxofibrosarcoma arising in patients $\leq$ 40 years were identified (23 females and 11 males; 14 to 40 years; median 34 years). Tumor sizes ranged from 1.5 to 31 cm (median 5 cm). Anatomic sites included: proximal extremity (17; 3 thigh), distal extremity (8), trunk (5), head/neck (3), intra-abdominal (1). Among tumors in the trunk and extremities where depth was known, 13 were superficial and 9 were deep-seated. Using the FNCLCC grading system, 9 cases were grade 1, 13 grade 2, and 12 grade 3. 3 cases harbored predominantly epithelioid morphology while 7 additional cases had foci with epithelioid features. FISH for *MDM2* amplification was negative for all cases tested (4/4), including the intraabdominal mass. NGS sarcoma fusion panel performed on a single case failed to show gene fusions and a comprehensive cancer profiling performed on another patient did not reveal any actionable variants. Available follow up information revealed that one patient experienced local recurrence after 13 months of diagnosis, while 2 developed distant metastasis (both patients had large (>20 cm) intramuscular tumors). Sites of metastasis included lung, bone and lymph nodes. Three patients were alive without disease (46 to 53 months; median 50 months).

Conclusions: Our study confirmed that myxofibrosarcoma arising in adolescents and young adults are rare but appear to show similar aggressive behavior to those tumors arising in their older adult counterparts. Interestingly, nearly one-third of cases in this age group showed some degree of epithelioid features, potentially resulting in diagnostic difficulty.

30 Genetic and Genomic Landscape of Myxoid Liposarcoma and their Association with Round Cell Phenotypes

Davsheen Bedi[1], Azfar Neyaz[1], Bao Riyue[1], Svetlana Yatsenko[2], Karen Fritchie[3], Arivarasan Karunamurthy[1], Ivy John[1]
[1]University of Pittsburgh Medical Center, Pittsburgh, PA, [2]University of Pittsburgh, Pittsburgh, PA, [3]Cleveland Clinic, Cleveland, OH

Disclosures: Davsheen Bedi: None; Azfar Neyaz: None; Bao Riyue: None; Svetlana Yatsenko: None; Karen Fritchie: None; Arivarasan Karunamurthy: None; Ivy John: None

Background: Limited studies have been published on myxoid liposarcoma (MLS) genomics. Herein, we explore the genetic and genomic landscape of MLS and their association with high grade features.

Design: We performed karyotype and whole-exome sequencing (WES) analysis on 19 MLS tumors. WES was performed on DNA isolated from unmatched tumor samples (n=19) on an Illumina NextSeq500 instrument using Agilent SureSelect Human All Exon V6 for exome capture and output reads were mapped to GRCh38 followed by duplicate removal and base quality score recalibration. Somatic variants were called using GATK4-MuTect2 with rigorous filtering to remove germline contamination, sequence or alignment artifacts, and variants of low quality. Total tumor mutational burden (TMB) was calculated using protein-changing mutations; synonymous mutations were removed.

Results: Complex karyotypes were identified in 10 of 19 MLS, of which high-grade features were seen in 7 of 11 complex tumors. A total of 762 somatic mutations were detected by WES, including 162 protein-changing mutations. The average TMB is 8.10

(ranging from 2 to 19) per exome, suggesting MLS is low-TMB cancer. Somatic mutational signature (v3.2) analysis revealed SBS86 (C>G predominant, chemotherapy treatment) enriched across all cases regardless of chemotherapy status. Higher TMB was observed in tumors with complex karyotypes compared to those with isolated chromosome aberrations (9.20±1.48 *vs*. 6.89±1.14, mean±S.E.M), and in high-grade tumors compared to low-grade (8.90±1.53 *vs*. 7.22±1.13).
Activating *PIK3CA* mutations (p.H1047R, p.H1047L, p.G1049R, p.E545K) were detected in 6/19 (32%) cases. Five out of six *PIK3CA* mutant tumors carry complex karyotypes, indicating a strong association between *PIK3CA* activation and genomic instability (5/10 (50%) *vs*. 1/9 (11%) in tumors with karyotype containing complex *vs*. isolated chromosome abnormality; *P*=0.14, odds ratio=7.15, two-sided Fisher's exact test). Three of six *PIK3CA* mutant tumors showed high-grade morphology. Other protein-changing mutations were present in *ATM* (1/19 cases), *EP300* (1/19), *FANCA* (1/19), *KMT2A/KMT2D* (3/19), *PTEN* (1/19), and *TP53* (1/19) genes.

Conclusions: *PIK3CA* mutations show a strong association with MLS with complex karyotypes. Increased mutational load (relatively higher TMB) is seen in MLS tumors with higher-grade features. MLS harbor highly enriched C>G transversions; while some could be related to chemotherapy, additional studies are required to evaluate their genetic etiopathogenesis.

31 Diagnostic Value of MDM2 RNA In Situ Hybridization for Low Grade Osteosarcoma: Consistency Comparison of RNA In Situ Hybridization with Fluorescence In Situ Hybridization and Immunohistochemistry

Chen Chen[1], Xin He[1], Min Chen[1], Tianhai Du[1], Wenyi Jing[1], Hongying Zhang[1]
[1]West China Hospital, Sichuan University, Chengdu, China

Disclosures: Chen Chen: None; Xin He: None; Min Chen: None; Tianhai Du: None; Wenyi Jing: None; Hongying Zhang: None

Background: Detection of MDM2 gene amplification via fluorescence in situ hybridization (FISH) and MDM2 immunohistochemistry (IHC) have been recognized as useful auxiliary tools for the diagnosis of low grade osteosarcoma (LGOS). MDM2 RNA in situ hybridization (RNA-ISH) has been recommended as an alternative diagnostic assay for well-differentiated liposarcoma/dedifferentiated liposarcoma recently. The aim of this study was to evaluate the diagnostic value of MDM2 RNA-ISH in LGOSs, compare it with MDM2 FISH and IHC and explore its feasibility in decalcified samples.

Design: Twenty-three LGOSs and 49 control samples of bone and soft tissue were included. *MDM2* RNA-ISH, FISH, IHC were performed on all undecalcified and formalin-fixed paraffin-embedded tissue. Nineteen out 23 LGOSs were evaluated by *MDM2* RNA-ISH and FISH in both decalcified and undecalcified samples.

Results: In undecalcified samples, two LGOSs were failed for MDM2 FISH and a total of 20/21 (95.2%) LGOSs showed positive results. 19 decalcified samples were failed for FISH. All control cases (n=49) were negative for MDM2 FISH. In 21 LGOSs with interpretable FISH results, 21(100%) cases were positive for RNA-ISH. One LGOS without MDM2 amplification was positive for RNA-ISH. The result of one FISH failed case was uninterpretable and the other showed no staining. In the control cases, only one undifferentiated pleomorphic sarcoma showed positivity for MDM2 RNA-ISH and the remaining cases were negative. The diagnostic sensitivity and specificity of MDM2 RNA-ISH in LGOSs were 100.0% and 96.2%, respectively. There was a great consistency between MDM2 RNA-ISH and FISH ($P<0.05$, kappa=0.932). In 19 decalcified samples, one was positive for RNA-ISH and the other showed no staining. In 21 LGOSs with interpretable FISH results, 76.3% (16/21) were positive for IHC. Two FISH failed cases showed focal positivity and no staining, respectively. All control cases except for one fibrous dysplasia were negative for IHC. In MDM2 IHC-positive LGOSs, 94.1% (16/17) were positive for RNA-ISH. There was a great consistency between MDM2 RNA-ISH and IHC ($P<0.05$, kappa=0.753).

Conclusions: MDM2 RNA-ISH equipped with high value in the diagnosis of LGOS, with consistent accuracy with FISH and higher sensitivity than IHC. But its specificity needs to be verified in more cases. Its success in decalcified sample indicates that it may have relatively low requirements on sample quality which needs to be investigated in further study.

32 Genome-Wide DNA Methylation Profiling Reveals Differentially Methylated Genes in Clinically Distinct Subsets of Solitary Fibrous Tumor

Jeffrey Cloutier[1], Hannah Beird[1], Nolan Maloney[2], Davis Ingram, Khalida Wani[1], Alexander Lazar[1], Wei-Lien (Billy) Wang[1], Elizabeth Demicco
[1]The University of Texas MD Anderson Cancer Center, Houston, TX, [2]Loma Linda University, Loma Linda, CA, [3]University of Toronto, Toronto, Canada

Disclosures: Jeffrey Cloutier: None; Hannah Beird: None; Nolan Maloney: None; Davis Ingram: None; Khalida Wani: None; Alexander Lazar: None; Wei-Lien (Billy) Wang: None; Elizabeth Demicco: None

Background: Solitary fibrous tumor (SFT) is a rare mesenchymal neoplasm characterized by a recurrent *NAB2-STAT6* fusion and metastatic progression in 10-30% of cases. The specific molecular alterations leading to aggressive behavior are not well understood, although *TERT* promoter mutations and/or *TP53* mutations may play a role in some cases. Epigenetic alterations are pervasive in oncogenesis but are largely unexplored in SFT. We examined genome-wide DNA methylation in a large series of SFT and demonstrate that biologically distinct SFTs have differential methylation profiles.

Design: A total of 85 SFTs were included in the study, including 75 primary tumors, 6 metastases, and 2 local recurrences (unknown status in 2). Tumors were located in the thorax (n=25) and extrathoracic soft tissue (n=58) (unknown in 2). 15 patients had a history of metastatic disease. Genome-wide DNA methylation was evaluated using Illumina MethylationEpic array. Methylation profiles were compared across several variables, including tumor behavior (benign vs malignant), tumor status (primary vs metastasis), and *TERT* promoter mutation status.

Results: After data QC and exclusion of X&Y chromosomes to remove bias on the basis of sex chromosomes, principal component analysis separated data into distinct groups sharing DNA methylation patterns. PC1 and PC2 segregated SFT according to tumor location (thoracic vs extrathoracic) and patient sex, respectively. Comparing tumors from patients with no history of metastasis vs those with a history of metastasis, 80 significantly differentially methylated gene probes were identified, including several cancer-associated transcription factor genes. *TERT* promoter mutation status correlated with 150 differentially methylated gene probes including genes involved in survival and autophagy. Immunohistochemical analysis to investigate expression of biologically relevant differentially methylated genes is ongoing.

Conclusions: The biological and behavioral heterogeneity of SFT is likely influenced by a combination of genetic and epigenetic alterations. We found that DNA methylation profiles are associated with distinct clinical features in SFT. DNA methylation patterns correlate with anatomic localization, suggesting that thoracic and extrathoracic tumors are epigenetically distinct. Tumors associated with metastatic behavior showed differential methylation of several cancer-associated genes. Together, these findings suggest that epigenetic alterations can influence tumor behavior in SFT.

33 Chromosome 8 Gain is a Frequent Copy Number Variation in Soft Tissue Sarcomas

Carina Dehner[1], Robert Bell[1], Kevin He[1], John Chrisinger[1], Amy Armstrong[1], John Shern[2], Marielle Yohe[3], Angela Hirbe[1]
[1]Washington University School of Medicine, St. Louis, MO, [2]Center for Cancer Research, National Cancer Institute, Bethesda, MD, [3]Center for Cancer Research, National Cancer Institute, National Institutes of Health, Bethesda, MD

Disclosures: Carina Dehner: None; Robert Bell: None; Kevin He: None; John Chrisinger: None; Amy Armstrong: None; John Shern: None; Marielle Yohe: None; Angela Hirbe: *Consultant*, Springworks Therapeutics; *Advisory Board Member*, AstraZeneca; *Grant or Research Support*, Tango Therapeutics

Background: Soft tissue sarcomas are rare mesenchymal neoplasms that frequently show complex chromosomal aberrations such as amplifications or deletions of DNA sequences or even whole chromosomes. We recently found that gain of Chromosome 8 is associated with worse overall survival in soft tissue sarcomas as a group and plays a role in high-grade transformation of malignant peripheral nerve sheath tumor (MPNST). Herein, we evaluated the role of chromosome 8 gain in a cohort of 7 different types of non-fusion driven soft tissue sarcomas using fluorescent-in-situ hybridization (FISH) testing.

Design: The departmental archive was searched for cases of undifferentiated pleomorphic sarcoma (UPS), well- and dedifferentiated liposarcoma (WDLPS and DDLPS), leiomyosarcoma (LMS), Neurofibromatosis 1 (NF1)-MPNST, non-NF1 MPNST, pleomorphic rhabdomyosarcoma (PRMS) and embryonal rhabdomyosarcoma (ERMS) with available tumor. Centromeric-enumerating (Vysis CEP8 D8Z2) was performed and 200 cells per tumor were counted. Average of Chr8 gain, percentage of cells with Chr8 gain and highest copy number of Chr8 were assessed.

Results: Sixty-five samples underwent Chr8 FISH: 13 cases of ERMS, 8 cases of PRMS, 8 cases of LMS, 8 cases of WDLPS and their 8 corresponding DDLPS, 10 cases of NF1-MPNST and 10 cases of non-NF1 MPNST. The highest Chr8 gain was noted in UPS with an average copy number of 3.71, followed by ERMS with 2.98 copies. UPS showed Chr8 gain in more than half of the counted cells per sample (average: 59%), followed closely by ERMS (average: 56%) (28-59%). The highest individual copy number per cells was seen in UPS with an average of 15.1 copies, followed by 12 copies in LMS (range: 6.5-15.1). There was no difference in copy number gain between WDLPS and its corresponding DDLPS (p = 0.7, 0.47 and 0.40, respectively).

Type of sarcoma	Average CEP8	Gain of Chr8 in %	Highest copy number of 8
UPS	3.714	59.2	15.125
WDLPS	2.325	28.6	8.000
DDLPS	2.454	36.3	6.571
LMS	2.964	44.9	12.00
PRMS	2.766	40.5	8.625
ERMS	2.975	56.2	7.385
Non-NF1 MPNST	2.716	42.9	9.188
NF1-MPNST	2.743	43.12	9.50

Figure 1 - 33

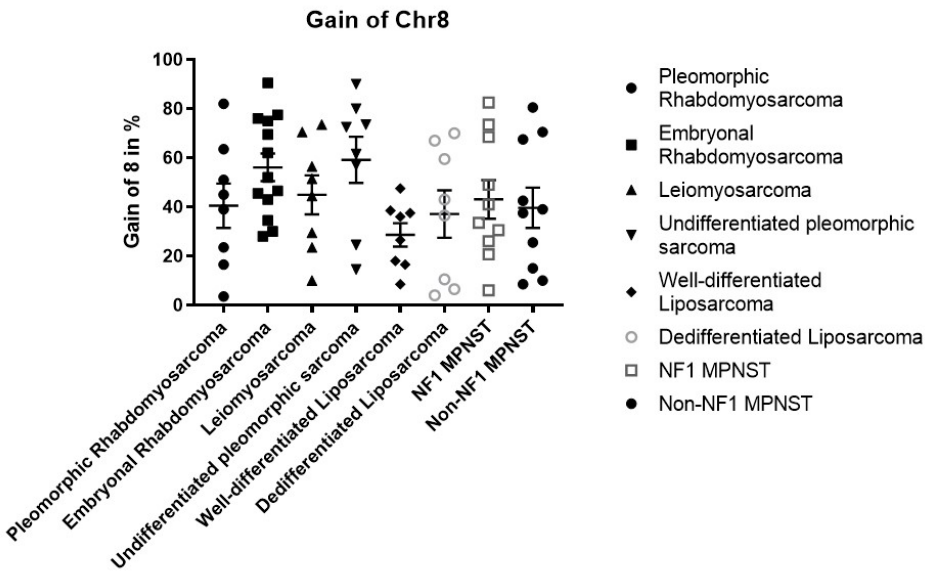

Conclusions: The pathogenesis of soft tissue sarcomas is poorly understood and many of them are associated with poor outcome supporting the need of new treatment approaches with better risk stratification. In our pilot study we show that Chr8 gain is commonly seen in soft tissue sarcomas, in particular in UPS, ERMS and LMS. Additionally, Chr8 gain does not appear to play a role in the dedifferentiation of retroperitoneal liposarcoma. Future studies looking at the outcome of these tumors in correlation with Chr8 and comparison to epithelial neoplasms are necessary to determine its prognostic relevance.

34 Molecular Characterization of Multifocal Granular Cell Tumors

Carina Dehner[1], Molly Schroeder[2], John Chrisinger[1]
[1]Washington University School of Medicine, St. Louis, MO, [2]Washington University in St. Louis, St. Louis, MO

Disclosures: Carina Dehner: None; Molly Schroeder: None; John Chrisinger: None

Background: Granular cell tumor (GrCT) is a distinctive neoplasm with neuroectodermal differentiation composed of cells with abundant granular cytoplasm and a predilection for the tongue, and superficial tissues of the head and neck. The prognosis is usually excellent, though malignant GrCT are extremely aggressive. The majority of GrCT present as solitary lesions, however multiple tumors occur in 10-15% of cases and are not thought to be associated with increased risk of aggressive behavior. Recent

data has shown that inactivating mutations in H^+-ATPase components, most commonly *ATP6AP1* or *ATP6AP2* are likely tumorigenic drivers. Herein we investigate the molecular alterations of multifocal GrCT to determine if there is evidence to suggest a clonal relationship versus molecularly distinct tumors.

Design: The pathology departmental archive was searched from 1988-2019 for patients with multifocal GrCT (≥ 2 tumor sites per patient) and 13 patients were identified with 2 or more synchronous lesions (range: 2 – 10 locations) leading to a total of 43 samples. Clinical parameters such as gender, tumor sites, follow up and associated syndromes were collected. Targeted next-generation sequencing for recently described potential driver mutations (*ATP6AP1, ATP6AP2, ATP6AP1L, ATP6V0A3, ATP6V0A4, ATP6V0B, ATP6V0C, ATP6V1A, ATP6V1D* and *PTEN*) was performed.

Results: Histologically none of the tumors showed atypical or malignant features. Sequencing results for 42 samples are shown in table 1 (one sample failed due to poor read quality). Tumors showed predominately mutually exclusive mutations in 33 of 42 samples. None of the multifocal tumors within a single patient showed the same potential driver alteration. Median follow up time was 18 years (7-29 years) and aggressive behavior was not observed. Syndromic associations were not noted.

Patient	Sample	Somatic Variation
P1	S_61	None observed
	S_72	*ATP6AP2* (c.706delG (p.Ala236fs)) 15% VAF
(F)	S_53	*ATP6AP1* (c.225_226delTA (p.Thr76fs)) 19% VAF
	S_7	*ATP6AP2* (c.978C>A (p.Tyr326*)) 24% VAF
P2	S3	None observed
	S32	*ATP6AP2* (c.589-2A>G (splice acceptor)) 13% VAF
(F)	S22	*ATP6AP1* (c.939T>G (p.Tyr313*)) 43% VAF
	S11	*ATP6AP1* (c.546delC (p.Tyr183fs)) 19% VAF
	S42	*ATP6AP1* (c.1085_1094delCAGGGCCCAG (p.Gly363fs)) 9% VAF
	S36	*ATP6AP1* (c.1087_1096delGGGCCCAGCA (p.Gly363fs)) 24% VAF
P3	S76	*ATP6AP1* (c.149G>A (p.Trp50*)) 36% VAF
(M)	S63	None observed
P4	S51	*ATP6AP1* (c.1167_1168insC (p.Ser391fs)) 14% VAF
(F)	S34	*ATP6AP1* (c.1242C>A (p.Tyr414*)) 8% VAF
P5	S54	*ATP6AP1* (c.127C>T (p.Gln43*)) 11% VAF
(F)		
P6	S52	None observed
(F)	S60	None observed
P7	S13	*ATP6AP1* (c.1083_1084delCA (p.Thr362fs)) 6% VAF
(F)	S59	None observed
P8	S71	*ATP6AP2* (c.508delC (p.Leu170fs)) 11% VAF
	S59	None observed
(F)	S57	*ATP6AP1* (c.685-2A>T (splice acceptor)) 24% VAF
	S50	*ATP6AP1* (c.364-2A>G *splice acceptor)) 15% VAF
	S38	*ATP6AP1* (c.50delC (p.Gln18fs)) 7% VAF
	S42	*ATP6AP1* (c.1192C>T (p.Gln398*)) 26% VAF
	S24	None observed
	S18	*ATP6AP2* (c.751delA (p.Met251fs)) 20% VAF
	S45	*ATP6AP2* (c.805_806delTT (p.Phe269fs)) 31% VAF
	S33	*ATP6AP1* (c.1208A>C (p.Gln403Pro)) 12% VAF *ATP6V0A4* (c.1155C>T (p.Val385Val)) 100% VAF Highest MAF = 15%
P9	S58	*ATP6AP1* (c.414G>A (p.Trp138*)) 15% VAF
	S43	*ATP6AP1* (c.1299C>T (p.Ser433Ser)) 18% VAF
(M)	S19	*ATP6AP2* (c.485delA (p.Asn162fs)) 27% VAF
P10	S30	*ATP6AP2* (c.24_28delGGCGT (p.Ala9fs)) 6% VAF
	S36	*ATP6AP1* (c.500_509delTGAAGCTCAA (p.Lys168fs)) 6% VAF
(F)		
P11	S32	*ATP6AP1* (c.1032_1036delCCTCG (p.Leu345fs)) 8% VAF
	S56	None observed
(F)		
	S25	*ATP6V0A4* (c.1662delC (p.Phe554fs)) 100% VAF

P12 (F)	S44	None observed
	S24	*ATP6AP1* (c.929C>T (p.Ser310Leu)) 7% VAF
P13 (M)	S15	*ATP6AP1* (c.414delG (p.Trp138fs)) 6% VAF *ATP6AP2* (c.165delA (p.Glu56fs)) 16% VAF
	S18	None observed
	S55	*ATP6AP2* (c.752delT (p.Met251fs)) 48% VAF

± Variants in trans
Table legend: Genomic variation detected in tumor-only sequencing of a small gene panel consisting of *ATP6AP1, ATP6AP2, ATP6AP1L, TCRIG1 (ATP6V0A3), ATP6V0A4, ATP6V0B, ATPV0C, ATP6V1A, ATP6B1D*, and *PTEN*.
"Apparently germline variation" is defined as that observed at variant allele frequency (VAF) between 45-55% in all samples from a patient. "Highest MAF" value is the greatest population minor allele frequency observed in aggregated gnomAD data.
Somatic variation is absent from gnomAD and COSMIC databases unless a frequency for their presence is noted.
Two somatic variants in *ATP6V0A4* (in S33 and S25) were observed at 100% VAF, suggesting the possibility of a loss of heterozygosity event in this region.
Transcripts:
ATP6V0C: NM_001694.4
ATP6AP2: NM_005765.2
ATP6AP1: NM_001183.6
TCIRG1 (*ATP6V0A3*): NM_006019.4
ATP6V0A4: NM_020632.3
ATP6V0B: NM_004047.5
ATP6V1A: NM_001690.4
PTEN: NM_ 000314.7
Conclusions: Benign appearing multifocal GrCT are not uncommonly encountered and our data suggests that many are genetically independent lesions. It remains unclear why certain patients show a propensity for these tumors in a non-syndromic setting; however, multifocal lesions do not appear to be associated with increased malignant potential.

35 Comprehensive Genomic Profiling of EWSR1/FUS-CREB Family of Translocation-Associated Tumors Uncovers Prognostically Significant Recurrent Genetic Alterations and Methylation-Transcriptional Correlates

Josephine Dermawan[1], Fabio Vanoli[1], Lei Zhang[1], Memorial Center[1], Tejus Bale[1], Brendan Dickson[2], Cristina Antonescu[1]
[1]Memorial Sloan Kettering Cancer Center, New York, NY, [2]Mount Sinai Health System, Toronto, Canada

Disclosures: Josephine Dermawan: None; Fabio Vanoli: None; Lei Zhang: None; Memorial Center: None; Tejus Bale: None; Brendan Dickson: None; Cristina Antonescu: None

Background: Recurrent gene fusions involving *EWSR1/FUS* with members of the cAMP response element binding protein (CREB) family (*ATF1*, *CREB1* and *CREM*) are shared amongst multiple tumor-types spanning a wide clinicopathologic spectrum.

Design: To elucidate the mechanisms underlying the divergent clinicopathologic spectrum of *EWSR1/FUS-CREB* family of translocation-associated tumors, we performed a comprehensive genomic analysis of fusion transcript variants, recurrent genetic alterations (mutations, copy number alterations), gene expression and methylation profiles across a large cohort of tumor types (Table 1).

Results: The distribution of the *EWSR1*/*FUS* fusion partners—*ATF1*, *CREB1*, and *CREM*—and exon involvement was significantly different across different tumor types (Figure 1). Our targeted sequencing showed that secondary genetic events are associated with tumor type rather than fusion type. Of the 39 cases that underwent targeted NGS testing, 18 (46%) had secondary OncoKB mutations or copy number alterations (29 secondary genetic events in total), of which 15 (52%) were recurrent. Recurrent, but mutually exclusive, *TERT* promoter and *CDKN2A* mutations were identified only in clear cell sarcoma (CCS) and associated with worse overall survival. *CDKN2A/B* homozygous deletions were recurrent in angiomatoid fibrous histiocytoma (AFH) and restricted to metastatic cases (Figure 2). mRNA upregulation of *MITF*, *CDH19*, *PARVB*, and *PFKP* was found in CCS compared to AFH and correlated with a hypomethylated profile. In contrast, *S100A4* and *XAF1* were differentially upregulated and hypomethylated in AFH but not CCS. A sarcoma methylation classifier was able to accurately match 100% of CCS cases to the correct methylation class; however, it was suboptimal when applied to other histologies.

Table 1. Study cohort demographics

Diagnosis	Female, n (%)	Male, n (%)	Mean age in years (range)	Total
Angiomatoid fibrous histiocytoma (AFH)	18 (51)	17 (49)	28.8 (2-79)	36
Clear cell odontogenic carcinoma (CCOC)	1 (100)	0	57.0	1
Clear cell sarcoma (CCS)	16 (40)	24 (60)	32.9 (7-71)	40
Clear cell sarcoma-like tumor of the gastrointestinal tract (GICCS)	14 (70)	6 (30)	39.0 (18-76)	20
Hyalinizing clear cell carcinoma of salivary gland (HCCC)	8 (80)	2 (20)	67.6 (55-86)	10
Malignant epithelioid neoplasm with predilection for mesothelial-lined cavities (ME)	7 (50)	7 (50)	37.2 (9-63)	14
Mesothelioma (Meso)	5 (62)	3 (38)	39.0 (15-78)	8
Myxoid mesenchymal tumor (MMT)	3 (60)	2 (40)	27.0 (12-48)	5
Primary pulmonary myxoid sarcoma (PPMS)	3 (100)	0	59.0 (43-82)	3
Total	74	60	36.9 (5-86)	137

Figure 1 - 35

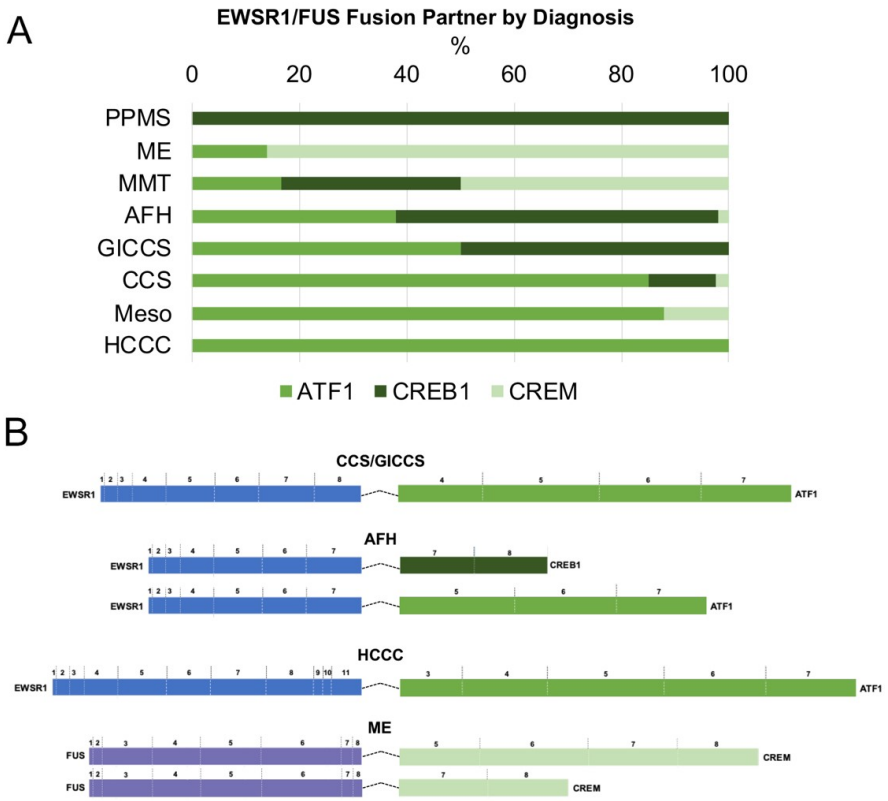

Figure 2-35

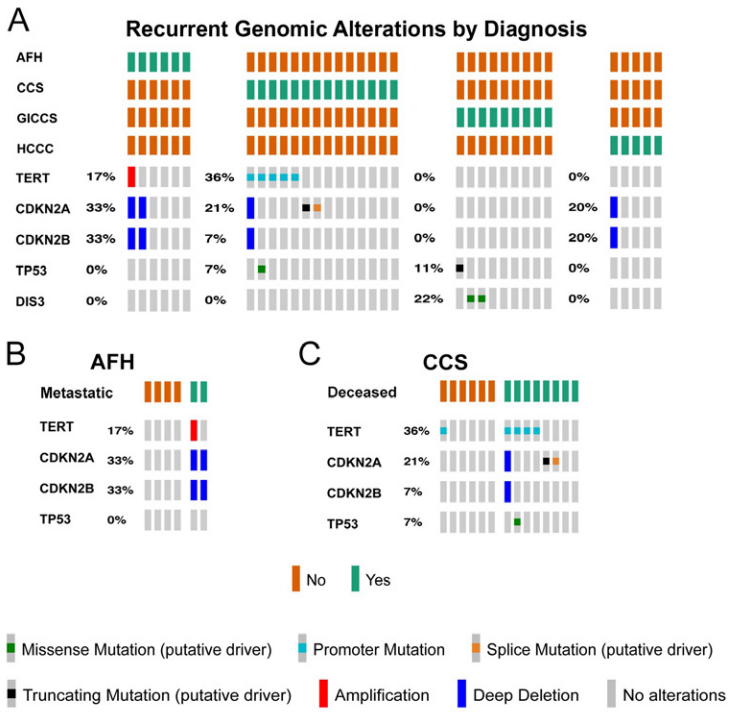

Conclusions: In conclusion, our comprehensive genomic profiling of *EWSR1/FUS-CREB* family of translocation-associated tumors uncovered mostly histotype rather than fusion-type associated correlations in transcript variants, prognostically significant recurrent secondary genetic alterations, and gene expression and methylation patterns.

36 The Incidence and Significance of Calcium Pyrophosphate Dihydrate Deposits (pseudogout) in Revision Arthroplasty Specimens

Josephine Dermawan[1], Fatimah Alruwaii[2], John Reith[2], Scott Kilpatrick[2]
[1]Memorial Sloan Kettering Cancer Center, New York, NY, [2]Cleveland Clinic, Cleveland, OH

Disclosures: Josephine Dermawan: None; Fatimah Alruwaii: None; John Reith: None; Scott Kilpatrick: None

Background: We recently evaluated the incidence and significance of calcium pyrophosphate dihydrate deposits (CPPD) in hip, knee, and shoulder primary total arthroplasty specimens, concluding that CPPD was more common in older patients and in the knees and shoulders when compared to the hips (PMID: 33720299). Given these findings, we now sought to determine the incidence and significance of CPPD in revision arthroplasties and whether such deposits might be correlated with periprosthetic joint infection (PJI), issues which have not been thoroughly evaluated in the literature.

Design: We retrospectively reviewed the clinicopathologic characteristics, especially focusing on CPPD, among consecutive hip, knee, shoulder, and elbow joint revision arthroplasties (n=1111) seen at our institution and signed out by the authors. Specific sites included 628 hips, 379 knees,101 shoulders, and 3 elbow specimens. Significant acute inflammation was defined as 5 or more neutrophils in 5 or more high power fields, and this was considered a "positive" result for periprosthetic joint infection (PJI), per Musculoskeletal Infection Society (MSIS) criteria. 190 cases (17.1%) were "positive" pathologically and thought to have PJI, more specifically 106 hips (16.9%), 74 knees (19.5%), 9 shoulders (8.9%), and 1 elbow (33.0%).

Results: Forty-seven cases (4.2%) had CPPD deposits in at least one section from one specimen of the revision arthroplasty case, more specifically 29 knees (7.7% of knees), 15 hips (2.4% of hips), 2 shoulders (2.0%), and 1 elbow (33.0%). The overwhelming majority (44, 93.6%) of cases of CPPD occurred in specimens which were negative for PJI, lacking significant acute inflammation; only 3 cases of CPPD, all associated with the knee, were found in patients considered positive for PJI at revision. The age range

among all patients in this series was 27-97 years (mean 65.1); those with CPPD were only slightly older, range 47-88 years (mean 68.6).

Conclusions: The distribution of CPPD among hip and knee revision arthroplasty specimens is similar to our experience with primary arthroplasties, with knees being significantly more frequently affected than the hips. However, shoulders were less commonly involved by CPPD than the hips or knees and also less often showed histologic evidence of PJI. CPPD appears more likely to be found in patients with aseptic loosening than in patients with PJI. The exact reasons behind CPPD being associated with an absence of PJI is unclear but deserves further investigation.

37 TMEFF2 Protein Expression and Clinicopathologic Profiles in Ewing Sarcoma

Jing Di[1], Subhasree Basu[2], Mike Russell[2], Tom Jorfi[2], Jackson Wong[2], Shaozhou Tian[2], Shadi Qasem[3]
[1]University of Kentucky College of Medicine, Lexington, KY, [2]Janssen R&D, LLC, Raritan, NJ, [3]University of Kentucky Healthcare, Lexington, KY

Disclosures: Jing Di: *Primary Investigator*, Janssen R&D, LLC; Subhasree Basu: *Employee*, The Janssen Pharmaceutical Companies of Johnson & Johnson; Mike Russell: *Employee*, Janssen R&D; Tom Jorfi: *Employee*, Janssen R&D Inc.; Jackson Wong: *Employee*, Janssen R&D; Shaozhou Tian: *Employee*, Janssen R&D; Shadi Qasem: *Primary Investigator*, Janssen Pharmaceuticals; *Primary Investigator*, Janssen Pharmaceuticals

Background: TMEFF2 is a conserved cell-membrane-bound proteoglycan that is often expressed at high levels in cells of prostatic ductal epithelial origin from normal early development through carcinogenesis. Bioinformatical analysis of major public cancer mRNA registry databases demonstrates TMEFF2 transcripts are present in other tumors such as Ewing sarcoma. The direct biological significance of mRNA expression is limited, and immunohistochemistry (IHC) studies are required to determine protein expression. In this study, we aim to define TMEFF2 distribution in Ewing sarcoma and evaluate TMEFF2 expression with clinicopathological findings.

Design: An extensive animal immunization campaign was conducted against specific regions of the TMEFF2 protein to generate a tool reagent (antibody) suitable for IHC studies. A proprietary TMEFF2 IHC assay was developed and utilized on 41 FFPE tumor materials of 32 Ewing sarcoma cases. Clinicopathological variables recorded included age, gender, and tumor site. H-scores were determined by 2 pathologists. One-way ANOVA, Chi-square, and Bartlett's test were used with $p<0.05$ considered significant.

Results: Detailed data are presented in [Table 1]. There were 51% (21/41) TMEFF2 positive cases with an average H-score of 48 (range 10-250). Higher average H-scores (90 and 70) were found in metastatic and recurrent cases vs primary tumors (31) ($p=0.0309$). Some tumors in the skin (2/3), brain (2/3), epidural (1/1), and urinary bladder (1/1) showed significantly intense expression of TMEFF2 compared to other locations ($p=0.0157$). [Figure 1]

Figure 1. Negative TMEFF2 stain from Ewing sarcoma in the lung (A,B), and positive TMEFF2 stain from the urinary bladder (C,D).

Table 1. TMEFF2 distribution

		TMEFF2 + n (total n) %	Average H-Score	p
Tissue	Primary	12 (27) 44	31	**0.0309***
	Metastatic	4 (10) 40	90	
	Recurrent	4 (4) 100	70	
Gender	F	8 (18) 44	36	0.3276
	M	13 (23) 57	57	
Location	Bone	9 (18) 50	30	**0.0157**
	Soft tissue	5 (8) 63	33	
	Skin	2 (3) 67	77	
	Lung	1 (7) 14	23	
	Brain/Epidural	3 (4) 75	145	
	Urinary bladder	1 (1) 100	180	
Age (yrs)	<15	12 (22) 55	51	0.9235
	15-19	2 (5) 40	36	
	>20	7 (14) 50	47	
*Bartlett's test				

Figure 1 - 37

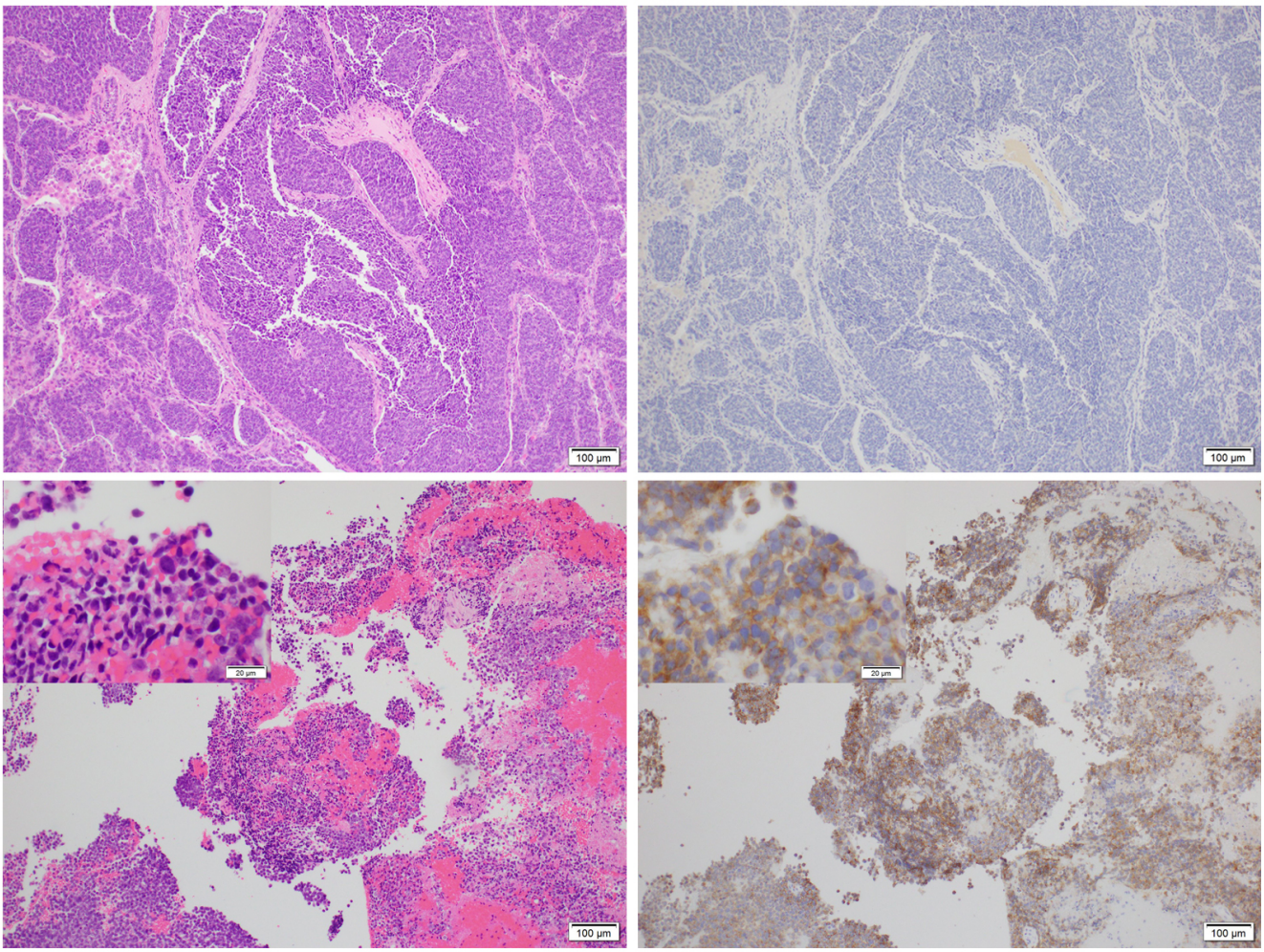

Conclusions: To our knowledge, this TMEFF2 IHC study was the first to demonstrate TMEFF2 protein expression in Ewing sarcoma. In addition, higher levels of TMEFF2 expression may be present in recurrent and metastatic tumors. The biological, prognostic, and therapeutic significance of our findings needs to be confirmed with additional studies with more robust tumor sets.

38 Droplet Digital (dd) PCR as a Novel Technology in Detecting CTNNB1 Mutations in Desmoid Fibromatosis

Jatin Gandhi[1], Erica Kao[2], Jose Mantilla Arango[1], Robert Ricciotti[1], Anshu Bandhlish[3], Yu Wu[1], Yajuan Liu[1], Eleanor Chen[1]
[1]University of Washington, Seattle, WA, [2]San Antonio Uniformed Services Health Education Consortium, San Antonio, TX, [3]University of Washington - Pathology, Seattle, WA

Disclosures: Jatin Gandhi: None; Erica Kao: None; Jose Mantilla Arango: None; Robert Ricciotti: None; Anshu Bandhlish: None; Yu Wu: None; Yajuan Liu: None; Eleanor Chen: None

Background: Desmoid fibromatosis (DF) is a locally aggressive soft tissue neoplasm characterized by infiltrative growth and frequent recurrences. It can mimic a range of benign and malignant processes, posing a diagnostic challenge in some instances. Molecularly, DF is characterized by alterations in the Wnt/β-Catenin pathway, with the majority showing sporadic mutations in *CTNNB1* while others have germline mutations in *APC* (Gardner syndrome). IHC staining for β-Catenin is often difficult to interpret due to non-specific reactivity and can be negative in up to 30% of cases. Prior studies have shown that some DFs lacking nuclear expression of β-Catenin may still carry activating *CTNNB1* mutations. ddPCR has been used effectively in detecting gene mutations in FFPE samples of various cancer types, suggesting its clinical utility. In this study we assess the diagnostic utility of ddPCR to detect *CTNNB1* mutations in DF with and without β-Catenin positivity, as well as in challenging cases.

Design: We identified 30 cases of DF, including 28 with nuclear β-Catenin expression by IHC and 2 without nuclear b-Catenin, as well as 7 (myo)fibroblastic lesions not classified as DF but for which DF was in the differential. Genomic DNA extracted from FFPE tissue blocks was subjected to ddPCR using primers for the most common point mutations in exon 3 of *CTNNB1* (S45F, S45P, T41A). Results were compared with IHC stains for β-Catenin. Clinicopathologic and demographic parameters were recorded.

Results: The patient age for DF ranged from 18-72 years (median, 44.5) with female predominance (F:M::1.8:1). Anatomic locations included neck/shoulder (n=9), extremities (n=6), chest wall (n=4), abdominal wall (n=4), mesentery (n=3), back (n=1) and breast (n=1). Tumor size ranged from 1.7 to 23 cm (median; 8.5 cm). 25 of 28 cases with nuclear β-Catenin on IHC showed a *CTNNB1* mutation by ddPCR (89%). The most frequent mutation was T41A (n=14; 50%) followed by S45F (n=8; 33%) and S45P (n=3;12%). The 2 cases without nuclear β-Catenin staining were negative for the three mutations tested. 2 of the 7 cases not previously classified as DF exhibited *CTNNB1* mutation (one each, S45F and S45P).

Conclusions: ddPCR is a sensitive and cost-efficient methodology to detect hotspot *CTNNB1* mutations in DF, especially diagnostically challenging cases. This method can also be applied as a targeted mutation assay to detect disease- defining point mutations in various tumor types.

39 Clinicopathologic Spectrum of NTRK fusion-positive Tumors Detected by Clinical RNA Sequencing Panel

Annie Garcia[1], Jacquelyn Reuther[2], Horatiu Voicu[2], Carrie Mohila[3], Adekunle Adesina[2], Deborah Schady[3], Wei-Lien (Billy) Wang[4], Alexander Lazar[4], Dolores Lopez-Terrada[5], Frank Lin[2], Rajkumar Venkatramani[2], Sharon Plon[2], Williams Parsons[2], Kevin Fisher[2], Angshumoy Roy[1]

[1]Baylor College of Medicine, Houston, TX, [2]Baylor College of Medicine/Texas Children's Hospital, Houston, TX, [3]Texas Children's Hospital, Houston, TX, [4]The University of Texas MD Anderson Cancer Center, Houston, TX, [5]Texas Children's Hospital, Baylor College of Medicine, Houston, TX

Disclosures: Annie Garcia: None; Jacquelyn Reuther: None; Horatiu Voicu: None; Carrie Mohila: *Stock Ownership*, Johnson and Johnson; Adekunle Adesina: None; Deborah Schady: None; Wei-Lien (Billy) Wang: None; Alexander Lazar: None; Dolores Lopez-Terrada: None; Frank Lin: None; Rajkumar Venkatramani: None; Sharon Plon: None; Williams Parsons: None; Kevin Fisher: None; Angshumoy Roy: None

Background: Gene fusions involving neurotrophic receptor tyrosine kinase (*NTRK*) genes are actionable targets approved for targeted therapy in any solid tumor. While generally infrequent in cancers, *NTRK* fusions are common in certain classic rare tumors where they are recurrently reported with ~100 different gene partners. However, overlapping clinical and histopathological features between classic and emerging *NTRK* fusion-positive entities pose practical challenges in developing a screening strategy to test for these fusions. Here we illustrate this by describing the varied clinical and histopathological features of a series of *NTRK* fusion-positive tumors detected in the clinical laboratory by targeted RNA sequencing.

Design: Solid tumors referred to the clinical laboratory for testing with a targeted fusion panel (Archer FusionPlex) were searched for *NTRK1*, *NTRK2* or *NTRK3* fusions. Electronic records were reviewed for clinical and laboratory findings. An *NTRK* fusion was considered an expected event if a classic fusion-positive entity, based on histopathology and/or immunohistochemistry (IHC), was provided as test indication.

Results: Eleven patients (6 males, 5 females; age 2 weeks – 30 years) were identified with diverse *NTRK* fusion-positive tumors in varied anatomical sites (Table 1). Fusions involved *NTRK1* (n=5*), NTRK2* (n=1) and *NTRK3* (n=5) with five different 5' gene partners. *ETV6/NTRK3* was the most common fusion (n=5) followed by *TPM3/NTRK1* (n=3), one tumor each with infrequent fusions (*LMNA/NTRK1*, *KANK1/NTRK2*) and a novel *DYNC1I2/NTRK1* fusion. Prior to fusion testing, clinical, histopathology and IHC features suggested an expected *NTRK* fusion-positive entity in 7/11 cases, including 4 infantile fibrosarcoma (IFS) cases, 1 glioblastoma, and 2 pan-TRK IHC-positive soft tissue tumors. Notably, the canonical *ETV6/NTRK3* fusion in IFS was detected in only 2/4 IFS tumors (cases 6, 7), with two others (cases 4, 11) harboring non-canonical/novel *NTRK* fusions (Table 1). Significantly, in 4/11 (36.3%) cases, the *NTRK* fusion was an unexpected finding (Table 1; cases 1, 5, 8, 10).

Case	Age	Sex	Location	Tumor (Initial diagnosis)	Pan-TRK IHC	Fusion panel results		
						Fusion	5' partner frequency (any tumor)	Diagnostic significance
01	9	M	Supra-renal	Round blue cell tumor (suggestive of Ewing)	NP	TPM3:NTRK1	Common	Unexpected
02	21	M	Para-vertebral	Spindle cell mesenchymal tumor of uncertain malignant potential	Positive (diffuse)	LMNA:NTRK1	Infrequent	Expected
03	30	F	Uterine Cervix	Atypical spindle cell proliferation; a low-grade sarcoma cannot be excluded	Positive	TPM3:NTRK1	Common	Expected
04	4Mo	M	Forearm	Congenital infantile fibrosarcoma	NP	TPM3:NTRK1	Common	Expected*
05	14	F	Nasal ala	Fibrohistiocytic proliferation	NP	ETV6:NTRK3	Common	Unexpected
06	10Mo	M	Orbit	Infantile fibrosarcoma	Positive (focal)	ETV6:NTRK3	Common	Expected
07	2W	M	Back	Infantile fibrosarcoma VS myofibroma	NA	ETV6:NTRK3	Common	Expected
08	2	F	Kidney	Undifferentiated Sarcoma	NP	ETV6:NTRK3	Common	Unexpected
09	6	F	Brain, frontal lobe	Epithelioid glioblastoma, recurrent	NP	ETV6:NTRK3	Common	Expected
10	6	M	Brain	Anaplastic ependymoma	NP	KANK1:NTRK2	Infrequent	Unexpected
11	3	F	Retro-peritoneum	Infantile fibrosarcoma	NP	DYNC1/2:NTRK1	Novel	Expected*

F, female; IHC, Immunohistochemical stain; M, male; Mo, month; NP, not performed; NA, not available; W, week; *non-canonical

Conclusions: *NTRK* fusion-positive entities presented with a wide clinical and histologic spectrum, in a third of which the finding was unexpected. Uncommon/novel *NTRK* fusions may be present in classic entities negative for canonical fusions by targeted testing and comprehensive fusion detection should be pursued in such cases. Positivity for pan-TRK IHC, diffuse or focal, may be helpful in uncommon clinical presentations.

40 Copy Number Alterations Outside 12q13-15 in Well-Differentiated/ Dedifferentiated Liposarcomas

Nicolas Giraldo Castillo[1], Chad Vanderbilt[2]
[1]Memorial Sloan Kettering Cancer Center, Baltimore, MD, [2]Memorial Sloan Kettering Cancer Center, New York, NY

Disclosures: Nicolas Giraldo Castillo: None; Chad Vanderbilt: *Consultant*, Paige AI

Background: Well-differentiated liposarcoma (WDLS) and dedifferentiated liposarcomas (DDLS) are rare malignant, locally aggressive mesenchymal neoplasms characterized by amplification of chromone 12q13-15, to include genes like MDM2, CDK4, and HMGA2. Previous studies in small cohorts of WDLS /DDLS suggest that there might be areas outside 12q13-15 with copy-number alterations (CNA) in these tumors. However, due to the limited sample size of these studies, the characterization of

recurrent CNA and their association with patient's clinical outcome remains unknown. In this study, we perform a large-scale genomic analysis of WDLS/DDLS to identify recurrent somatic mutations and CNA events associated with poor prognosis.

Design: We studied the prevalence of somatic mutations, CNA, and structural variants in n=81 WDLS and n=248 DDLS samples sequenced by MSK-IMPACT panel using the cBioPortal platform. We then assessed the prognostic impact of the most common genomic events using Cox Proportional-Hazards modeling for overall survival (OS.) Relevant findings were validated in an additional cohort of n=167 DDLS from the TCGA.

Results: Preliminary analysis of n=329 WDLS/DDLS showed recurrent amplifications in 6q21 (including TNFAIP3 in 18%, IFNGR1 in 12%, and LATS1 in 12%), 5p15.33 (including TERT in 12%, and TRIP13 in 10%), and 1q21-23 (including SDHC in 8% and MCL1 in 7%) regions. In addition, amplification of JUN was seen in 12% of cases. A small fraction of cases showed focal deletions, including the 9p21 region (MTAP 4%, CDKN2AP14ARF 4%, and CDKN2AP16INK4A 3%) and ATRX (3%.) Somatic mutations were relatively uncommon and included ATRX (4%), TP53 (3%), and ERBB4 (2%.) Although JUN and 5p15.33 amplification events were independent, tumors with alteration in any of these two regions were enriched in dedifferentiated histology (chi-squared p=0.001 and 0.01, respectively) and associated with shorter OS (p=0.008 and 0.01, respectively.) Analysis from additional n=167 TCGA DDLS cases confirmed that both JUN and 5p15.33 amplification were associated with poor prognosis (p=0.002 and p=0.002, respectively.)

Conclusions: This large-scale genomic analysis reveals genomic events potentially associated with progression of WDLS into DDLS and identified TERT/TRIP13 and JUN CNA as potential prognostic biomarkers in these two entities.

41 Primary Inflammatory Myofibroblastic Tumor of the Liver: Clinicopathologic and Genetic Study of 10 Cases Including a Subset of ETV6-NTRK3 Fusion

Qianqian Han[1], Xin He[1], Min Chen[1], Xiaojun Pang[2], Zhang Zhang[1], Hongying Zhang[1]
[1]West China Hospital, Sichuan University, Chengdu, China, [2]Mianyang Hospital of Traditional Chinese Medicine, Mianyang, China

Disclosures: Qianqian Han: None; Xin He: None; Min Chen: None; Xiaojun Pang: None; Zhang Zhang: None; Hongying Zhang: None

Background: Inflammatory myofibroblastic tumor (IMT) is a borderline myofibroblastic tumor, most frequently arising in mesentery, retroperitoneum, pelvis and lung, and rarely in the liver. The purpose of this study was to analyze the clinicopathological and molecular characteristics of primary liver IMT.

Design: 10 primary liver IMTs were identified, accounting for 2.6% of all diagnosed IMTs (10/384) over the past 10 years at our medical centre. The clinicopathological data was collected and analyzed by immunohistochemistry, fluorescence in situ hybridization (FISH), reverse transcription polymerase chain reaction, next generation sequencing (NGS) and Sanger sequencing.

Results: 4 males and 6 females were reviewed, age ranged from 1 year to 48 years (median 35 years, including 3 children). The main morphological features included compact fascicular spindle cell proliferation, extensive myxoid stroma, and sparse tumor cells arranged in a hyaline stroma. Tumors of 9 cases showed mild to moderate cellular atypia, 1 case exhibited obvious atypia with large and round nuclei with prominent nucleoli. Mitotic figures (0~2/10HPF) were observed. Positive SMA staining was shown in 9 cases (90%), ALK cytoplasmic expression in 6 cases (6/10, 60%) and pan-TRK nuclear reactivity in 3 cases (3/10, 30%). *ALK* gene rearrangement was detected in 3 of 5 ALK-positive cases undergone FISH and/or NGS detection, of which one case contained *ALK* double fusion transcripts (*TFG-ALK* and *FCHSD2-ALK*). All 3 pan-TRK-positive cases exhibited *ETV6-NTRK3* fusion confirmed by NGS and/or Sanger sequencing, but FISH only determined positive results in 1 case. Unavailable immunostaining or gene rearrangement was detected in 1 case (1/10, 10%). All tumors undergone completely resection survived without disease (follow-up time was 3 to 96 months), except one biopsy case died of tumor 12 months later.

Conclusions: Primary liver IMT is extremely rare and should be differentiated from metastatic IMT and inflammatory pseudotumor. ALK overexpression/*ALK* rearrangement IMTs was the majority, consistent with classical IMTs; Notably, an *ALK* double fusion IMT was detected, which had not been reported so far. Secondly, the proportion of *ETV6-NTRK3*-rearranged IMTs was higher than that of IMT in other anatomical location. And we should be aware of the possibility of false-negative results by FISH detection. Early detection and complete resection with negative margins are very important for the favourable prognosis.

42 Clinicopathologic Features and Prognostic Predictors of Dedifferentiated Chondrosarcoma

Yin (Rex) Hung[1], Ivan Chebib[2], Emily Berner[2], Quinn Taylor-Black[1], Martin Selig[1], Vikram Deshpande[2], Jason Hornick[3], Santiago Lozano-Calderon[2], G. Pétur Nielsen[2]
[1]Massachusetts General Hospital, Boston, MA, [2]Massachusetts General Hospital, Harvard Medical School, Boston, MA, [3]Brigham and Women's Hospital, Harvard Medical School, Boston, MA

Disclosures: Yin (Rex) Hung: None; Ivan Chebib: None; Emily Berner: None; Quinn Taylor-Black: None; Martin Selig: None; Vikram Deshpande: None; Jason Hornick: None; Santiago Lozano-Calderon: None; G. Pétur Nielsen: None

Background: Dedifferentiated chondrosarcoma is aggressive and rare. Data on its clinicopathologic/molecular features and their prognostic significance remain limited.

Design: We searched surgical pathology files from 1999-2021 for dedifferentiated chondrosarcomas, reviewed clinicopathologic features, quantified extents/amounts of dedifferentiation, and, in selected cases, performed H3K27me3 immunohistochemistry and IDH1/2 molecular testing. Statistical analysis (cox proportional hazard models and log-rank tests) was performed in python 3.8 (package: lifelines).

Results: In this consecutive series of 67 patients (26 women, 41 men; age 39 to >89 [median 61] yr; 2 with Ollier disease), 58 presented *de novo*, and 9 had conventional chondrosarcomas 0.6-13 (median 6) yr prior. Pathologic fracture and distant metastases were noted in 27 and 7 patients at presentation, respectively. The tumors involved femur (n=27), pelvis (22), humerus (7), tibia (4), scapula/ribs (4), spine (2), and clivus (1). Of 60 surgically resected tumors, total sizes/dedifferentiated components could be assessed in 56. The tumors ranged from 4-46 cm (median 12 cm) in size and contained 1-99% (median 70%) dedifferentiated components, which harbored osteosarcomatous (n=26), rarely rhabdomyosarcomatous (2) or angiosarcomatous (1) elements. The associated cartilaginous components were predominantly Grade 1-2, rarely Grade 3 (n=3) or enchondromas (2). Loss of H3K27me3 expression was seen in 5 of 49 (10%) cases; IDH1/2 R132/172 mutations were detected in 16 of 23 (70%) cases tested. In the entire cohort, the median overall survival (OS) and progression-free survival (PFS) were 11.8 and 5.4 months, respectively. Prognostic factors for worse OS/PFS included metastatic disease at presentation and pathologic fracture. Neoadjuvant radio/chemotherapy was associated with improved PFS. No associations between age, sex, tumor location, or IDH/H3K27me3 status and OS/PFS were identified. While there was no prognostic significance of total tumor size or percentage of dedifferentiation alone, the size of the dedifferentiated component (>3 cm) was predictive of worse OS (8.7 vs 58.9 mo; HR=4.71, 95% CI: 1.60-13.84; p<0.005; Figure 1), but not PFS (HR=1.63, 95% CI: 0.62-4.28; p=0.33).

Figure 1 - 42

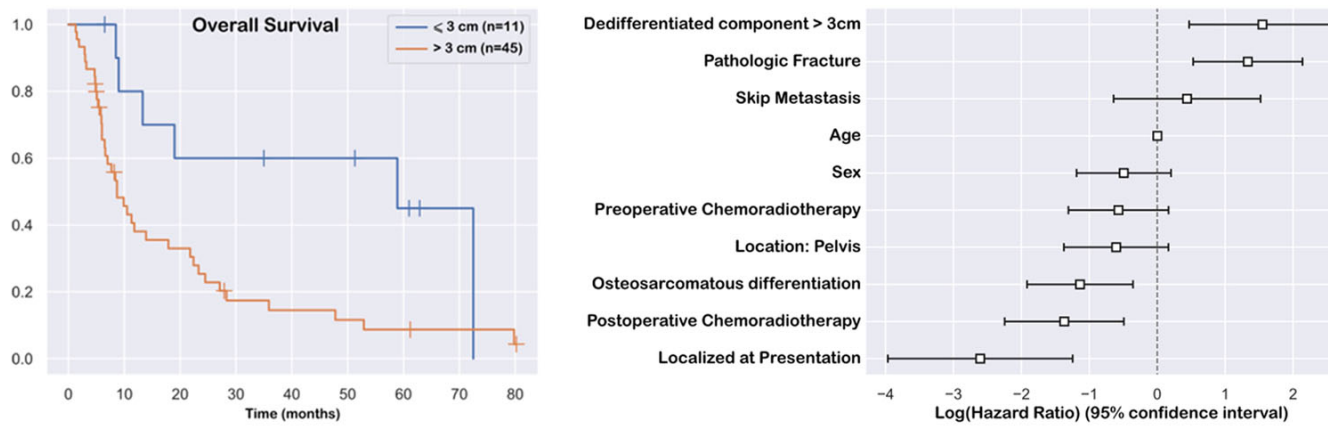

Conclusions: Dedifferentiated chondrosarcomas usually arise in femur/pelvis, present *de novo* or after initial conventional chondrosarcoma diagnosis, and pursue a dismal clinical course. The size of the dedifferentiated component predicts outcome better than total tumor size or percentage of dedifferentiation.

43 Classification of Small Round Cell Tumors Using Convolutional Neural Networks

Nishat Khan[1], Christopher Chandler[1], Jonathan Henriksen[1], Linda Shapiro[1], Nicholas Reder[1], Robert Ricciotti[1]
[1]*University of Washington, Seattle, WA*

Disclosures: Nishat Khan: None; Christopher Chandler: None; Jonathan Henriksen: None; Linda Shapiro: None; Nicholas Reder: *Employee*, Lightspeed Microscopy, Inc.; *Employee*, Lightspeed Microscopy, Inc.; Robert Ricciotti: None

Background: Small round cell tumors (SRCTs) are a diverse group of neoplasms seen by all subspecialties generally characterized morphologically by crowded small cells with basophilic nuclei and scant cytoplasm. Differentiating SRCTs from one another is a common challenge in surgical pathology and can have major clinical implications for the patient. Immunohistochemical staining and molecular studies are often necessary for diagnosis. We hypothesized that we could use convolutional neural networks (CNNs) to classify SRCTs using whole slide images (WSI) of hematoxylin and eosin (H&E) stained slides.

Design: Following IRB approval, we searched our institutional pathology archives for 8 different types of SRCTs and retrieved all available histologic slides. Retrieved cases included Ewing sarcoma (n=34), alveolar rhabdomyosarcoma (ARMS) (n=11), round cell liposarcoma (n=24), mesenchymal chondrosarcoma (MCSA) (n=11), olfactory neuroblastoma (n=20) follicular lymphoma (n=51), Merkel cell carcinoma (n=47), and small cell lung carcinoma (n=47). At least one representative H&E-stained slide from each case was scanned at 40x resolution using an Aperio ScanScope AT2 whole slide scanner. Regions of interest (ROI) were annotated using QuPath (vers. 2.3). Image patches were generated from unannotated WSI and ROIs using a sliding window approach and a training, validation, and test set breakdown of 50%, 20%, and 30% respectively. Residual Network (ResNet) was used for training and classification. Classifier accuracy was compared for all 8 diagnoses (8-class) as well as performance in differentiating sarcoma from non-sarcoma neoplasms (2-class) using unannotated WSI and pathologist directed ROIs.

Results: We achieved an overall 8-class accuracy of 73.47% (unannotated WSI) to 78.52% (ROI) and a 2-class (sarcoma vs non-sarcoma) accuracy of 84.43% (WSI) to 88.33% (ROI) (Table 1). Our classifier was least accurate in differentiating ARMS from MCSA but case numbers for these two neoplasms were small.

Eight class classifier		
Diagnosis	Accuracy for WSI	Accuracy for ROI
Lymphoma (n=51)	87.32%	92.30%
Small cell lung carcinoma (n=47)	87.24%	91.54%
Merkel cell carcinoma (n=47)	87.13%	91.03%
Olfactory neuroblastoma (n=20)	70.11%	76.08%
Ewing sarcoma (n=34)	78.47%	82.59%
Round cell liposarcoma (n=24)	73.23%	79.43%
Alveolar rhabdomyosarcoma (n=11)	52.01%	58.11%
Mesenchymal chondrosarcoma (n=11)	52.20%	57.06%
	Average accuracy 73.47%	Average accuracy 78.52%
Two Class Classifier		
Diagnostic Group	Accuracy for WSI	Accuracy for ROI
Sarcoma (n=80)	79.51%	85.01%
Non-sarcoma (n=165)	89.35%	91.63%
	Average accuracy 84.43%	Average accuracy 88.33%

Conclusions: We show that SRCTs can be successfully classified from H&E stained WSI alone using CNNs. Classifier accuracy improved significantly with increasing case counts, suggesting performance could be improved by including more examples of each neoplasm. Pathologist directed ROIs improved classifier accuracy over unannotated WSI alone. Our findings suggest that CNN analysis of WSIs has the potential to improve diagnostic accuracy, help reduce workup from ancillary testing and reduce cost.

44 Targeted DNA and RNA Sequencing of Soft Tissue Spindle Cell Tumors Reveals a Rare MET-TFG and a Novel PWWP2A-RET Gene Fusions as well as Additional Recurrent PIK3CA Point Mutations

Natálie Klubíčková[1], Kemal Kosemehmetoglu[2], Michal Michal[3], Michael Michal[3]
[1]Charles University, Faculty of Medicine in Plzen, Plzen, Czech Republic, [2]Hacettepe University, Ankara, Turkey, [3]Biopticka laborator s.r.o., Plzen, Czech Republic

Disclosures: Natálie Klubíčková: None; Kemal Kosemehmetoglu: None; Michal Michal: None; Michael Michal: None

Background: Spindle cell soft tissue tumors may harbor fusions of various kinase genes, several of which are targetable by novel small inhibitory molecules. Apart from the *ETV6-NTRK3* fusion in infantile fibrosarcoma, fusions of other kinase genes such as *NTRK1/2/3, RET, MET, RAF1,* or *BRAF* have been recently reported in various mesenchymal tumors with similar morphology. We aimed to share our institutional experience with these rare tumors and specifically focused on determining whether they – in addition to gene fusions – harbor any other molecular abnormalities.

Design: 15 tumors affecting both pediatric and adult patients were collected. The following morphological patterns were observed: lipofibromatosis-like neural tumor (LNT, n=2) (Fig.1B) and fibroblastic tumor with perivascular hyalinization patterns (FTPH, n=4) (Fig.1A) – both considered low-grade (LG), and high-grade (HG) fibrosarcoma-like pattern (FS, n=10) (Fig. 1C). Immunohistochemistry for S100 protein, CD34, SMA and panTrk was performed. Targeted RNA sequencing using Archer FusionPlex Kits (n=14) or targeted DNA and RNA sequencing (n=11) using the Illumina TruSight Oncology 500 was carried out. FISH was used in 1 case. When possible, clinical follow-up was obtained.

Results: Clinicopathological features are summarized in Table. All cases with the *ETV6-NTRK3* fusion displayed FS morphology. Other detected fusions were associated with various morphological patterns. Case 2 harbored an *EML4-NTRK3* fusion and contained both LG FTPH and HG FS areas. Using FISH, homozygous loss of *CDKN2A* was detected only in the HG area. The patient DOD 30 months after the diagnosis. Additionally, 2 cases with a *PIK3CA* mutation and 1 case with a *MAP3K1* mutation were detected, all being associated with HG FS morphology. Only 1 case with an LG LNT pattern and a *PIK3CA* mutation was found. Four patients with locally advanced or recurrent disease are being treated with *NTRK* or *RET* inhibitors in combination with other modalities, 3 of them are currently disease-free and 1 is AWD.

Case No.	Age/Sex	Location	Size (cm)	MR	Immunohistochemistry				**Fusion**	Mutation	MSI/TMB	T	Outcome/ Length (months)
					S100	CD34	SMA	Trk					
1	37 years/F	instep	max. dim. 1.3	LNT	-	+++	-	++	*LMNA-NTRK1*	*PIK3CA* pm	NA	S	NED/30
2	3 years/M	upper lip and orbit	NA	FS	+++	+++	-	+++	*EML4-NTRK3*	*CDKN2A* loss	NA	S +CHT	Mediastinal MET (max. dim. 10 cm); DOD/30
				FTPH	++	+++	-	+++		-	NA		
3	10 months/M	NA	NA	LNT	+	-	+	+++	*TPM3-NTRK1*	-	NA	NA	NA
4	4 months/M	forearm	NA	FS	-	-	+	++	*ETV6-NTRK3*	*MAP3K1* pm	low/low	S +CHT +TT-L	NED/13
5	3 years/F	lower eyelid	NA	FS	+	+++	-	+++	*LMNA-NTRK1*	*PIK3CA* pm	NA/low	S +TT-E	LR 2x before our diagnosis; NED/NA
6	6 months/F	foot	NA	FS	-	++	+	++	*ETV6-NTRK3*	*PIK3CA* pm	NA	CHT +TT-L	NED/11
7	43 years/M	hip	5.5 x6.2 x6.3	FTPH	++	+++	-	+++	*LMNA-NTRK1*	-	low/low	NA	NA
8	1 day/M	duodenum	NA	FS	-	-	++	+++	*TPM3-NTRK1*	NA	NA	NA	NA
9	5 months/M	cheek	NA	FS	-	+	-	+	*ETV6-NTRK3*	-	NA	NA	NA
10	2 weeks/F	coccygeal region	max. dim. 1.5	FS	-	-	-	-	*PWWP2A-RET*	-	NA	CHT +TT	AWD/NA
11	6 years/F	orbit	max. dim. 2	FTPH	++	-	-	-	*MYH10-RET*	NA	low/NA	S +CHT	NA
12	34 years/M	forearm	NA	FTPH	-	+++	-	-	*NCOA4-RET**	-	NA	NA	LR 1x; lost to follow-up
13	1 day/F	back	max. dim. 18	FS	-	+++	-	-	*TFG-MET*	NA	NA	S	NED/24
14	56 years/M	knee	1.5 x1 x1	FS	-	+++	+++	-	*ITSN1-RAF1*	-	low/low	NA	NA
15	5 months/M	RP	max. dim. 5	FS	+++	-	+++	-	*OSBP-BRAF**	-	NA	S +CHT	NED/24

Legend: AWD - alive with disease; CHT - chemotherapy; DOD - died of disease; E - entrectinib; F - female; L - larotrectinib; LR - local recurrence; MET - metastasis; MR - morphology review; MSI - microsatellite instability; NA - not available; NED - no evidence of disease; pm - point mutation; RP - retroperitoneum; S - surgery; T - treatment; TMB - tumor mutation burden; TT - targeted therapy;
* - cases already reported

Figure 1 - 44

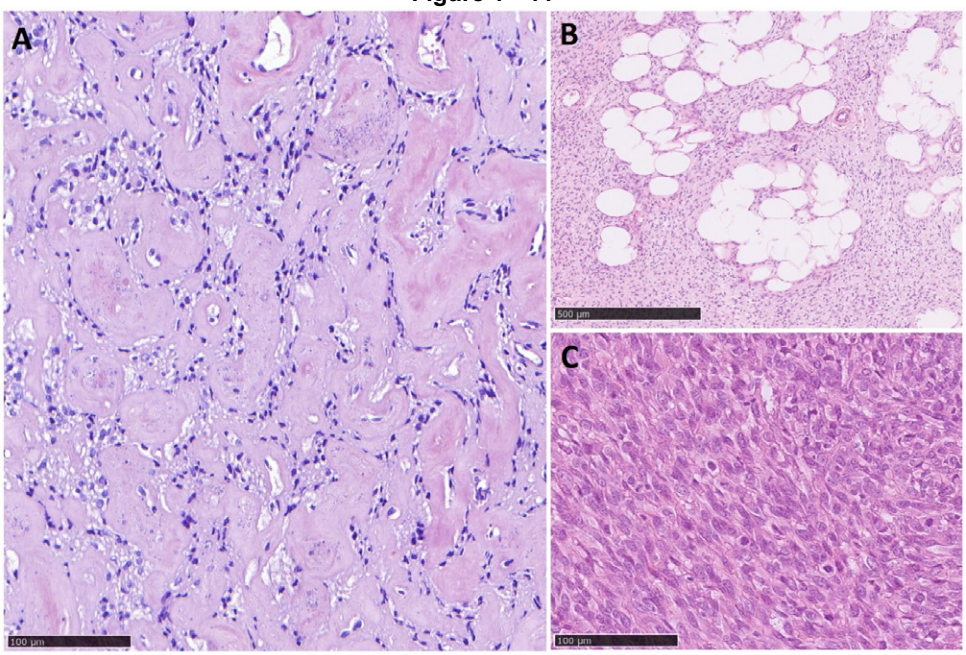

Figure 1. Morphological patterns observed in the tumors. **A.** LG fibroblastic tumor with perivascular hyalinization. **B.** LG lipofibromatosis-like neural tumor. **C.** HG fibrosarcoma-like tumor.

Figure 2 - 44

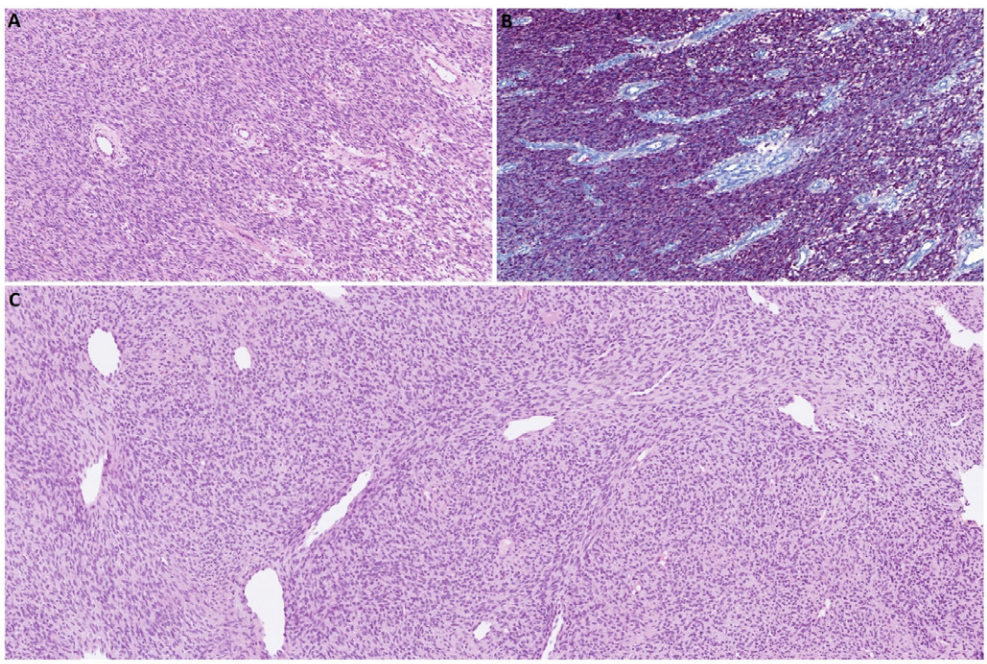

Figure 2. A. Case 13 harboring a rare *TFG-MET* fusion exhibited classic FS morphology. **B.** Diffuse S100 protein expression in case 13. **C.** Case 10 with a novel *PWWP2-RET* fusion again showing FS morphology.

Conclusions: Besides identifying several rare or novel kinase fusions genes, our analysis also revealed various additional mutations including recurrent *PIK3CA* point mutations. Although their significance is unknown, they might be responsible for progression of tumors with LG morphology (LNT, FTPH) into tumors with HG morphology and/or acquisition of a more aggressive biological potential. Targeted therapy is effective and significantly aids in successful treatment.

45 Clinicopathologic Characteristics of Giant Cell Tumor of Bone with Malignant Transformation

Sandor Krisztian Kovacs[1], Yin (Rex) Hung[2], G. Pétur Nielsen[1]
[1]Massachusetts General Hospital, Harvard Medical School, Boston, MA, [2]Massachusetts General Hospital, Boston, MA

Disclosures: Sandor Krisztian Kovacs: None; Yin (Rex) Hung: None; G. Pétur Nielsen: None

Background: Giant cell tumor of the bone (GCTB) is locally aggressive and rarely undergoes malignant transformation. Denosumab, a RANKL inhibitor, has been approved to treat locally advanced/unresectable GCTB. Clinical studies demonstrated the safety of denosumab; rare reports of malignancy arising in denosumab-treated GCTB have been noted. Clinicopathologic features and the biology of malignant transformation in GCTB remain poorly understood.

Design: Surgical pathology files from 1990-2021 were searched for GCTB with malignant transformation. Clinicopathological features were reviewed. Immunohistochemistry was performed in selected cases.

Results: Of >800 GCTB patients, malignant transformation was identified in 13 (<2.0%; 8 men, 5 women; age 16-57 [median 33] years). They presented 8-206 months after the initial diagnosis of GCTB, involving long bones (femur, tibia, fibula, humerus) in 11 and pelvis in 2 patients. The tumor sizes ranged from 3.4-18.0 cm (median 6 cm). Four of 13 patients were known to have received denosumab for initial GCTB for 7-24 months (median 20 months), with an interval of 11-33 months (median 20 months) between treatment initiation and malignant transformation. Their initial GCTB all showed the characteristic morphology for giant cell tumor of bone. After malignant transformation, histologic features included focal to prominent necrosis, overt nuclear atypia, conspicuous mitotic figures, and areas diagnostic of high-grade sarcoma. At least 6 of 13 tumors showed areas suggestive of residual GCTB component adjacent to sarcoma. By immunohistochemistry, H3.3-G34W was positive in 5 of 7 tumors tested. Of the five patients with available follow-up, one developed multiple metastases in lymph nodes, and one died of disease at 16 months after the diagnosis of malignant GCTB.

Conclusions: GCTB with malignant transformation usually arises months to years after the initial GCTB diagnosis. In this cohort, 4 of 13 patients were known to have denosumab treatment prior to sarcomatous transformation of GCTB. Additional investigations are needed to better characterize underlying mechanisms in sarcomatous transformation.

46 Copy Number Alterations in Epstein-Barr Virus associated Smooth Muscle Tumour, Leiomyoma and Leiomyosarcoma

Victor Lee[1], Naw Wah Wah[1], Noorjehan Omar[2]
[1]National University of Singapore, Singapore, Singapore, [2]Hospital Kuala Lumpur, Kuala Lumpur, Malaysia

Disclosures: Victor Lee: None; Naw Wah Wah: None; Noorjehan Omar: None

Background: There are three clinical subtypes of EBV associated smooth muscle tumours (EBV-SMT): EBV-SMT in post-transplant patients, EBV-SMT in patients with HIV, and EBV-SMT in patients with congenital immunodeficiency. Although the pathologic characteristics of EBV-SMT have been well characterized, the genomic profiles of these tumors are not well studied. Furthermore, conventional histological criteria of malignancy are not reliable in predicting clinical outcomes in EBV-SMT. This study aims to characterize copy number alterations in EBV-SMT, leiomyoma and leiomyosarcoma and correlate CNA with clinicopathological characteristics.

Design: Copy number profiles were generated from 20 FFPE tumour tissues using the OncoScan® FFPE assay (Affymetrix) and data analysis was performed using the OncoScan® Console (v1.3) software and Chromosome Analysis Suite (ChAS). Final data analysis included EBV-SMT (n=6), leiomyomas (n=6) and leiomyosarcomas (n=7), occurring in extra-uterine locations in adults. CNApp was used to further analyze data from ChAS. GRCh38 was used for analysis. Copy number scores were computed by CNApp considering segments from the input file and default thresholds for classifying broad and focal events. BCS, FCS and GCS represent broad, focal and global CNA scores. BCS, FCS and GCS were computed based on length and amplitude of segments. Student's t-test was used for pair wise comparison of the distribution of GCS, FCS and BCS in EBV-SMT, leiomyoma and leiomyosarcoma. P val<0.05 were considered statistically significant.

Results: EBV-SMT, leiomyoma and leiomyosarcoma can be differentiated based on copy number alterations (Fig. 1). Genomic instability and focal CNAs are the highest in leiomyosarcoma and the lowest in leiomyoma (Fig.2). The presence of only 17 5Mb regions that differentiate EBV-SMT and leiomyoma ($p<0.05$) indicates that EBV infection does not lead to as much genomic

instability as in leiomyosarcoma. There are 187 5Mb regions that differentiate EBV-SMT and leiomyosarcoma ($p<0.05$). These findings correlate with the clinical behaviours of these tumours.

Figure 1 - 46

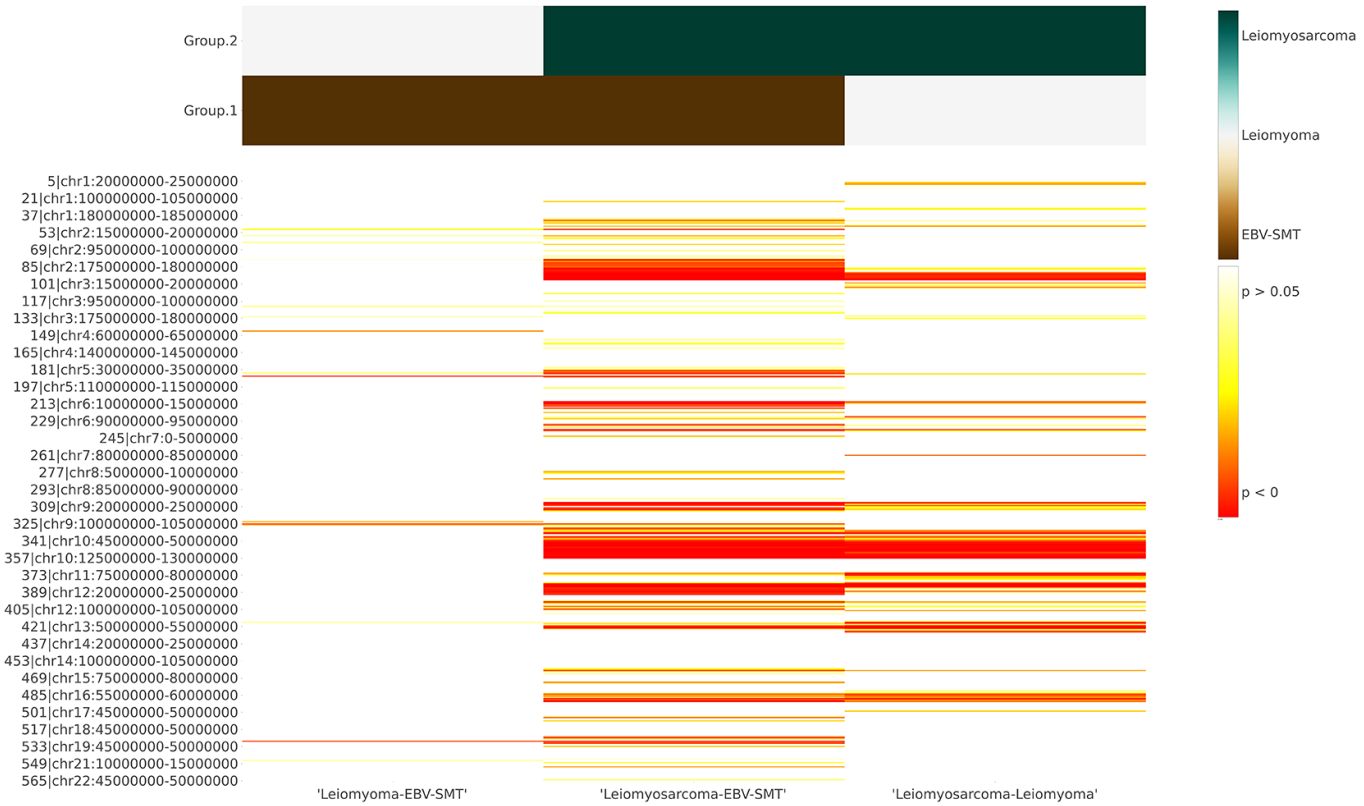

Figure 2 - 46

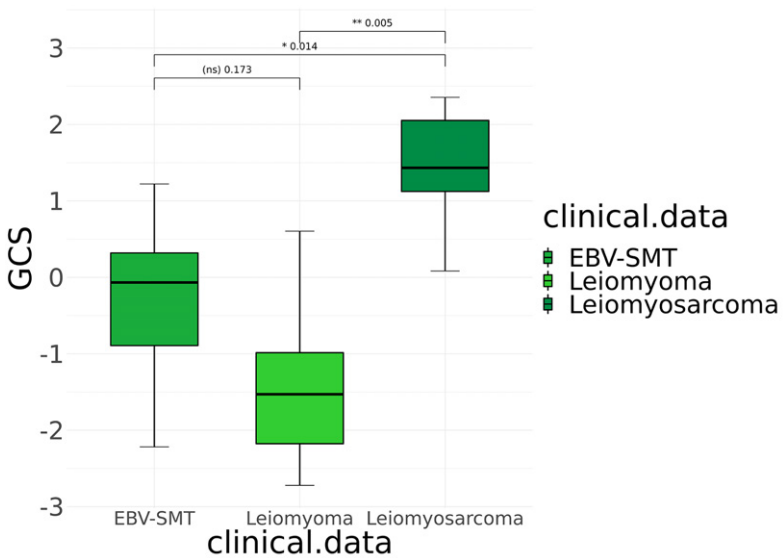

Conclusions: This study has identified CNAs unique to EBV-SMT which differentiate it from leiomyoma and leiomyosarcoma. Global and focal copy number alteration burden in EBV-SMT is significantly lower than that in leiomyosarcoma. These findings correlate with the clinical outcome where EBV-SMT progress slowly and tend to have better prognosis compared to leiomyosarcoma which are much more aggressive.

47 Immunohistochemical Analysis of Proteins of Metabolism in Chordoma Tumor Microarrays

Sherry Lee[1], Ida Micaily[1], Tingting Zhan[2], Raymond ONeill[1], John Abraham[3], MD Martinez-Outschoom[2], Atrayee Basu Mallick[1], Wei Jiang[1]
[1]Thomas Jefferson University Hospital, Philadelphia, PA, [2]Thomas Jefferson University, Philadelphia, PA, [3]Fox Chase Cancer Center, Philadelphia, PA

Disclosures: Sherry Lee: None; Ida Micaily: None; Tingting Zhan: None; Raymond ONeill: None; John Abraham: None; MD Martinez-Outschoom: *Advisory Board Member*, Seagen; *Advisory Board Member*, Astra Zeneca; *Grant or Research Support*, Otsuka; *Advisory Board Member*, EUSA; Atrayee Basu Mallick: *Advisory Board Member*, Daichi Sanyo; *Consultant*, Novartis; Wei Jiang: None

Background: Chordoma is a rare and aggressive primary bone malignancy. Standard treatment is *en bloc* surgical excision coupled with radiation therapy. Depending on its location and recurrence, chordoma can cause significant morbidity and mortality. Previously we found that expressions of several proteins involved in mitochondrial metabolism, Translocase of the Outer Mitochondrial Membrane complex subunit 20 (TOMM20), TP53 Induced Glycolysis and Apoptosis Regulator (TIGAR), and Monocarboxylate Transporter 1 (MCT1), show positive correlation with histological grade of chondrosarcoma. Furthermore, TOMM20 promoted chondrosarcoma growth *in vivo*.

Design: Clinical data for patients diagnosed with chordoma were collected via retrospective chart review. Tumor microarrays were built from 61 chordoma specimens. Expressions of TOMM20, TIGAR, and MCT1 were evaluated by immunohistochemistry (Figure 1) and semi-quantitative analysis of staining intensity and percentage of positive tumor cells. Intensity of staining was graded from 0 to 3+ with 0 having no staining to 3+ with strongest staining. Percent of positive tumor cells was graded from 0 to 2 with 0 having <10%, 1 10-50%, and 2 >50% of tumor cells. Composite scores were calculated by multiplying grade of intensity and grade of positive tumor cells. Two-tailed unpaired t-test and one-way ANOVA were used to determine significant differences in composite scores between groups.

Results: Forty-one patients, 27 male and 14 female, with an average age of 57 at the time of chordoma diagnosis were included in the study. Twenty-seven patients had primary disease and 14 had recurrent and/or metastatic disease. Average composite scores of MCT1, TIGAR, and TOMM20 expression were compared by disease status and anatomic location (Table 1). Higher expression of TOMM20 was seen in recurrent and metastatic chordomas compared to primary lesions. Comparing composite scores of primary lesions in patients with primary disease only versus those with recurrent disease showed that TOMM20 expression is significantly higher in primary lesions followed by a history of recurrence.

Table 1. Expressions of proteins of metabolism in chordomas by disease status and anatomic location. CI: confidence interval; *p<0.05.

	Disease status			**Anatomic location**		
Protein	Primary (n=37)	Recurrent and metastatic (n=24)		Base of skull (n=35)	Mobile spine (n= 13)	Sacrum (n=13)
MCT1 mean (95% CI)	3.1 (2.5 - 3.8)	3.7 (2.9 - 4.5)		3.4 (2.7 - 4.0)	3.2 (2.1 - 4.2)	3.5 (1.9 - 5.0)
TIGAR	4.6 (4.0 - 5.2)	4.6 (3.8 - 5.4)		4.9 (4.3 - 5.5)	4.5 (3.5 - 5.5)	3.8 (2.6 - 5.1)
TOMM20	2.4* (1.8 - 3.0)	3.7* (2.9 - 4.5)		2.7 (2.0 - 3.5)	3.2 (2.5 - 3.8)	2.8 (1.6 - 4.1)

Figure 1 - 47

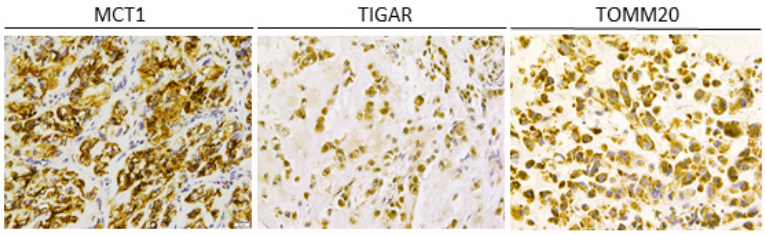

Figure 1. Representative images of staining patterns of MCT1, TIGAR, and TOMM20 on chordoma tumor microarrays.

Conclusions: Identifying novel signaling pathways promoting chordoma's growth and recurrence is critical to develop targeted therapy for treating chordoma. Recurrent/metastatic disease showed increased expression of TOMM20, a potential marker to predict chordoma disease progression. Primary chordoma tumors that progress to recurrent/metastatic disease also exhibit higher expression of TOMM20.

48 Myoepithelial Tumors of Soft Tissue in Children and Young Adults

Suzanna Logan[1], Karen Fritchie[2], Andrew Folpe[1]
[1]Mayo Clinic, Rochester, MN, [2]Cleveland Clinic, Cleveland, OH

Disclosures: Suzanna Logan: None; Karen Fritchie: None; Andrew Folpe: None

Background: Primary myoepithelial tumors of soft tissue and bone are rare in children (≤ 21 years old). Although some reported myoepitheliomas in young patients have behaved in an aggressive fashion, their natural history has not been fully elucidated. Furthermore, the morphologic, immunohistochemical, and molecular genetic features of these rare tumors have not been comprehensively described. To these ends, we report a series of 23 myoepithelial tumors of soft tissue and bone in children.

Design: Cases coded as "myoepithelioma" or "myoepithelial carcinoma" occurring in patients ≤ 21 years old were retrieved from the authors' consultation files (2009-2019). Cases were classified as "myoepithelial" based on a combination of characteristic morphology and immunophenotype (co-expression of keratins and some combination of S100 protein, SOX10, smooth muscle actins, desmin, caldesmon, or GFAP). Histologically malignant tumors displayed some combination of nuclear atypia, high cellularity, elevated mitotic activity, and necrosis. SMARCB1/SMARCA4 expression and *EWSR1* gene rearrangement status were recorded. Clinical follow-up, including surgery, adjuvant therapy, local recurrence, metastasis, and current status were obtained.

Results: The 23 cases occurred in 9 males and 14 females (ages 12 wks to 21 yrs, median 12 yrs). Sites of disease included trunk, extremities, and skull. Most (19/23, 83%) were histologically malignant, comprising sheets, fascicles, and organoid arrays of cytologically malignant epithelioid and round cells. Matrix production was seen in one case. Other notable morphologic features included primitive appearing spindled or round cells. SMARCB1 expression was lost in 1/13 cases (8%); SMARCA4 expression was retained in 4 tested cases (all SMARCB1 intact). *EWSR1* gene rearrangement was identified in 3/12 (25%) cases. Clinical follow up (11 patients, range 2-119 mos, median 30.5 mos) showed metastases to lymph nodes, lung, and brain, in 4/9 patients with histologically malignant tumors, 2 of whom died of disease (2 and 10 mos after diagnosis).

Table 1. Clinicopathologic characteristics of histologically malignant (1-19) and benign (20-23) myoepithelial tumors.

Pt No.	Age/Sex	Location	Size (cm)	Primary Therapy	Local Recurrence (mo)	Metastasis (mo)	Follow-Up (mo)	Molecular
Histologically malignant								
1	12w/M	axilla/chest wall	7	Wide excision (lymph node metastases and brachial plexus/skeletal muscle infiltration present upon primary excision) Chemotherapy initiated with poor response, discontinued shortly	-	Regional LN, 0	DOD, 2	NP
2	15/F	breast	12	Excision, negative margins	N	N	NED, 119	NP
3	11/F	foot	3	Excision (margin status unknown)	N/A	N/A	N/A	NP
4	10m/M	thigh	6	N/A	N/A	Extracranial and intradural, 14	N/A	*EWSR1* neg (FISH)*
5	19/M	thigh mass	9.5	Wide excision, adjuvant RT (margin status unknown)	N	N	NED, 82	*EWSR1* and *TFE3* neg (FISH)
6	22m/M	hand	N/A	5th ray resection, negative margins Epitrochlear/axillary lymph node biopsies, negative	N	N	NED, 63	NP
7	2/F	supraorbit and pericranium	2	N/A	N/A	N/A	N/A	*EWSR1* pos (FISH)
8	2/F	thigh	N/A	N/A	N/A	N/A	N/A	*EWSR1* neg (FISH)
9	10/F	knee	N/A	N/A	N/A	N/A	N/A	*EWSR1*, *FUS*, *SYT* neg (FISH)
10	12/F	thigh	3.5	N/A	N/A	N/A	N/A	*EWSR1, DDIT3* neg (FISH)
11	12/M	foot	5	Excision, positive margins, adjuvant CRT	-	Pulmonary, 1	DOD, 10	*SMARCB1* deletion (NGS)
12	17/M	index finger	1.7	N/A	N/A	N/A	N/A	*SS18-SSX1/2* neg (RT-PCR)
13	15/F	thigh, focal invasion into femoral cortex	8.5	En bloc resection, negative margins	N	N	NED, 36	*EWSR1*, *FUS*, and *SYT* neg (FISH)
14	9/F	paraspinal	4.5	Excision (unknown margin status), adjuvant CRT	N	N	NED, 23	*EWSR1* and *SS18* neg (FISH)
15	7/F	palm	N/A	N/A	N/A	N/A	N/A	NP
16	12/F	flank	3.3	Primary excision, positive margins Re-excision, negative margins	N	Regional lymph nodes, 4	NED, 25	*EWSR1* pos, *TFE3* neg (FISH)
17	6/F	leg	4	N/A	N/A	N/A	N/A	*EWSR1* neg (FISH)
18	20/F	skull	3	N/A	N/A	N/A	N/A	*EWSR1* pos (FISH)
19	18/M	thigh	3.5	N/A	N/A	N/A	N/A	NP
Histologically benign								
20	15/F	elbow	2.3	Excision, negative margins	N	N	NED, 113	NP
21	21/F	chest	3.2	Excision, negative margins	N	N	NED, 24	NP
22	12/M	ear	0.7	N/A	N/A	N/A	N/A	NP
23	8/M	leg	0.7	N/A	N/A	N/A	N/A	NP

CRT: chemoradiation therapy, DOD: died of disease, FISH: fluorescence *in-situ* hybridization, N: no, N/A: not available, NED: no evidence of disease, NGS: next-generation sequencing, NP: not performed, RT-PCR: reverse-transcription polymerase chain reaction

*Additional copies of *EWSR1* FISH probe present in approximately 70% of cells

Conclusions: Myoepithelial tumors of soft tissue in children are often histologically malignant, and may behave in an aggressive fashion, with rapidly spreading disease and fatal outcome. In contrast, histologically benign myoepithelial tumors in this age group appear to have a favorable prognosis, although data are very limited. SMARCB1/SMARCA4 loss and *EWSR1* rearrangement are uncommon features of soft tissue myoepithelial tumors in young patients.

49 Molecular Analysis of Myxoinflammatory Fibroblastic Sarcoma (MIFS) with High-Grade (HG) Progression Reveals a Novel BRAF-MKLN1 Gene Fusion and Frequent BRAF and VGLL3 Gene Amplifications

Michael Michal[1], David Suster[2], Natálie Klubíčková[3], Zdenek Kinkor[1], Kvetoslava Michalova[1], Antonina Kalmykova[4], Saul Suster[5], Michal Michal[1]

[1]Biopticka laborator s.r.o., Plzen, Czech Republic, [2]Rutgers New Jersey Medical School/Rutgers University, Newark, NJ, [3]Charles University, Faculty of Medicine in Plzen, Plzen, Czech Republic, [4]Medical Laboratory CSD Lab, Kyiv, Ukraine, [5]Medical College of Wisconsin, Milwaukee, WI

Disclosures: Michael Michal: None; David Suster: None; Natálie Klubíčková: None; Zdenek Kinkor: None; Kvetoslava Michalova: None; Antonina Kalmykova: None; Saul Suster: None; Michal Michal: None

Background: MIFS is defined as a low-grade sarcoma with a high propensity for local recurrence and a very low metastatic potential. About half of MIFS harbor *VGLL3* amplifications, while a smaller subset has *BRAF*, *OGA* (*MGEA5*) or *TGFBR3* rearrangements. Although the existence of HG variant of MIFS was already proposed in previous studies, the conclusions were based on morphological findings and lacked molecular data. As a result, the concept of HG MIFS has not been widely accepted and such tumors remain to be classified as HG myxofibrosarcomas. Our aim was to ascertain whether any immunohistochemical (IHC) or molecular evidence linking these neoplasms to conventional MIFS could be identified.

Design: 6 cases exhibiting both typical morphological features of conventional (C-) MIFS as well as HG sarcomatous areas were collected and stained for several IHC markers including those known to be frequently expressed in C-MIFS. FISH analysis, as well as NGS using the Archer FusionPlex Sarcoma kit, was performed.

Results: The clinical, IHC, and molecular features are summarized in the Table. All tumors were located on the extremities above the fascia. 5 tumors exhibited C-MIFS areas with low/moderate atypia and 1-3 mitoses/2 mm^2 gradually transforming into HG MIFS areas (representing at least 20% of the lesion) with severe atypia and 8-15 mitoses/2 mm^2. Morphologically, tumors contained all diagnostic features of MIFS as defined by the WHO (Figures 1 and 2). Case 6 exhibited only HG MIFS areas. All 4 cases with follow-up pursued an aggressive course. All cases showed IHC expression of cyclin D1, factor XIII and CD10. 5/6 and 2/6 cases stained with D2-40 and CD34, respectively. No expression was noted for S100 protein, AE1/3, desmin, and MDM2. 3/5 analyzable cases harbored *VGLL3* amplification. Case 2 revealed a novel *BRAF-MKLN1* gene fusion which was confirmed by FISH. The FISH analysis also revealed *BRAF* gene amplification in this case as well as in case 4.

Case	Age/sex	Location	Size (cm)	Follow-up	Mib-1	*OGA* + *TGFBR3* FISH	*BRAF* FISH (break + enumeration)	*VGLL3* gene AMP by FISH	NGS
1	76/M	R forearm	6,5x4x2,5	NA	50 %	Neg	Neg	Neg	Neg
2	73/M	L distal arm	4x3x3	NA	70 %	Neg	Break + AMP	Neg	*BRAF-MKLN1*
3	76/F	Lower leg	4.5x2x1.8	R; lungs mets; DOMD	30 %	Neg	Neg	NA	Neg
4	66/F	R elbow	7.6x6x1.5	3xR; LN + lung mets; DOMD	20 %	Neg	Neg	AMP	Neg
5	48/F	R shoulder	6 in diam.	R; lung mets; lost to follow-up	70 %	Neg	Neg	AMP	Neg
6	69/F	R hip	5 in diam.	R; multiple lung and pleural mets; DOMD	80 %	Neg	Low AMP	AMP	Neg

Legend: DOMD – died of metastatic disease; R – recurrence; NA – not available; AMP – amplification; NGS –Archer FusionPlex sarcoma kit

Figure 1 - 49

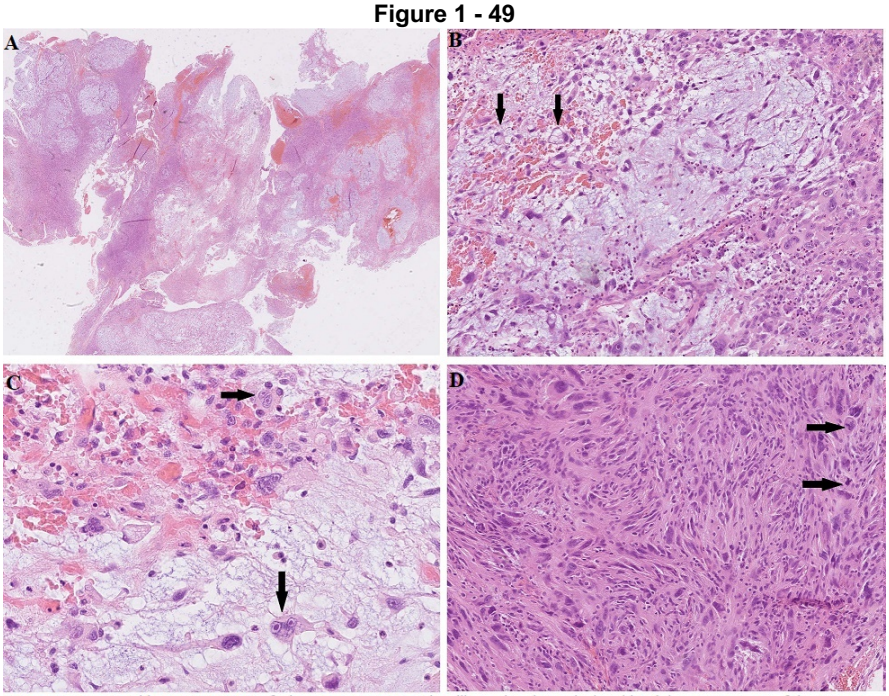

Figure 1. Case 2 with *BRAF-MKLN1* fusion. **A.** Low power view illustrating the typical multinodular arrangement of the tumor with alternating hyalinized and myxoid areas; **B.** The C-MIFS areas exhibited typical MIFS morphology i.e. spindled to epithelioid cells with ample eosinophilic cytoplasm, lipoblast-like cells are seen (arrows). A subpopulation of cells showed enlarged nuclei with mild atypia and prominent virocyte-like nucleoli focally resembling RS-like cells. Admixed inflammatory infiltrate was present. In some areas, the immune cells were engulfed by the neoplastic cells (emperipolesis). The mitotic activity in the C-MIFS area was minimal; **C.** High power view demonstrating typical example of RS-like cells, a multivacuolated lipoblast-like cell is seen in the center of the picture as well; **D.** HG MIFS area exhibited high cellularity, severe atypia of neoplastic cells and increased mitotic activity (arrows).

Figure 2 - 49

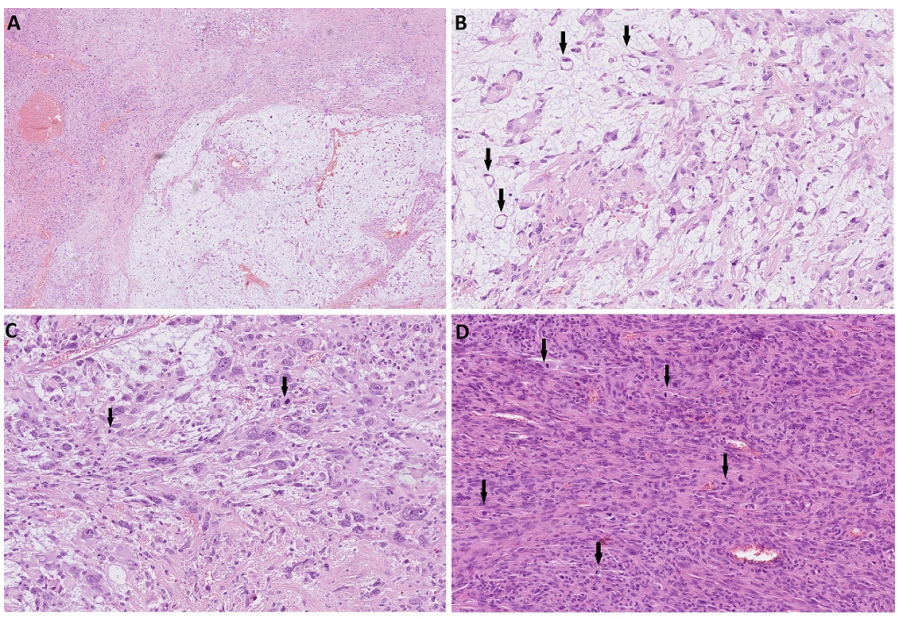

Figure 2. Case 1. A. Low power view showing the transition from C-MIFS area (right) to HG MIFS area (left); **B.** The C-MIFS areas exhibited typical MIFS morphology i.e. spindled to epithelioid cells with ample eosinophilic cytoplasm, lipoblast-like cells are seen (arrows). A subpopulation of cells showed enlarged nuclei with mild atypia and prominent virocyte-like nucleoli. The mitotic activity in the C-MIFS area was minimal; **C.** Transition area exhibiting classical C-MIFS morphology but increased mitotic activity (arrows). Prominent RS-like cells are seen. Admixed inflammatory infiltrate was present. In some areas, the immune cells were engulfed by the neoplastic cells (emperipolesis); **D.** HG MIFS area exhibited high cellularity, severe atypia of neoplastic cells and increased mitotic activity (arrows).

Conclusions: Our IHC and molecular results support the hypothesis that the studied cases are indeed related to C-MIFS. Recognizing HG variant of MIFS may prevent undercalling cases with HG areas but predominantly C-MIFS morphology as low-

grade sarcomas. Moreover, it seems that *BRAF* rearrangements are significantly more common in tumors with HG MIFS morphology than in myxofibrosarcomas. Since they can be potentially targeted by BRAF inhibitors, recognizing such lesions as HG MIFS might help in identifying eligible patients and improving their outcome.

50 Solitary Fibrous Tumor with Pure Round Cell Morphology: Immunohistochemical and Molecular Study of 15 Cases

Michael Michal[1], Konstantinos Linos[2], Natálie Klubíčková[3], Kvetoslava Michalova[1], Elaheh Mosaieby[3], Michal Michal[1], Brian Rubin[4]

[1]Biopticka laborator s.r.o., Plzen, Czech Republic, [2]Dartmouth-Hitchcock Medical Center, Lebanon, NH, [3]Charles University, Faculty of Medicine in Plzen, Plzen, Czech Republic, [4]Cleveland Clinic, Cleveland, OH

Disclosures: Michael Michal: None; Konstantinos Linos: None; Natálie Klubíčková: None; Kvetoslava Michalova: None; Elaheh Mosaieby: None; Michal Michal: None; Brian Rubin: None

Background: SFT is an uncommon fibroblastic tumor composed of a mixture of spindled, ovoid and round cells. The morphological spectrum of SFT is extraordinarily broad. While many uncommon morphologies e.g. lipomatous, myxoid and giant cell angiofibroma patterns are relatively well-known, a pure round cell variant is not widely recognized. In such cases, the IHC workup includes the application of small round cell tumors (SRCT) markers. However, very little is known about their expression in SFT.

Design: 15 SFT cases exhibiting pure round cell morphology were collected. Since a confident diagnosis was impossible on morphological grounds, the molecular detection of *NAB2-STAT6* fusion (PCR or Archer FusionPlex) and/or diffuse strong nuclear STAT6 expression (Abcam, clone YE361) was required. The WHO risk assessment model was used for the assignment of risk groups. A large panel of IHC markers commonly used in the workup of SRCT was applied and the reliability of CD34 expression was investigated as well. 6 cases were also analyzed for secondary molecular aberrations using Archer VariantPlex Solid Tumor kit.

Results: The clinicopathological features are summarized in the Table. Although insufficient data often hampered the exact assignment of the risk group, (at least) intermediate (IR) to high-risk (HR) cases predominated (10/14). All three cases with a follow-up developed distant metastases. All cases retained diffuse STAT6 expression, including 7 cases with molecular confirmation. CD34 expression was often reduced or negative. In keeping with previous studies, BCOR was frequently (5/7 cases) positive. Other recurrently expressed markers were cytokeratins (CKs) CAM5.2/OSCAR/AE1/3 (collectively 5/14), MyoD1 (2/8), Fli-1 (2/3) and CD99 (6/10). Positivity with desmin, synaptophysin, TTF1 and calretinin was observed in individual cases. Apart from BCOR, Fli-1, desmin and (rarely) CKs, which showed diffuse expression, all other markers were only focally positive. Diffuse membranous CD99 expression was not observed. Case 9 harbored mutations of *TP53* and *TERT* promoter, the latter was also detected in case 2.

Case	Age/ sex	Location	Size (cm)	Risk group	NAB2-STAT6 fusion	STAT6	CD 34	CD 99	BCOR	CAM5.2/ OSCAR/ AE1/3	Fli-1	Myo D1	Desmin	Synaptho -physin	TTF1	Calre-tinin	Other negative IHC
1	55/M	Pelvis	NA	IR	+	+++	++	+	-	NA/-/-	NA	-	++	-	-	F	NKX2.2, S100, SOX10, Melan A, INSM1, CD45, CD20
2	71/M	Pelvis	9x8x4	IR	+	+++	+++	NA	NA	NA/-/-	NA	-	-	+	-	-	NKX2.2, S100, SOX10, Melan A, INSM1, CD45, CD20
3	48/M	Cranial base	NA	NA	+	+++	-	F	++	NA/++/-	NA	-	-	-	-	-	NKX2.2, S100, SOX10, Melan A, INSM1, CD45, CD20
4	F/85	Sacral bone	11x6x5	IR	+	+++	+++	F	++	-/NA/-	NA	F	-	-	-	-	NKX2.2, S100, SOX10, Melan A, INSM1, CD45, CD20
5	36/F	Auditory canal	NA	LR	+	+++	F	-	-	NA/-/-	+++	-	-	-	-	-	NKX2.2, S100, SOX10, Melan A, INSM1, CD45, CD20
6	83/M	Pleura	2.5	LR	+	+++	+++	-	+	NA/NA/-	-	-	-	-	-	-	NKX2.2, S100, SOX10, Melan A, INSM1, CD45, CD20
7	73/F	Back	4.9	LR	NA	+++	+	-	+	NA/NA/F	NA	-	-	-	+	-	NKX2.2, S100, SOX10, Melan A, INSM1, CD45, CD20
8	69/F	Thigh	NA	HR	NA	+++	+	-	F	NA/NA/-	NA	+	-	-	-	-	NKX2.2, S100, SOX10, Melan A, INSM1, CD45, CD20
9	61/F	Pineal region	NA	HR	+	+++	+++	NA	NA	NA/NA/NA	NA	NA	NA	NA	NA	NA	S100
10	68/F	Pelvis	NA	At least IR	NA	+++	+++	F	NA	NA/NA/+	NA	NA	-	NA	NA	-	S100
11	78/M	Prepatellar mass	7	IR	NA	+++	+++	NA	NA	+/NA/NA	+++	NA	-	NA	NA	NA	S100
12	64/F	Parotid	NA	At least IR	NA	+++	-	NA	NA	-/NA/-	NA	NA	-	NA	NA	NA	S100, Melan A
13	57/F	Posterior thigh	NA	At least IR	NA	+++	+++	F	NA	NA/NA/+	NA	NA	-	NA	NA	NA	S100
14	68/M	Pelvis	NA	At least IR	NA	+++	+	F	NA	NA/NA/-	-	NA	-	NA	NA	NA	S100, CD45
15	64/F	Thigh	3cm	LR	NA	+++	NA	NA	NA	NA/-/-	NA	NA	NA	NA	NA	NA	S100, SOX10

Legend: NA – not available; LR – low risk; IR – intermediate risk; HR – high risk; F – focal expression; focal = up to 5% of tumor cells positive; + = 6-33%; ++ = 34-66%; +++ = 67-100%

Figure 1 -50

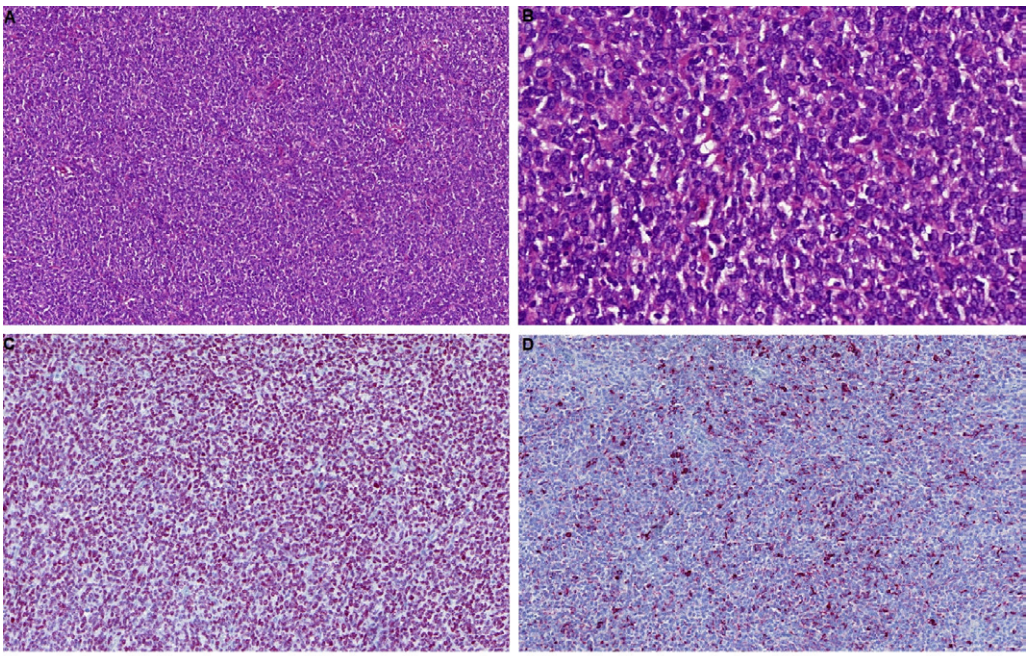

Figure 1. A. and B. Case 1 composed of sheets of uniform small round blue cells. The diagnosis of such SFT cases on morphological grounds is impossible. **C.** Diffuse strong nuclear STAT6 expression in case 1. **D.** Misleading multifocal desmin expression was noted in case 1.

Figure 2 - 50

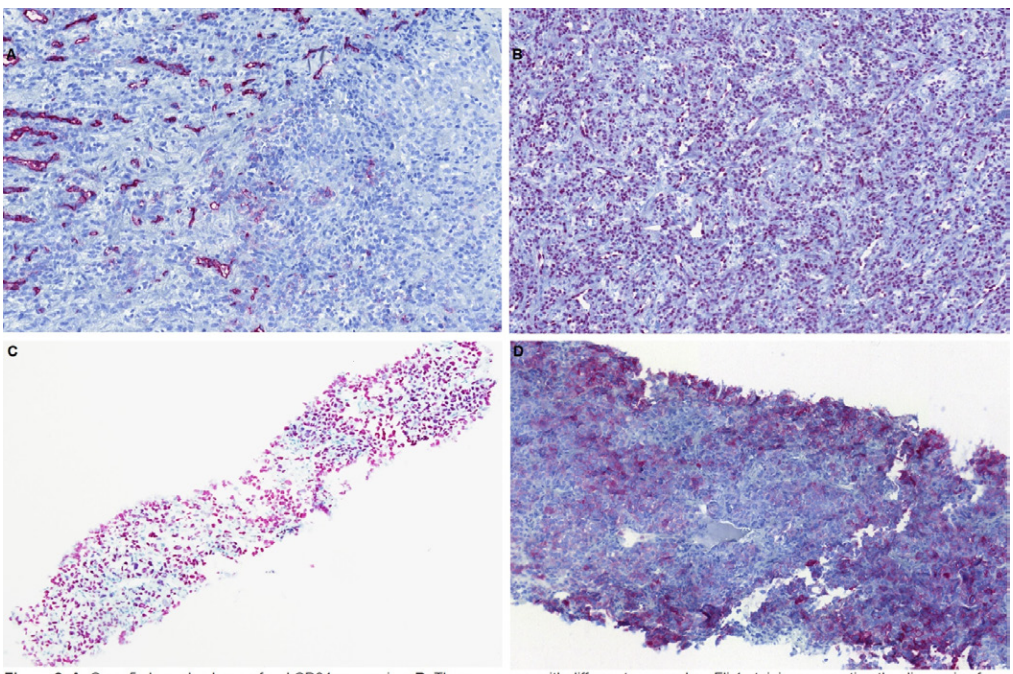

Figure 2. A. Case 5 showed only very focal CD34 expression. **B.** The same case with diffuse strong nuclear Fli-1 staining suggesting the diagnosis of Ewing sarcoma (submitting diagnosis). **C.** Case 3 with strong nuclear BCOR expression. **D.** The same case also showed a prominent OSCAR positivity.

Conclusions: Round cell SFTs often correspond to IR or HR SFT risk groups. Unexpected/aberrant IHC expression is commonly encountered, with frequent BCOR and CK positivity being the most misleading. Since diffuse STAT6 expression is retained, awareness of this uncommon morphological variant of SFT, leading to the appropriate use of STAT6 IHC is the key to proper diagnosis.

51 Ischemic Fasciitis of the Upper Extremity: A Series of 14 Cases Highlighting an Unusual Presentation

Gabriel Oaxaca[1], Steven Billings[2], Jennifer Ko[1]
[1]Cleveland Clinic, Cleveland, OH, [2]Cleveland Clinic, Lerner College of Medicine, Cleveland, OH

Disclosures: Gabriel Oaxaca: None; Steven Billings: None; Jennifer Ko: None

Background: Ischemic fasciitis is a rare pseudosarcomatous fibroblastic/myofibroblastic proliferation thought to arise from ischemia related to sustained or repeated pressure on soft tissues overlying bony protuberances. This lesion is classically associated with elderly immobile or debilitated patients and prototypically arises within the limb girdles and sacral regions. We report a fourteen case series of ischemic fasciitis outside the typical clinical presentation arising in the upper extremity.

Design: Cases of ischemic fasciitis were retrieved from both in-house and consultation files. Cases outside of the upper extremities (arm, elbow, forearm), were excluded. Available patient information was obtained via the medical record.

Results: Fourteen cases were identified from in-house (8) and consultation (6) files. The patients (11M:3F) had a mean age of 59 years (range 23-79). The lesions presented in the arm (2/14; 14%), elbow (5/14; 36%), and forearm (6/14; 43%). One lesion was described as extending from the elbow to the forearm (1/14; 7%). Ischemic fasciitis was not considered as a clinical diagnosis. Two (14%) were originally diagnosed as bursitis, one (7%) as a cyst. Detailed clinical history on three patients revealed: one elderly patient using elbows for stabilization on tables; a lab technician who described possible friction of the elbow; and a resident physician who rested his arms on surfaces doing extended computer work. All cases displayed typical features with central fibrinoid necrosis surrounded by a reactive proliferation of stellate/ganglion fibroblasts/myofibroblasts admixed with inflammatory cells and a reactive vascular proliferation (Figure 1). Additionally, 2/14 (14%) demonstrated prominent myxoid degeneration (Figure 2), and 2/14 (14%) were relatively paucicellular and set in a sclerotic background, consistent with end stage/burned out lesions.

Figure 1 - 51

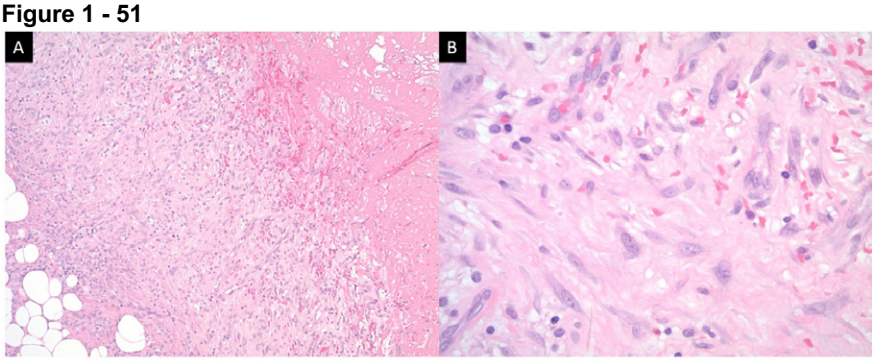

Figure 1: Medium power view demonstrating interface between fibrinoid degeneration and reactive fibroblastic/myofibroblastic proliferation (A), High power view highlighting classic fasciitis features including erythrocyte extravasation, mixed inflammatory infiltrate, and stellate fibroblasts/myofibroblasts (B).

Figure 2 – 51

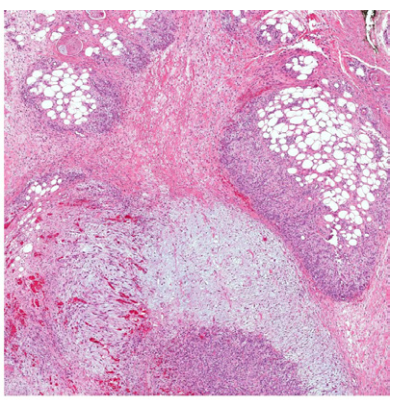

Figure 2: Lower power view demonstrating fibrinoid as well as myxoid degeneration.

Conclusions: Ischemic fasciitis of the upper extremity has a younger mean age than conventional cases. The younger mean age at diagnosis may be related to occupational issues. Recognition of the typical histopathologic features and knowledge that this entity may present outside the expected location may aid in the diagnosis of ischemic fasciitis at non-classical sites.

52 Optimization of a Deep Convolutional Neural Network for Spatial Quantification of Necrosis in Archival Osteosarcoma Cases

Michael Occidental[1], Nicolas Coudray[2], Luis Chiriboga[3], Aristotelis Tsirigos[2], George Jour[3]
[1]NYU Langone Health, New York, NY, [2]New York University School of Medicine, New York, NY, [3]New York University, New York, NY

Disclosures: Michael Occidental: None; Nicolas Coudray: None; Luis Chiriboga: None; Aristotelis Tsirigos: None; George Jour: None

Background: Osteosarcoma (OSA) is a rare primary malignant bone tumor associated with an average 60% 5-year survival rate. Tumor necrosis quantification by human eye has been shown to be a significant prognostic factor for outcome in the neoadjuvant setting. Herein, we aim to test the performance of a deep convoluted neural network (DCNN) in tissue segmentation (viable vs necrotic) as well as quantification of necrosis in archival primary (neoadjuvant setting) and metastatic OSA cases.

Design: Twenty-two (15 male, 8 females; 4 biopsies, 18 excision) cases including 10 metastatic and 10 primary OSA post neoadjuvant chemotherapy. The age of the patients ranged from 8-24 years old at the time of diagnosis (median = 17 years). 103 slides were scanned at 40x magnification using the Aperio AT2 scanner. Manual annotations were done by BST pathologist. Four areas of interest (AOI) were selected: Viable Tumor (VT), Necrotic Tumor (NT), Non-neoplastic Tissue (NNT) and Artifact (A). Google Inception v3 algorithm was deployed. 299 x 299-pixel tiles were generated from AOI at 20x magnification. Three-fold cross validation and subsequent testing was performed per slide and per patient at 42, 200, and 300 epochs until reaching acceptable performance (Figure 1A, B). Receiver operating characteristic (ROC) analysis was performed. Necrosis quantification was performed using the ratio NT/(NT+VT). Pearson correlation was used for correlation of human versus machine necrosis ratio calculation ($p<0.01$).

Results: Acceptable performance was reached at 200 epochs/cutoff ~150,000 iterations (Figure 1B-F). Automated segmentation of AOI by DCNN after training by patient and by slide showed micro AUC = 0.92 and 0.96 and a macro AUC = 0.92 and 0.95, respectively (Table 1). Performance was maintained across both primary and metastatic specimens for all 4 AOI's (Table 1). Necrosis quantification showed excellent correlation between DCNN and pathologist generated percent necrosis per slide and per patient ($R2=0.97$, $p=2.16E-22$ and $R2=0.99$, $p=1.46E-12$, respectively).

	Per Patient:				Per Slide:	
	42 epochs		300 epochs		200 epochs	
	Area Under the Curve (AUC)	Standard deviation (SD)	AUC	SD	AUC	SD
Macro average	0.920	0.029	0.921	0.024	0.953	0.011
Micro average	0.937	0.019	0.935	0.250	0.967	0.008
Viable Tumor	0.899	0.068	0.917	0.044	0.969	0.008
Necrotic Tumor	0.940	0.030	0.934	0.033	0.964	0.013
Normal Tissue	0.921	0.032	0.920	0.035	0.967	0.004
Artifacts	0.918	0.023	0.913	0.035	0.911	0.036

Figure 1 - 52

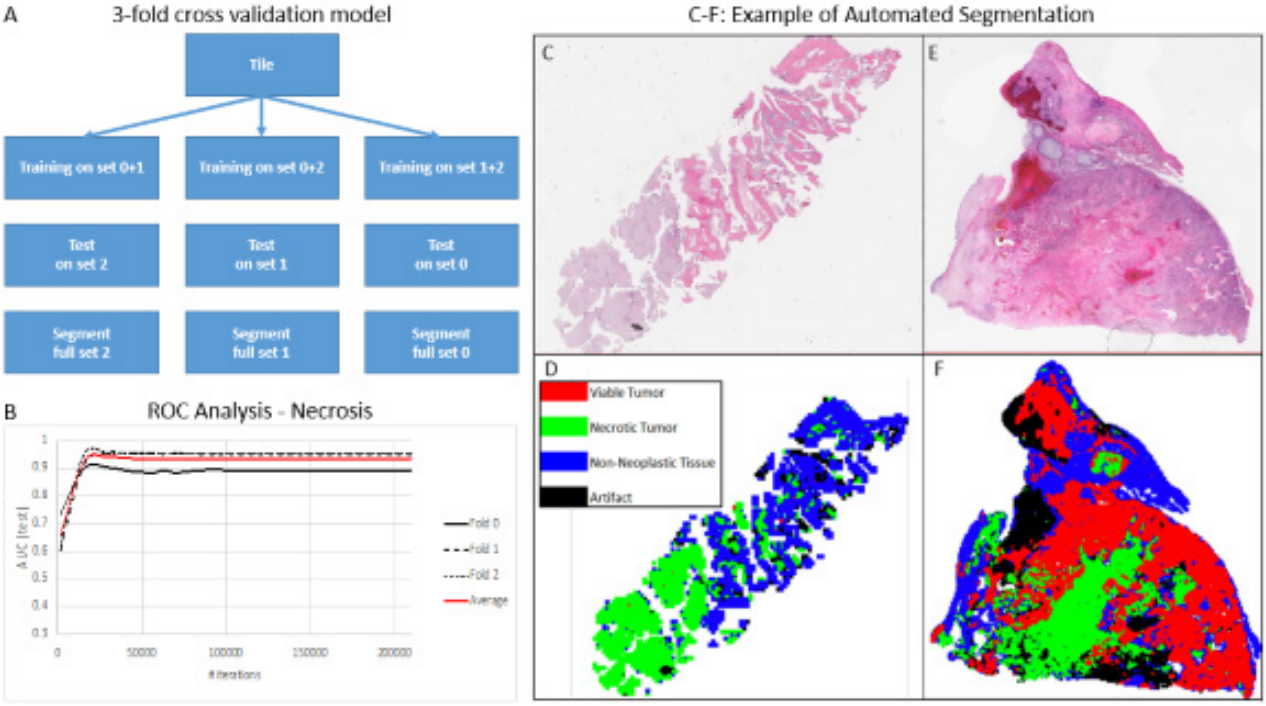

Conclusions: DCNN shows excellent performance in accurate automated tissue segmentation and quantification of necrosis in both primary and metastatic OSA**.** Validation of this optimized tool on a larger cohort and additional correlative analysis with outcome is underway in neoadjuvant setting in primary OSA cases.

53 Primary Clear Cell Sarcoma of Bone: Clinicopathological Study of a Rare Presentation

Igor Odintsov[1], Jyothi Jagannathan[2], G. Pétur Nielsen[3], Jason Hornick[4]
[1]Brigham and Women's Hospital, Boston, MA, [2]Brigham and Women's Hospital, Dana-Farber Cancer Institute, Harvard Medical School, Boston, MA, [3]Massachusetts General Hospital, Harvard Medical School, Boston, MA, [4]Brigham and Women's Hospital, Harvard Medical School, Boston, MA

Disclosures: Igor Odintsov: None; Jyothi Jagannathan: None; G. Pétur Nielsen: None; Jason Hornick: *Consultant*, Aadi Biosciences, TRACON Pharmaceuticals

Background: Clear cell sarcoma is an uncommon malignant mesenchymal neoplasm of young adults with a predilection for tendons and aponeuroses of distal extremities, a distinctive nested growth pattern, melanocytic differentiation, and usually an *EWSR1-ATF1* fusion. Rare cases of primary bone clear cell sarcoma (PB-CCS) have been reported. The purpose of this study was to evaluate the clinicopathological features of a series of PB-CCS.

Design: PB-CCS cases were retrieved from consult and surgical files. Immunohistochemical and molecular analyses were performed, and clinical and pathologic features were evaluated. Clinical follow-up information was obtained from medical records.

Results: Three cases of PB-CCS (2 consults and one in-house) were identified out of 109 CCS diagnosed between 2010 - 2021. Two patients were female, and one patient was male; ages were 19, 21, and 47 yrs. Two tumors arose in the long bones of the lower extremities (femur, fibula). One tumor involved the sacrum and pre-sacral soft tissue (favored to represent a bone primary). One tumor also involved regional lymph nodes at presentation. All tumors except one showed characteristic histologic features, in the form of nests and fascicles of uniform epithelioid to spindle cells with prominent nucleoli and pale eosinophilic to clear cytoplasm; one tumor showed unusual focal pleomorphism and more notable nuclear atypia. By immunohistochemistry, HMB-45 was positive in 2/3 cases, S100 in 2/3 cases, MiTF in 1/1, and SOX10 in 1/1. All cases were confirmed to harbor *EWSR1* rearrangement; in 2 cases, *EWSR1-ATF1* fusion was documented. Clinical follow up was available in 2 cases. Both patients died of disease, 5 years and 21 months after diagnosis. The third case was recently reviewed.

#	Age	Sex	Site	Immunohistochemistry	Molecular tests	Follow up
1	21	F	Right sacrum	Positive – S100, vimentin Negative – keratin, desmin, SMA, Melan-A, E-Cadherin, tyrosinase, CD56, HMB-45, EMA	FISH For EWSR1 rearrangement	DOD 5 years
2	19	F	Right femur	Positive - S100, HMB-45, CD117	FISH for EWSR1 rearrangement, t(12:22)	DOD 21 months
3	47	M	Right fibula	Positive - SOX10, MITF, HMB-45 Negative - S100	By report, genetic studies showed an EWSR1-ATF1 fusion.	AWD 4 months

Conclusions: CSS rarely presents in the skeleton. At such locations, distinction from metastatic melanoma is particularly challenging. Clinical and pathologic features are similar to conventional CCS of deep soft tissue. PB-CSS may pursue an aggressive clinical course.

54 RNA Sequencing Analysis of Non-Uterine Leiomyosarcomas for Outcome Risk Prediction

Makiko Ogawa[1], Atsushi Tanaka[1], Kei Namba[1], Narasimhan Agaram[1], Michael Roehrl[1]
[1]Memorial Sloan Kettering Cancer Center, New York, NY

Disclosures: Makiko Ogawa: None; Atsushi Tanaka: None; Kei Namba: None; Narasimhan Agaram: None; Michael Roehrl: None

Background: Non-uterine high-grade leiomyosarcomas (LMS) are rare but frequently lethal neoplasms. LMS often exhibit aggressive behavior, recur locally, and some metastasize to other organs. Thus, better understanding tumor biology and developing novel therapies for LMS are needed to predict individual risk, to tailor treatment, and to improve clinical outcomes. In this study, we sought to use mRNA sequencing to explore differentially expressed genes that may play a role in driving aggressiveness and metastatic propensity of LMS.

Design: We selected 20 LMS cases, including 10 low-risk cases (disease-free survival (DFS) of more than 5 years) and 10 high-risk cases (DFS less than 3 years) that were all histologically high-grade and not distinguishable. Total RNA was extracted from frozen tissues and subjected to deep mRNA sequencing. Differential expression analyses and gene pathway enrichment analyses were performed.

Results: After processing RNA-Seq data, about 18,000 gene transcripts were quantified. Comparing high-risk cases to low-risk cases, we discovered 90 differentially expressed genes, 64 up-regulated genes and 26 down-regulated genes. In upstream regulator analyses, several inflammation-associated genes are associated with high-risk LMS, such as TNF, IL1, IL6, and IFN gamma. In canonical pathway analyses, inflammatory pathways such as tumor microenvironment pathway, IL17 signaling, TREM1 signaling, and HIF1 alpha signaling are also found up-regulated in high-risk tumors.

Conclusions: Our study identified differentially expressed genes and pathways that may drive aggressiveness and metastatic propensity of non-uterine high-grade LMS. We are currently correlating our RNA-Seq differences with measurement at deep proteomic level to construct a multiomic outcome risk prediction model for LMS that can help guide adjuvant therapy decisions for LMS patients after surgery.

55 CD30 Expression in Proximal-type Epithelioid Sarcoma

Chinelo Onyenekwu[1], Reena Singh[2]
[1]Medical College of Wisconsin, Milwaukee, WI, [2]Medical College of Wisconsin Affiliated Hospitals, Milwaukee, WI

Disclosures: Chinelo Onyenekwu: None; Reena Singh: None

Background: Proximal-type Epithelioid Sarcoma (PES) is a rare, clinically aggressive sarcoma characterized by positive keratin and absent INI-1 expression. The recent approval of tazemetostat, an oral EZH2 inhibitor, has added to the limited therapeutic

options of surgery and radiation. CD30 expression is commonly seen in lymphomas and embryonal carcinoma, and less commonly in solid malignancies. Brentuximab vedotin is an antibody drug conjugate approved for the treatment of classical Hodgkin lymphoma and CD30-expressing T-cell lymphomas. In addition to clinical trials for solid tumors, there are reports of treatment of angiosarcoma and inflammatory myofibroblastic tumor with brentuximab. The aim of this study was to evaluate CD30 expression in ES as a potential therapeutic target.

Design: Immunohistochemistry (IHC) was performed using a mouse monoclonal anti-CD30 antibody on 20 confirmed PES cases (positive keratin expression, loss of INI-1, appropriate clinical and tumor characteristics). Membranous staining in >5% of cells was considered positive.

Results: Twenty cases from 14 patients (9 males, 5 females) were evaluated. Five patients had primary and metastatic material available, while the remainder had material from the primary lesion only. By IHC, 2 of 20 (10%) cases, representing primary and metastatic lesions from one patient, were diffusely positive (>90% of tumor cells) for CD30 (Figure 1A-B). IHC for CD45, TIA1 and ALK were negative in the CD30-positive cases.

Figure 1 - 55

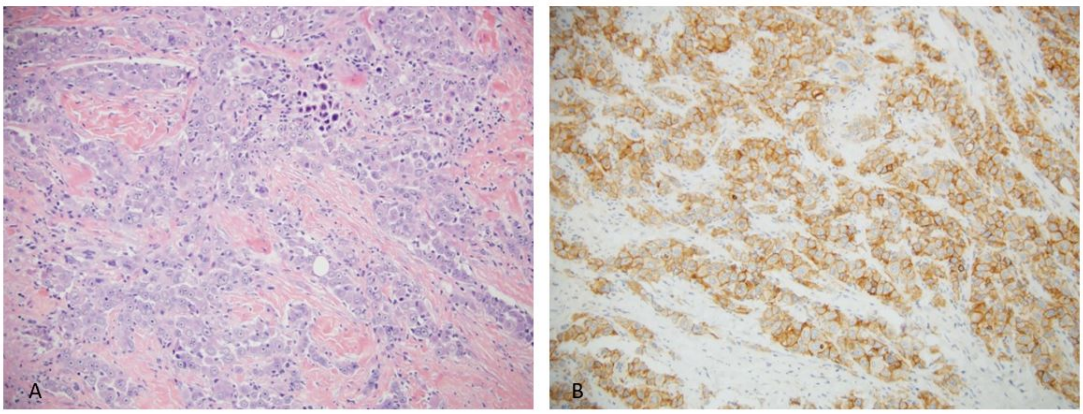

Hematoxylin and eosin-stained section of PES at 200X (A). CD30 IHC performed on the same case at 200X (B). PES: Proximal-type Epithelioid Sarcoma

Conclusions: CD30 expression appears to be a rare event in PES. More investigation is needed to determine use of anti-CD30 therapy in PES and CD30 expression in the classical variant of epithelioid sarcoma.

56 Mesenchymal Neoplasms of the Tongue: A Clinicopathologic Study of 52 Cases

Domenika Ortiz Requena[1], Jaylou Velez Torres[2], Julio Diaz-Perez[2], Laurence Briski[3], Elizabeth Montgomery[2], Andrew Rosenberg[3]

[1]University of Miami Miller School of Medicine/Jackson Memorial Hospital, Miami, FL, [2]University of Miami Miller School of Medicine, Miami, FL, [3]University of Miami Health System, Miami, FL

Disclosures: Domenika Ortiz Requena: None; Jaylou Velez Torres: None; Julio Diaz-Perez: None; Laurence Briski: None; Elizabeth Montgomery: None; Andrew Rosenberg: None

Background: Neoplasms of the tongue are relatively common, and the vast majority are epithelial in phenotype. Although uncommon, a diverse array of mesenchymal neoplasms (MN) may arise in this anatomic site. To increase our understanding of these lesions, we review our experience, the largest reported to date, of MNs of the tongue and describe their clinicopathologic features.

Design: The pathology archives from 2013-2021 and the consultation files of one of the authors, were queried for all MNs of the tongue. We reviewed their histologic slides and ancillary studies and obtained the clinical data from the medical records.

Results: We identified 52 lesions from 29 men and 23 women (M:F = 1.26:1) with a mean age of 53 years (range, 1-94 years). Forty-six tumors were in the oral tongue, and 6 were in the base of the tongue. There were 41 benign tumors: 15

hemangiomas (29%), 7 granular cell tumors (13%), 4 lobular capillary hemangiomas (8%), 3 schwannomas (6%), 4 lipomas (8%), 2 chondromas (4%), 2 myofibromas (4%), 1 solitary circumscribed neuroma (2%), 1 ectomesenchymal chondromyxoid tumor (2%), 1 lymphangioma (2%), and 1 perineurioma (2%). There were 6 sarcomas: 1 Kaposi sarcoma (2%), 1 alveolar soft part sarcoma (2%), 1 leiomyosarcoma (2%), 1 malignant rhabdoid tumor (2%), 1 spindle cell rhabdomyosarcoma with a *EP300-VGLL* fusion (2%), and 1 undifferentiated pleomorphic sarcoma (2%). In addition, there were 4 solitary fibrous tumors (8%)—all with low risk of progression based on risk stratification criteria—and 1 atypical glomus tumor (2%) with a *NOTCH2* rearrangement and *TLL2* mutation. Forty-three patients underwent surgical excision, and 1 patient (with hemangioma) underwent embolization. The patient with spindle cell rhabdomyosarcoma developed postoperative numbness at the surgical site and was disease free through 17 months of follow-up. The patient with leiomyosarcoma declined adjuvant radiation and developed metastasis to the lung at 22 months. The patient with alveolar soft part sarcoma had metastases to the lung at the time of diagnosis and received adjuvant chemotherapy. The remaining 24 patients (with follow-up data ranging from 0.3-48 months) had no local or distant recurrence.

Conclusions: MNs of the tongue are uncommon. Most are benign and are usually characterized by either endothelial, adipocytic, or schwannian differentiation. The mainstay of treatment is surgical excision with extent of excision determined by tumor type. Adjuvant therapy is reserved for high-grade sarcomas.

57 Epithelioid and Spindle Cell Hemangioma: A Clinicopathologic Series of 16 Primary Bone and Soft Tissue Tumors Highlighting a Predilection for the Hands and Feet, Frequent Multicentricity, and Indolent Behavior

David Papke[1], Jyothi Jagannathan[2], Brendan Dickson[3], Christopher Fletcher[1]
[1]Brigham and Women's Hospital, Boston, MA, [2]Brigham and Women's Hospital, Dana-Farber Cancer Institute, Harvard Medical School, Boston, MA, [3]Mount Sinai Health System, Toronto, Canada

Disclosures: David Papke: None; Jyothi Jagannathan: None; Brendan Dickson: None; Christopher Fletcher: None

Background: Epithelioid and spindle cell hemangioma (ESCH) was initially described in 1999 in a series of primary bone tumors. Its pathogenesis and relationship to other vascular neoplasms remain poorly understood.

Design: 16 cases from the consultation and institutional archives of one of the authors were studied to determine the clinicopathologic characteristics of ESCH. Next-generation RNA sequencing is being performed on 7 tumors.

Results: Eight patients (50%) were male. Age at presentation ranged from 20-78 years (median: 38.5 y). Seven patients (44%) had tumor(s) limited to bone, six (38%) had tumor(s) limited to soft tissue, two (12%) had unifocal elbow tumors involving bone and soft tissue, and one had multiple soft tissue and bone tumors. Six patients (38%) had multiple tumors, all in a unilateral anatomic region in the wrist, hand, ankle, or foot. For the 10 patients with unifocal disease, tumor sites were: soft tissue of the hand (3 tumors), bones of the feet (2), soft tissue of the forearm (2), elbow (2) and vertebra (1). In imaging studies, primary bone tumors were lobulated, expansile and lytic. Five tumors demonstrated cortical breakthrough. Tumor size ranged from 0.8–7.2 cm (median: 1.7 cm).

ESCH is composed of lobules of epithelioid and spindled endothelial cells with bland, vesicular nuclei. Neoplastic cells showed orderly vasoformative growth, with hemorrhagic stroma and no atypia or multilayering. In bone, the lobules infiltrated between trabeculae; soft tissue tumors were circumscribed. Immunohistochemistry demonstrated positivity for CD31 (12/12 tumors) and ERG (4/4). When positive, SMA highlighted orderly vasoformative architecture (11/13 tumors). FOSB was diffusely positive in one of 14 tumors (7%) and showed focal staining in two.

Clinical follow up was available for 11 patients so far (69%; range: 5 mo-11 y; median: 3.5 y). Seven had no evidence of disease. Six tumors (55%) recurred locally, four within a year, one at 2.4 years, and one thrice at 2, 3 and 5 years. Three patients were alive with multifocal, stable bone tumors (at 3.9, 4.5, and 6 y). No tumors metastasized.

Conclusions: ESCH is a benign vascular neoplasm with a predilection for hands and feet and frequent multicentricity. Although ESCH and epithelioid hemangioma behave similarly, the difference in FOSB positivity rates suggests that they are probably distinct. Given that most recurrences and primary tumors behaved indolently, watchful waiting would be reasonable for patients with multicentric disease.

58 GLI1 Expression in Soft Tissue Tumors with GLI1 Rearrangements or Amplification

Paige Parrack[1], Adrián Mariño Enríquez[1], Christopher Fletcher[1], Jason Hornick[2], David Papke[1]
[1]Brigham and Women's Hospital, Boston, MA, [2]Brigham and Women's Hospital, Harvard Medical School, Boston, MA

Disclosures: Paige Parrack: None; Adrián Mariño Enríquez: None; Christopher Fletcher: None; Jason Hornick: *Consultant*, Aadi Biosciences; *Consultant*, TRACON Pharmaceuticals; David Papke: None

Background: *GLI1* alterations occur in several tumor types, including pericytoma with t(7;12), gastroblastoma, and an emerging class of nested *GLI1*-rearranged or amplified mesenchymal neoplasms (GLIMN). These tumor types have non-specific immunophenotypes, making diagnosis difficult without molecular studies. GLI1 immunohistochemistry (IHC) is sensitive for gastroblastoma, but its utility in distinguishing nested GLIMN and other neoplasms with *GLI1* rearrangements from morphologic mimics is unknown.

Design: GLI1 IHC was performed using a mouse monoclonal antibody (clone C-1, 1:600 dilution) on 104 tumors, including: 1) a "*test cohort*" of 23 tumors, including 10 nested GLIMN (7 with confirmed *GLI1* alterations), 10 pericytomas with t(7;12), 2 gastroblastomas, and 1 *GLI1*-rearranged myoepithelial carcinoma (MEC); 2) an "*NGS cohort*" of 7 other tumors with *GLI1* amplification detected by NGS, including 3 dedifferentiated liposarcomas (DDLPS), 1 leiomyosarcoma, 1 alveolar rhabdomyosarcoma, 1 intimal sarcoma, 1 osteosarcoma; and 3) a "*control cohort*" of 10 DDLPS with unknown *GLI1* amplification status and 64 morphologic mimics, including 10 paragangliomas, 5 solitary fibrous tumors, 5 Ewing sarcomas, 5 *BCOR*-rearranged sarcomas, 5 myoepitheliomas, 5 myopericytomas, 5 glomus tumors, 5 atypical carcinoids, 4 epithelioid schwannomas, and 15 GIST (5 *PDGFRA*-mutant, 5 SDH-deficient, 5 *KIT*-mutant). The positive staining threshold was set to >5% of neoplastic cells at moderate staining intensity.

Results: GLI1 IHC was positive in 17/23 test cohort tumors (73.9%) [7/10 nested GLIMN, 8/10 pericytomas with t(7;12), 1/2 gastroblastomas, and 1/1 MEC] and in 3/7 NGS cohort tumors. Consistent with its reported rate of *GLI1* amplification, 1/10 control cohort DDLPS was positive. GLI1 IHC was positive in only 2/64 (3.1%) mimics (1 Ewing sarcoma and 1 *BCOR*-rearranged sarcoma). The staining pattern of GLI1 was nuclear and cytoplasmic in 18 cases and only nuclear in 5. IHC on archival sections >5 years old often showed limited or no staining; restricting analysis to sections <5 years old, GLI1 IHC was 86.7% sensitive and 96.9% specific for test cohort tumors, with expression in 6/6 nested GLIMN, 5/7 pericytomas with t(7;12), 1/1 gastroblastoma, and 1/1 MEC.

Conclusions: GLI1 IHC is moderately sensitive and highly specific among test cohort tumors. Given its specificity, in the context of appropriate tumor morphology, GLI1 IHC may be a useful diagnostic adjunct for these rare tumor types.

59 Novel Genomic Aberrations in Lymphatic Anomalies

Thuy Phung[1], Yulong Fu[2], Joyce Lee[3], Alex Hastie[3], Hayk Barseghyan[2]
[1]University of South Alabama, Mobile, TX, [2]Children's National Medical Center, Washington, DC, [3]San Diego, CA

Disclosures: Thuy Phung: None; Yulong Fu: None; Joyce Lee: None; Alex Hastie: None; Hayk Barseghyan: None

Background: Lymphatic anomalies are a type of developmental vascular anomalies characterized by the presence of abnormally-formed lymphatic vessels within internal organs and soft tissues that can lead to impaired lymphatic function and high morbidity. Little is known about the molecular basis of these diseases. To gain further insights into the genomic landscape of lymphatic anomalies, we performed optical genome mapping (OGM) of human lymphatic anomaly cell lines. OGM is a technique for constructing genome-wide high-resolution maps of labeled long DNA molecules to reveal genomic structural variations.

Design: We established primary endothelial cell lines from patient-derived lymphatic anomaly tissues using immunoaffinity purification with anti-CD-31-antibody to select for endothelial cells. The cells were analyzed by OGM using Bionano Saphyr system. Genomic DNA (gDNA) was isolated from 1.5 million freshly cultured cells per sample using Bionano Prep SP Kit, and labeled 750 ng gDNA using Bionano DLS labeling chemistry followed by counterstaining of the DNA backbone. Labeled whole genomic DNA was analyzed in Saphyr scanner. Bioinformatics algorithms convert images into molecules, and assembly algorithms align molecules to construct consensus genome maps. Data collection consisted of 1,350 Gb of molecules that were >150 Kb in length with effective coverage of 335X and 80% percent of molecules aligned to reference human genome hg38.

Results: We successfully purified endothelial cells from lymphatic anomaly tissues with >99% purity. The cells showed lymphatic differentiation as determined by stains for lymphatic endothelial markers CD31 and Prox-1. Analysis by OGM revealed a number of

chromosomal aberrations found in lesional cells and not in Bionano Database of normal cells, and these include 4 insertions, 14 deletions, 3 inversion breakpoints and 1 duplication. Further analysis of these structural variants showed a 7.4-Kb deletion in *PIN4* gene locus. We confirmed this deletion by long-range PCR. Transcriptomic profiling of lymphatic anomaly cells by RNASeq revealed reduction in mRNA expression levels of *PIN4* in these cells as compared with known expression levels in normal tissues in Genotype-Tissue Expression database.

Conclusions: We have uncovered novel genomic aberrations in lymphatic anomalies using OGM, including a novel deletion in *PIN4* gene locus. Future studies are aimed to determine the biological significance of *PIN4* in the pathogenesis of lymphatic anomalies.

60 Novel Genomic Structural Variations in Angiosarcomas

Thuy Phung[1], Joyce Lee[2], Alex Hastie[2], Hayk Barseghyan[3]
[1]University of South Alabama, Mobile, TX, [2]San Diego, CA, [3]Children's National Medical Center, Washington, DC

Disclosures: Thuy Phung: None; Joyce Lee: *Employee*, Bionano Genomics, Inc.; *Stock Ownership*, Bionano Genomics, Inc.; Alex Hastie: None; Hayk Barseghyan: None

Background: Angiosarcomas are malignant vascular tumors with a number of known molecular aberrations, such as c-Myc gene amplification, and PTPRB and PLCG1 mutations. Most known molecular aberrations in angiosarcomas have been identified by standard technologies, such as FISH and next generation sequencing (NGS). However, potentially significant large genomic aberrations, such as gene fusion, large amplification and deletions, may not be detectable by NGS. To gain further insights into the genomic landscape of angiosarcomas, we performed optical genome mapping (OGM) of primary human angiosarcoma cell lines. OGM is a technique for constructing genome-wide high-resolution maps of labeled long DNA molecules to reveal genomic structural variations.

Design: Three primary human angiosarcoma cell lines (HAMON, ASM5 and MO-LAS-B) were cultured and harvested for genomic DNA isolation. 1.5 million cells were used for each sample run. High quality intact genomic DNA was prepared using BionanoPrep SP Kit. DNA was purified using Nanobind disk, followed by DNA homogenization and subsequent labeling of DNA with DLE-1 dye. Labeled whole genomic DNA was analyzed in Bionano Saphyr scanner, and bioinformatics algorithms convert images into molecules, and assembly algorithms align molecules to construct consensus genome maps.

Results: OGM analysis of angiosarcoma cells revealed multiple unique structural aberrations, including large insertions, deletions, inversion breakpoints, duplications, inter-chromosomal translocation and intra-chromosomal translocation. Further analysis showed the following findings: 354-Kb deletion in *Plexin D1* gene locus that regulates the migration of endothelial cells and is required for normal development of the heart and vasculature; reciprocal t(4;9) translocation in *UGT8* (UDP Glycosyltransferase 8) gene locus that is involved in biosynthesis of galactocerebrosidase; reciprocal t(6;22) translocation involving *HIRA* (Histone Cell Cycle Regulator) and *EYS (*Eyes Shut Homolog) gene loci; and 14 Mb inversion interrupting RYR2 (Ryanodine Receptor 2) and TAF1A (TATA-Box Binding Protein Associated Factor) gene loci.

Conclusions: These findings demonstrate the utility of optical genome mapping as a tool to uncover large genomic structural variations to better understand the molecular pathogenesis of malignant vascular tumors. Future studies are aimed to determine the biological significance of these structural variations in angiosarcomas.

61 Periosteal Chondrosarcoma: A Monocentric Retrospective Analysis of 54 Patients with Idh1/2 Mutational Analysis

Alberto Righi[1], Marina Pacheco[2], Lucia Barra[1], Marco Gambarotti[1], Marta Sbaraglia[3], Sofia Asioli[4], Stefania Cocchi[1], Stefania Benini[5], Angelo Dei Tos[6]
[1]IRCCS Istituto Ortopedico Rizzoli, Bologna, Italy, [2]Gamboa, Panama, [3]Azienda Ospedaliera Padova, Italy, [4]University of Bologna, Bologna, Italy, [5]Instituto Ortopedico Rizzoli di Bologna, Bologna, Italy, [6]University of Padua, Padua, Italy

Disclosures: Alberto Righi: None; Marina Pacheco: None; Lucia Barra: None; Marco Gambarotti: None; Marta Sbaraglia: None; Sofia Asioli: None; Stefania Cocchi: None; Stefania Benini: None; Angelo Dei Tos: None

Background: Periosteal chondrosarcoma is a rare cartilaginous neoplasm that arises on the surface of bone and, by definition, invades the underlying cortex and/or measures more than 5 cm. To date, only small series of this rare entity have been published and in a handful of cases, *IDH1* Arg132 somatic mutations have been shown to be present.

Design: We describe the clinicopathologic features of primary periosteal chondrosarcoma, determine the potential impact on survival and perform molecular screening of *IDH1* and *IDH2* gene mutations.

Results: Our series includes 55 cases of periosteal chondrosarcoma. Age ranged from 16 to 77 years (median, 37) with a male prevalence (62%). Forty-three cases involved the long bones of the extremities; of these 19 cases arose in the femur, 18 in the humerus and 6 in the tibia. The majority (91%) of tumors involving the long bone were metaphyseal. Twelve tumors occurred in flat bones, vertebrae and small tubular bones of feet. All but 7 cases were surgically removed with adequate margins. Macroscopically, tumor size ranged from 3.5 to 18 cm. Eleven cases measured less than 5 cm. Applying the WHO grading system for central chondrosarcomas, 23 (42%) were grade 1; 27 (49 %), grade 2; three (5 %), grade 3 and two (4%) presented areas of dedifferentiation. Soft tissue infiltration was present in 21/48 cases (43%). Involvement of medullary canal was seen in 12/45 cases (27%) of cases. Mutational analysis was feasible in 32 cases, in 9 of which (28%) heterozygous mutations in codon 132 of *IDH1* gene were detected. No *IDH2* mutations were found. During follow-up (median: 137 months), 4 patients had local recurrences at intervals ranging from 1 to 84 months. Six patients developed metastasis to the lungs within 5 to 158 months of surgical treatment. At last follow-up, all 6 patients that developed lung metastasis died of disease, two patients died of unrelated causes, and the remaining 46 patients were alive without disease. OS and DFS was not found to be statistically associated with gender, location of tumor, tumor size, type of surgical margins, histologic grade, medullary/soft tissue infiltration or *IDH1* gene status.

Conclusions: 1. periosteal chondrosarcoma exhibits a clinical behaviour that overalls with grade 1 and 2 central chondrosarcoma. 2. Somatic heterozygous mutations of codon 132 of *IDH1*, are present in one third of periosteal chondrosarcomas. 3. Neither clinicopathological parameters nor the status of *IDH1* Arg132 seem to be predictors of outcome.

62 Ultra-rare Undifferentiated Round Cells Sarcoma Prevalence and Survival After Genomic Classification

Alberto Righi[1], Marco Gambarotti[1], Emanuela Palmerini[1], Margherita Maioli[1], Stefania Cocchi[1], Giovanna Magagnoli[1], Stefania Benini[2], Elisa Carretta[1], Tommaso Frisoni[1], Marta Sbaraglia[3], Angelo Dei Tos[4]
[1]IRCCS Istituto Ortopedico Rizzoli, Bologna, Italy, [2]Instituto Ortopedico Rizzoli di Bologna, Bologna, Italy, [3]Azienda Ospedaliera Padova, Italy, [4]University of Padua, Padua, Italy

Disclosures: Alberto Righi: None; Marco Gambarotti: None; Emanuela Palmerini: None; Margherita Maioli: None; Stefania Cocchi: None; Giovanna Magagnoli: None; Stefania Benini: None; Elisa Carretta: None; Tommaso Frisoni: None; Marta Sbaraglia: None; Angelo Dei Tos: None

Background: Over the last decade, the category of undifferentiated round cell sarcomas (URCS -defined by the absence of Ewing sarcoma-associated translocations), has emerged. Among this group of ultra-rare tumors, the two relatively most frequent new entities are represented by CIC and BCOR- rearranged sarcomas.

Design: In order to understand the prevalence and the prognosis of these ultra-rare tumors, we retrieved all cases of Ewing sarcoma and other URCS diagnosed at the Rizzoli Orthopaedic Institute between 1920 and 2020. All URCS with available material were analyzed with fluorescence in-situ hybridization (FISH), and reverse transcription quantitative polymerase chain reaction (RT-qPCR) in order to identify cases of CIC-rearranged and BCOR- rearranged sarcoma. Negative cases were further analyzed with the Archer FusionPlex Sarcoma Panel. Survival was analyzed in patients with available follow-up.

Results: Our series include 1994 cases. Twenty cases negative for Ewing sarcoma translocations lacked material for further genetic analysis and were excluded from the present study. This left 1974 cases, which were classified as follows: 1925 as Ewing sarcomas (97.50%), 25 as CIC-rearranged sarcomas (1.25%), 16 as *BCOR-CCNB3* rearranged sarcomas (0.80%), one each as CIC-*LEUTX, EWSR1-NFATC2, FUS-NFATC2* rearranged sarcoma (0.05% each), and 5 as unclassified URCS (0.30%). Microscopically non-Ewing sarcomas exhibited morphological variation including variable round, epithelioid and spindle cell morphology. In stark contrast with Ewing sarcoma only 4/43 (9.3%) of non-Ewing sarcomas (2 *CIC*-rearranged sarcomas, 1 *BCOR-CCNB3* sarcoma, and 1 URCS), featured diffuse expression of CD99. In 41 cases with available follow-up (22 CIC-rearranged, 11 *BCOR-CCNB3* rearranged, *1 FUS-NFATC2, 1 CIC-LEUTX*, and 5 unclassified URCS) the 3-years overall survival (OS) was 32.7% in *CIC*-rearranged sarcomas, 81.8% in BCOR-CCNB3 sarcomas, and 60% in URCS (p 0.057), while in the literature Ewing sarcoma shows a 65-70% cure rate for localized disease and a 5-year survival rate of <30% for metastatic and early-relapsing cases. The patient with *CIC-LEUTX* sarcoma died 13 months from diagnosis, and the patient with *FUS-NFATC2* was alive without disease at 8 years from onset.

Conclusions: Undifferentiated round cell sarcoma can be further characterized by a combination of morphologic observation ad molecular techniques, which is also helpful in differentiating them from Ewing sarcoma. The survival difference among different entities underscores the need of their accurate subclassification.

63 Does MDM2 Amplification Ratio Relate with Dedifferentiation and Predict Prognosis in Well differentiated/Dedifferentiated Liposarcomas?

Ariannette Robledo Gomez[1], Shefali Chopra[2]
[1]Keck Hospital of USC, LAC+USC Medical Center, Los Angeles, CA, [2]Keck School of Medicine of USC, Los Angeles, CA

Disclosures: Ariannette Robledo Gomez: None; Shefali Chopra: None

Background: The assessment of MDM2 gene amplification ratio (AR) by fluorescence *in situ* hybridization (FISH) is used for diagnosing well differentiated liposarcoma (WDLPS) and dedifferentiated liposarcoma (DDLPS). Dedifferentiated liposarcomas carry risk of metastatic disease and may benefit from neoadjuvant therapy. This study was undertaken to evaluate if there is a significant difference in amplification factor in dedifferentiated and well dedifferentiated liposarcoma and whether it can be added to the diagnostic algorithm to help identify patients on core biopsies which might benefit from neoadjuvant chemotherapy.

Design: All resection cases from 2017 to present diagnosed as well differentiated (WDLPS), cellular well differentiated / low grade dedifferentiated (LGDDLPS) liposarcomas or dedifferentiated liposarcomas (DDLPS) with MDM2 amplification were retrieved from pathology search database of our institution after IRB approval.

Results: 77 total liposarcoma cases with MDM2 amplification were evaluated (57 of the body cavities and 22 of the extremities). The mean MDM2 amplification ratio of liposarcomas by site and differentiation are described in table 1. The MDM2 AR for all WDLPS ranged from 2.1-12.2 (mean= 6.3), for LGDDLS it ranged from 4.2-10.0 (mean=7.18) and for DDLPS the AR ranged from 5.1-12.5 (mean=8.15). DDLPS had a higher mean amplification ratio (p= 0.0036) when compared to WDLPS. 41 cases had recurrence (36 body cavity; 5 extremities) of these 25 were WDLS, 2 were LGLPS and 14 were DDLPS. The mean amplification ratio for recurrent body cavity liposarcomas was 7.64 vs 7.14 in non-recurrent (p= 0.453). In extremity liposarcomas the mean amplification ratio for recurrent tumors was 3.76 vs 5.05 in non-recurrent (p= 0.233). Metastasis was seen in 9/19 of DDLPS cases. The mean amplification ratio for metastatic DDL was 8.1 vs 7.48 non-metastatic (p= 0.760).

Table 1. Mean MDM2 amplification ratio by site and differentiation

	Well Differentiated Liposarcomas (WDLPS)	Cellular well differentiated/low grade dedifferentiated (LGDDLPS)	Dedifferentiated liposarcoma (DDLS)
Body cavity	7.06 (n=31)	7.76 (n=7)	7.96 (n=19)
Extremities	4.69 (n=18)	5.25 (n=2)	6.95 (n=2)
All	6.30 (n=48)	7.18 (n=9)	8.15 n=20)

Conclusions:

- There was significant difference between the mean MDM2 amplification ratio of DDLPS and WDLPS and it likely predicts dedifferentiation.
- All DDLPS in our series had an amplification ratio of >5 but 70% of WDLPS also had an AR >5; hence determining a cutoff for an individual case for giving neoadjuvant therapy is not feasible.
- The MDM2 amplification ratio is higher in body cavity liposarcomas than extremity liposarcomas.
- There was no significant difference in the amplification factor in metastatic and recurrent category in each group hence not a separate predictor of prognosis.

64 USP6 Fusion Partners Identified by Next Generation Sequencing in Nodular Fasciitis and Cellular Fibroma of Tendon Sheath: An Institutional Experience

Shannon Rodgers[1], Harshita Mehrotra[2], Laura Favazza[1], Kyle Perry[2]
[1]Henry Ford Hospital, Detroit, MI, [2]Henry Ford Health System, Detroit, MI

Disclosures: Shannon Rodgers: None; Harshita Mehrotra: None; Laura Favazza: None; Kyle Perry: None

Background: Nodular fasciitis (NF) is a self-limited proliferation of fibroblasts and myofibroblasts often arising in subcutaneous tissues in the upper extremities, head, neck, and trunk. Fibroma of tendon sheath (FTS) is a myofibroblastic proliferation usually seen in association with tenosynovial tissue in the digits or hand. Both NF and FTS exhibit rearrangements of the *USP6* gene. While the majority of NF exhibit a *MYH9-USP6* fusion transcript, only a minority of FTS cases have been shown to contain *MYH9* as a *USP6* fusion partner. We aim to assess the identity and distribution of *USP6* fusion partners in NF and FTS on which NGS was performed within our institution.

Design: An LIS search was performed for NF and FTS from years 2017-21 with available ancillary sequencing studies. In these cases, RNA was extracted using standard protocols for formalin fixed paraffin embedded tissues (minimum 20 ng RNA). RNA sequencing was performed using Archer Fusion Sarcoma panel using primers flanking exons 1-3 of the *USP6* gene. Assay acceptability criteria included minimum depth of coverage 200X for RNA assays and percent uniformity of coverage >70%. Other RNA panel quality matrix included Reads After Trimming > 2,000,000 and average unique RNA start sites per GSP2 Control >= 10.

Results: The initial language search resulted in 20 cases with a diagnosis of NF or FTS. Of these, RNA sequencing was performed on 13 cases. 7 of 13 cases were positive for a *USP6* gene fusion. Basic patient demographics, diagnoses and sequencing findings are presented in Table 1. Of the *USP6* fusion positive cases, 6 were NF, and 1 was FTS. 4/7 were males with a median age 20 years (range 7 to 57), and median size 2.5 cm (range 1.0 to 5.5). Fusion partners were *COL1A1*, *MYH9*, *SPARC*, *CTNNB1*, *RUNX2*, *HDLBP*, and *RRBP1*.

No	Age at diagnosis	Sex	Diagnosis	Site of Tumor	Largest tumor dimension (cm)	Molecular profile (gene fusion)
1	7	F	Nodular fasciitis	Right flank	1.3	*COL1A1-USP6*
2	16	M	Nodular fasciitis	Back	4.5	*MYH9-USP6*
3	57	M	Nodular fasciitis	Right Calf	1	*CTNNB1-USP6*
4	45	F	Nodular fasciitis	Left forehead	1.5	*HDLBP-USP6*
5	19	F	Nodular Fasciitis	Left forehead	1.1	*RRBP1-USP6*
6	56	M	Nodular fasciitis	Right knee	5.5	*MYH9-USP6*
7	20	M	Cellular Fibroma of Tendon Sheath	Right hand	2.4	*SPARC-USP6*

Conclusions: While the *MYH9* gene was the most common partner for *USP6* in this study, the *MYH9-USP6* transcript was present in less than half of this limited cohort. To our knowledge, the *HDLBP-USP6* fusion identified represents a yet undescribed fusion in NF. Furthermore, while a *SPARC-USP6* fusion transcript has been previously identified in a conventional FTS, we report a *SPARC-USP6* fusion in a cellular FTS, illustrating the morphologic and molecular diversity of these lesions.

Assessment for *USP6* rearrangement has proven an invaluable tool for the diagnosis of both FTS and NF. While this institutional series is limited, the findings further attest to the expanding diversity of *USP6* fusion partners in these entities.

65 Mesenchymal Neoplasms With ACTB-GLI1 Fusion: Towards a Better Understanding of This Enigmatic and Evolving Tumor Type

Nathalie J. Rodrigues Simoes[1], Julie Tse[2], William Faquin[3], Andrew Rosenberg[4], Darcy Kerr[5]
[1]Dartmouth-Hitchcock Medical Center, Lebanon, NH, [2]Foundation Medicine, Inc., Boston, MA, [3]Massachusetts General Hospital, Harvard Medical School, Boston, MA, [4]University of Miami Health System, Miami, FL, [5]Dartmouth-Hitchcock Medical Center, Geisel School of Medicine at Dartmouth, Lebanon, NH

Disclosures: Nathalie J. Rodrigues Simoes: None; Julie Tse: *Employee*, Foundation Medicine, Inc.; William Faquin: None; Andrew Rosenberg: None; Darcy Kerr: None

Background: Until recently, "pericytoma with t(7;12)" was considered a distinctive, benign myopericytic tumor. However, evidence documents that neoplasms harboring the associated *ACTB-GLI1* fusion can exhibit malignant behavior and lack histological features of myopericytoma. Indeed, mesenchymal tumors with *GLI1* fusions, most often with *ACTB* as a gene partner, and tumors with high-level *GLI1* amplification, are proposed as an emerging epithelioid mesenchymal neoplasm of uncertain phenotype. We collected a cohort of these lesions in an effort to gain a better understanding of their morphologic, immunophenotypic, and biologic spectrum.

Design: We searched the archives of a commercial lab and an academic medical center for neoplasms with documented *ACTB-GLI1* fusions. Previously published cases were excluded.

Results: The 12 identified cases affected adults (7 male, 5 female) with a median age of 45 years (range: 26-69). The most common anatomic site was somatic soft tissue (5/10). Other sites included: epidural (2), bone (2), and ovary (1). The remaining 2 cases represented lung metastasis with an unknown primary site. Three cases were recurrent tumors. Morphologically, all tumors demonstrated an epithelioid-to-round cell morphology, with 3 cases additionally showing spindle cell features. Solid growth, fine tumor-associated vascularity, microcystic pattern, and myxoid to edematous stroma were commonly observed. By immunophenotype, tumors were positive for CD56 (2/2), and a subset stained positively for S100 (3/8), CD99 (2/5), epithelial markers (keratins/EMA) (2/7), SMA (2/4), MSA (1/2), chromogranin (1/5), and synaptophysin (1/5). All cases tested were negative for desmin (6) and SOX10 (3). Tumor mutational burden was assessed in 7 cases with an average mutational burden of 2.3 mutations/Mb (range 0-5.31); these tumors were classified as microsatellite stable. Limited clinical follow-up showed 2 metastases and 3 recurrences.

Abbreviations: +, positive; -, negative; (f), focal; (w), weak; synapto, synaptophysin; chromo, chromogranin

Case number	Sex	Age	Location	Select Immunophenotypic Features	Initial Pathology Diagnosis
1	M	33	Right leg soft tissue	+ S100, MelanA (f), TFE3 - Synapto, chromo, desmin, SOX10	Unique S100-positive sarcoma
2	F	59	Right leg soft tissue	+ CD56, S100 (f), SMA (f), Ki67 40% - Keratins, EMA, desmin, SMA, MSA, synapto, chromo	Malignant epithelioid neoplasm
3	M	69	Ilium with soft tissue extension	+ CD56	Malignant neoplasm with epithelioid morphology, favor sarcoma
4	M	30	Lung metastasis	N/A	Metastatic extraskeletal myxoid liposarcoma
5	M	46	Right pelvis soft tissue	N/A	Undifferentiated round cell sarcoma, high grade
6	M	56	Epidural spine	+ NSE (f)(w), CD99 (f)(w) - Pankeratin, S100	Poorly differentiated malignant tumor
7	M	36	Lung metastasis	+SMA (f), MSA (f), CD34 (f) - EMA, S100, desmin	Metastatic undifferentiated round cell neoplasm
8	M	56	Thoracic vertebra T9 bone	+ Chromo (f), synapto (f) - Keratin, PAX8, S100	Epithelioid and spindled cell tumor with neuroendocrine differentiation
9	F	26	Epidural tumor	+ S100, SOX9, CD10, Ki67 <10% - SMA, SOX10, CD31, EMA, synapto, chromo, desmin	Unclassified malignant epithelioid neoplasm
10	F	34	Left foot nodule	N/A	Low-grade malignant neoplasm of uncertain type
11	F	42	Ovary	+ Pankeratin, EMA, CD10 - Synapto, SAL14, CD31, CD34, AE1/AE3, WT1, calretinin, desmin	Spindled and epithelioid neoplasm
12	F	51	Right neck, level 5 mass	+ ERG (f), SMARCA4, and SMARCB1 (retained) - Pankeratin, desmin, SMA, SOX10, S100, EMA, chromo, and NSE	Atypical spindled and epithelioid neoplasm of uncertain malignant potential

Figure 1 - 65

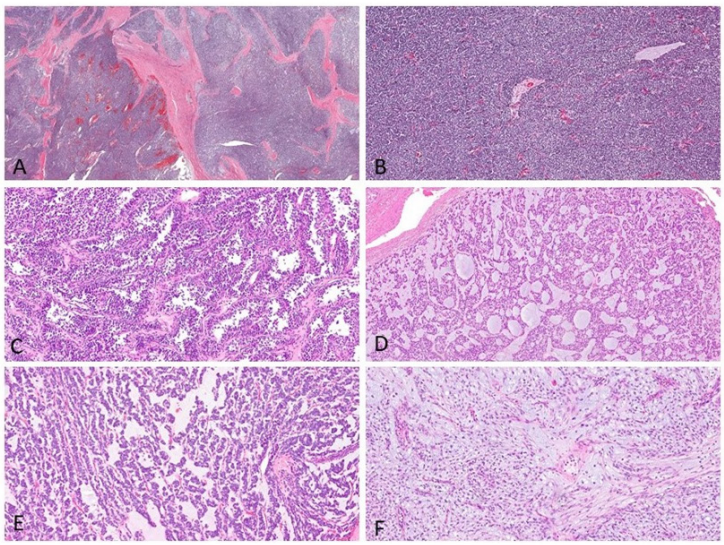

Figure 1. Histology of mesenchymal tumors with *ACTB- GLI1* fusion. A) Solid growth pattern with fibrous septae was atypical. B) Tumors frequently showed a delicate microvascular capillary network. C) A pseudo-alveolar pattern was occasionally seen. D) Myxoid matrix was a prominent feature in many cases. A subset of cases showed E) A reticular arrangement or F) A spindle cell component

Conclusions: To our knowledge, this represents the largest cohort to date of an emerging translocation-associated mesenchymal tumor that harbors *ACTB-GLI1* fusion. While united by a common genetic abnormality, tumors showed diverse morphologic, immunophenotypic, and clinical features. Overlap with myopericytoma was minimal, and therefore the category of uncertain phenotype seems appropriate. Although clinical follow-up was limited, our results in this selected cohort further confirm the potential of malignant biologic behavior in that 17% metastasized and 25% recurred locally.

66 PAX8 Expression in Non-Epithelial Neoplasia

Douglas Rottmann[1], May Chan[2], Dafydd Thomas[3], Rajiv Patel[1]
[1]Michigan Medicine, University of Michigan, Ann Arbor, MI, [2]University of Michigan, Ann Arbor, MI, [3]University of Michigan Hospitals, Ann Arbor, MI

Disclosures: Douglas Rottmann: None; May Chan: None; Dafydd Thomas: None; Rajiv Patel: None

Background: The paired box genes are highly conserved transcription factors involved in the lineage derivation of many tissues in vertebrates. PAX8 controls the development of the thyroid gland and mesonephric and Mullerian tracts. Therefore, PAX8 immunohistochemistry (IHC) is commonly used as a lineage marker for neoplasms. PAX8 expression is not limited to carcinomas. Synovial sarcomas are reported to be positive for PAX8 and more recently, Ewing sarcoma and solitary fibrous tumor are reported to be positive in a subset of cases. Despite the expanding list of PAX8-positive tumors, there has not been a systematic review of its expression in mesenchymal and non-epithelial tumors. We aim to examine the expression of PAX8 by IHC in mesenchymal tumors.

Design: Tissue microarrays (TMAs) comprising numerous different sarcomas were selected for use based on the breadth of tumors included. Included were one TMA of mostly synovial sarcomas (14 SS, 2 MPNST, and 1 DDLPS), one of small round blue cell tumors (7 *CIC-DUX4* sarcomas and 9 Ewing sarcomas), and three of various sarcomas and gastrointestinal stromal tumors (127 cases), all with normal tissue controls. One slide of each TMA was stained for PAX8 (rabbit polyclonal, Cell Marque, 1:500 dilution) and the controls showed appropriate staining. Each core was evaluated for presence of tumor and were scored on a semiquantitative scale for intensity (0: no staining, 1+: faint to weak, 2+: moderate, 3+: strong). A review of the English-language literature for PAX8 staining in mesenchymal neoplasms was performed.

Results: In total, 143 sarcomas and 13 gastrointestinal stromal tumors (GISTs) in our TMAs had at least one evaluable core. If any level of staining is considered positive, then 67 cases (43%) were positive for PAX8. If a stricter cutoff is applied, requiring at least 2+ staining for positivity, then only 24 cases (15%) would be considered positive. The majority of cases had only rare to scattered positive cells. Table 1 synthesizes the literature and the data from our TMAs.

Diagnosis	Literature (positive/total)	TMAs (positive/total)	Overall positivity rate
Adult-type fibrosarcoma	0/1 (0%)	1/1 (100%)	50%
Alveolar soft part sarcoma	0/3 (0%)	-	-
Angiomyolipoma	12/13 (92%)	-	-
Angiosarcoma	0/11 (0%)	3/11 (27%)	14%
Epithelioid angiosarcoma	-	1/2 (50%)	50%
BCOR-CCNB3 sarcoma	3/6 (50%)	-	-
Benign mesothelial proliferations	50/98 (51%)	-	-
Adenomatoid tumor	0/32 (0%)	-	-
Benign cystic mesothelioma	0/1 (0%)	-	-
WD papillary mesothelioma	50/65 (77%)	-	-
Biphenotypic sinonasal sarcoma	18/18 (100%)	-	-
Chordoma	1/22 (5%)	-	-
CIC-rearranged sarcoma	0/1 (0%)	6/7 (86%)	75%
Clear cell sarcoma of kidney	11/70 (16%)	-	-
Congenital infantile fibrosarcoma	5/5 (100%)	-	-
Congenital mesoblastic nephroma	18/47 (38%)	-	-
Desmoid fibromatosis	5/5 (100%)	-	-
DSCRT	0/7 (0%)	-	-
Endometrial stromal sarcoma	1/6 (17%)	-	-
Epithelioid sarcoma	0/1 (0%)	-	-
Ewing sarcoma	29/101 (29%)	10/13 (77%)	34%
Gastrointestinal stromal tumor	1/16 (6%)	5/13 (38%)	21%
Hemangioblastoma	3/14 (21%)	-	-
Histiocytic sarcoma	1/2 (50%)	-	-
Infantile myofibromatosis	5/5 (100%)	-	-
Leiomyoma	0/9 (0%)	-	-
Leiomyosarcoma	0/10 (0%)	5/11 (45%)	24%
Grade 1	-	0/2 (0%)	0%
Grade 2	-	0/1 (0%)	0%
Grade 3	-	5/8 (63%)	63%
Liposarcoma	1/10 (10%)	5/17 (29%)	22%
Well-differentiated	1/4 (25%)	1/4 (25%)	25%
Dedifferentiated	0/6 (0%)	1/4 (33%)	10%
Low-grade myxoid	-	1/2 (50%)	50%
High-grade myxoid	-	0/1 (0%)	0%
Pleomorphic	-	1/3 (33%)	33%
NOS	-	1/3 (33%)	33%
Malignant mesothelioma	36/516 (7%)	-	-
Malignant rhabdoid tumor	8/41 (20%)	-	-
Mesenchymal chondrosarcoma	-	1/3 (33%)	33%
Metanephric stromal tumor	0/16 (0%)	-	-
MPNST	7/11 (64%)	3/12 (25%)	43%
Triton tumor	0/1 (0%)	1/1 (100%)	50%
Myxofibrosarcoma	-	1/3 (33%)	33%
Neuroblastoma	0/11 (0%)	0/4 (0%)	0%
Ossifying renal tumor of infancy	0/1 (0%)	-	-
Osteosarcoma (MFH-like)	-	0/1 (0%)	0%
Perivascular cell tumor	0/22 (0%)	-	-
Rhabdomyosarcoma	30/72 (42%)	7/16 (44%)	42%
Alveolar	24/35 (69%)	1/4 (25%)	64%
Embryonal	3/20 (15%)	3/6 (50%)	23%
Pleomorphic	-	1/4 (25%)	25%
Spindle cell	1/10 (10%)	1/1 (100%)	18%
NOS	2/7 (29%)	1/1 (100%)	38%
Schwannoma	3/18 (17%)	-	-
Solitary fibrous tumor	28/100 (28%)	-	-
Synovial sarcoma	10/39 (26%)	15/28 (54%)	37%
Monophasic SS	-	9/21 (43%)	43%
Biphasic SS	-	6/7 (86%)	86%
UPS/MFH	-	4/14 (29%)	29%
Wilms tumor	60/60 (100%)	-	-

Table. Cases stained for and positive for PAX8 in both the literature and among our TMAs, as well as the percent positivity. For the TMAs, the percentage of cases with any positivity and the new total positivity rate (literature and TMAs) are calculated. DSRCT = desmoplastic small round cell tumor, MFH = malignant fibrous histiocytoma, MPNST = malignant peripheral nerve sheath tumor, NOS = not otherwise specified, UPS = undifferentiated pleomorphic sarcoma, WD = well-differentiated.

Figure 1 - 66

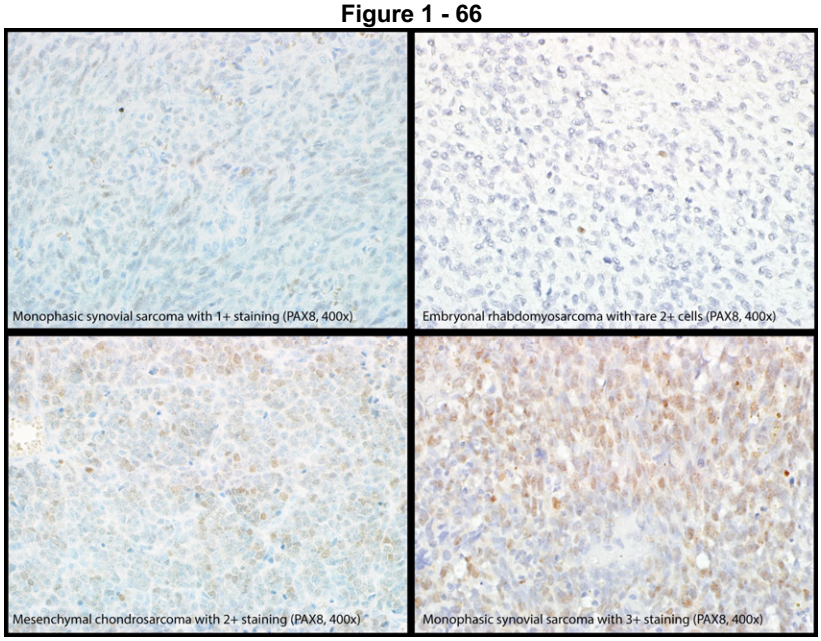

Conclusions: We provide a large, detailed collection of PAX8 staining in mesenchymal neoplasms, including 143 sarcomas and 13 gastrointestinal stromal tumors. Among these, 62 sarcomas and 5 GISTs have at least some positivity. We also report the first PAX8-positive cases of angiosarcoma, *CIC*-rearranged sarcoma, fibrosarcoma, leiomyosarcoma, and undifferentiated pleomorphic sarcoma. Most tumors in our cohort had only rare positive cells; however, some cases showed diffuse expression.

67 Pseudomyogenic Hemangioendothelioma of Bone: A Case Series with Uncommon FOSB Fusions

Douglas Rottmann[1], Konstantinos Linos[2], John Gross[3], John Reith[4], Scott Kilpatrick[4], Jorge Torres-Mora[5], Julia Bridge[6], Rajiv Patel[1], David Lucas[7], Scott Lauer[6]

[1]Michigan Medicine, University of Michigan, Ann Arbor, MI, [2]Dartmouth-Hitchcock Medical Center, Lebanon, NH, [3]The Johns Hopkins Medical Institution, Baltimore, MD, [4]Cleveland Clinic, Cleveland, OH, [5]Mayo Clinic, Rochester, MN, [6]University of Nebraska Medical Center, Omaha, NE, [7]Michigan Medicine, Ann Arbor, MI

Disclosures: Douglas Rottmann: None; Konstantinos Linos: None; John Gross: None; John Reith: None; Scott Kilpatrick: None; Jorge Torres-Mora: None; Julia Bridge: None; Rajiv Patel: None; David Lucas: None; Scott Lauer: None

Background: Pseudomyogenic hemangioendothelioma (PMHE) is a rare endothelial neoplasm of intermediate malignant potential. PMHE usually involve the soft tissues of the extremities and are often multifocal. PMHE does not usually involve the bone, although rare cases have been reported to arise from it. Histologically, PMHE are composed of spindle to epithelioid cells with bright eosinophilic cytoplasm. They typically express markers of both epithelial and endothelial differentiation. Most PMHE harbor a *SERPINE1-FOSB* fusion, while a minority have other *FOSB* fusions. We report twelve cases of PMHE arising in bone, four with uncommon fusions.

Design: The index patient presented to the University of Nebraska Medical Center for left knee pain that impaired ambulation. On X-ray, he was found to have lytic foci within the left distal femur, patella, proximal tibia, and fibula. A biopsy showed spindled and epithelioid cells with bright eosinophilic cytoplasm. The tumor cells were positive for ERG, CD31, and cytokeratin AE1/AE3 (focal), supporting the diagnosis of PMHE. Next generation sequencing identified an *ACTB-FOSB* fusion. The patient is currently undergoing therapy with sirolimus and zoledronic acid.

Results: We performed text searches of the pathology archives at the University of Michigan, University of Nebraska, Dartmouth-Hitchcock, Johns Hopkins University, Cleveland Clinic Foundation, and Mayo Clinic for additional cases of PMHE arising in bone. We excluded cases that predominantly involved soft tissue. In total, we identified 12 cases of primary bone PMHE, including 7 with follow up (see table). In our series, intraosseous PMHE occurred in young patients (range 4-35, average 18.5 years), often involved the pelvis or lower extremity (11/12, 92%), and was commonly polyostotic (8/12, 67%). All cases had similar histologic features to

the index case and a comparable immunophenotype, including a CD31+ CD34- ERG+ pattern. Three cases had NGS, identifying *CLTC-FOSB* (previously reported), *ACTB-FOSB*, and *WWTR1-FOSB* fusions (previously reported).

Case	Pt age	Pt sex	Tumor site	Immunohistochemistry	Molecular findings	Follow up
1	11	M	Femur, tibia, fibula, patella	AE1/3 + (focal), ERG +, CD31 +, CD34 -	*ACTB-FOSB* fusion	AWD (8 mo)
2	17	M	Fibula	AE1/3 + (focal weak), ERG +, CD31 + (focal), CD34 -	*CLTC-FOSB* fusion	NED (28 mo)
3	27	F	Sacrum	AE1/3 -, ERG +, CD31 +, CD34 -	No molecular	No follow up
4	15	M	2nd and 4th toes	AE1/3 +, CD31 +, CD34 -	No molecular	NED (11 yr)
5	23	M	2nd, 3rd, and 5th toes	AE1/3 +, CD31 +, CD34 -	No molecular	No follow up
6	23	M	Iliac, clavicle, 6th rib, femur	AE1/3 +, CK7 +, ERG +, CD31 +, Fli-1 +	No molecular	AWD (3 yr)
7	4	M	Femur, tibia	AE1/3 +, ERG +, CD31 +	*FOSB* FISH negative	NED (1 yr)
8	19	M	Tibia, talus	AE1/3 +, ERG +, CD31 +, FOSB +	No molecular	No follow up
9	15	M	T2 vertebra	AE1/3 +, ERG +, CD31 +, CD34 -	*ACTB-FOSB* fusion	No follow up
10	35	F	Calcaneus, fibula	AE1/3 +, ERG +, CD31 + (focal)	No molecular	NED (4 yr)
11	26	M	Femurs, pelvis, sacrum, lumbar vertebrae	AE1/3 +, ERG +, Fli-1 +	No molecular	No follow up
12	7	F	Femur	AE1/3 +, ERG +, CD31 +, FOSB +	*WWTR1-FOSB* fusion	NED (2 yr)

Table. Clinicopathologic data for the cases included in this series. AWD = alive with disease, F = female, M = male, NED = no evidence of disease, pt = patient.

Conclusions: Pseudomyogenic hemangioendothelioma is a rare tumor that often involves bone, but rarely arises in it. We present a brief case series of twelve cases of PMHE primary to the bone, four of which show uncommon fusions of *FOSB*. Similar to soft tissue PMHE, bone PMHE may be multifocal, as seen in 8 of our 12 cases, or radiologically aggressive with expansile remodeling of bone. Recognition of this entity avoids misdiagnosis and may obviate mistreatment.

68 Immune Cell Densities in Dedifferentiated Liposarcoma and Chondrosarcoma: Toward Understanding the TIME in Dedifferentiated Sarcomas

Karen Schoedel[1], William Li[2], Megan Zilla[2], Rebekah Belayneh[2], Rebecca Watters[2], Tullia Bruno[2], Anette Duensing[3], Douglas Hartman[2], Kurt Weiss[2]
[1]UPMC Presbyterian Hospital, Pittsburgh, PA, [2]University of Pittsburgh Medical Center, Pittsburgh, PA, [3]UPMC Hillman Cancer Center, Pittsburgh, PA

Disclosures: Karen Schoedel: None; William Li: None; Megan Zilla: None; Rebekah Belayneh: None; Rebecca Watters: None; Tullia Bruno: None; Anette Duensing: None; Douglas Hartman: *Speaker*, Philips; *Consultant*, Iqvia; Kurt Weiss: None

Background: Dedifferentiated sarcomas usually represent the most aggressive forms of sarcomas from which they derive. Subsets of immune cells in dedifferentiated liposarcoma (DDLPS), particularly B-cells in tertiary lymphoid structures (TLS), are associated with improved survival and better response to immune checkpoint inhibitors. In this study we explore differences in subset immune cell densities with respect to DDLPS and dedifferentiated chondrosarcomas (DDCS). We hypothesize that the differences in immune cell subsets account for differences in patient outcome.

Design: 28 cases of DDCS and 42 cases of DDLPS were obtained from the Department of Pathology files. Representative FFPE tissue blocks of the dedifferentiated components were selected and immunohistochemical stains for CD4, CD8 and CD20 were applied. Automated image analysis was performed to quantitate immune cell densities per mm^2 of tumor area. DDCS and DDLPS cohorts were compared with respect to immune cell densities. Multivariate analysis using binary logistic regression was performed and a Kaplan-Meier plot was generated using the log rank test.

Results: CD4 positive T-cell density is higher in DDLPS and associated with significantly decreased mortality. CD20 B-cell populations are similar in both tumors.

Immune Cell	Average Density DDLPS mm2	Average Density DDCS mm2	Odds ratio	95% Confidence Interval	P value
CD4	269	142	0.996	0.992-1.000	**0.038**
CD8	171	105	1.005	1.000-1.010	0.055
CD20	24	25	0.982	0.956-1.009	0.193

DDLPS shows a significantly better overall survival as compared to DDCS (p=0.000074).

Figure 1 - 68

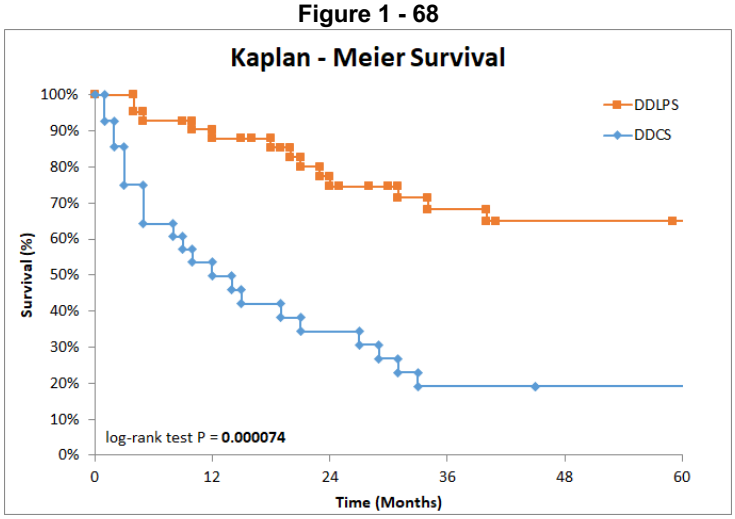

Conclusions: The constituents of the tumor immune microenvironment (TIME) are different such that CD4 cell density is increased in DDLPS as compared to DDCS, although CD20 cell density is similar. Differences in the TIME may contribute to overall survival differences. Further studies, particularly gene expression profiling, are required to evaluate potential functional differences in the TLS of dedifferentiated sarcomas.

69 Clinicopathological Analysis of 9 Cases of TFE3-rearranged Epithelioid Hemangioendothelioma to Further Broaden Its Morphological Spetrum

Meng-yuan Shao[1], Meng Sun[2], Lu Zhao[2], I Weng Lao[2], Lin Yu[2], Jian Wang[3]
[1]Fudan University Shanghai Cancer Center, Shanghai Medical College, Fudan University, Shanghai, China, [2]Fudan University Shanghai Cancer Center, Fudan University, Shanghai, China, [3]Fudan University Shanghai Cancer Center, Shanghai, China

Disclosures: Meng-yuan Shao: None; Meng Sun: None; Lu Zhao: None; I Weng Lao: None; Lin Yu: None; Jian Wang: None

Background: TFE3-rearranged epithelioid hemangioendothelioma (EHE) as a new molecular subtype has been included into the fifth edition of "WHO Classification of Soft Tissue and Bone Tumors". Herein, we report 9 cases of TFE3-rearranged EHE to explore the differences of clinicopathological characteristics between it and classic EHE, and further broaden its morphological spectrum.

Design: The clinicopathologic data of 9 cases of TFE3-rearranged EHE diagnosed in the Department of Pathology of Fudan University Shanghai Cancer Center were collected. Morphological observation, immunohistochemical staining, fluorescence in situ hybridization (FISH) and next generation sequencing (NGS) detection were performed.

Results: Among 9 patients, 4 were males and 5 were females. The age ranged from 33 to 61 years old, with an average age of 46 years old. Six cases occurred in the somatic soft tissue, 2 in the lung, and 1 in the bone. The tumor size was

0.8~4.0cm(mean,2.4cm). Microscopically, 4 cases had relatively well-defined borders; 5 cases had unclear borders, infiltrating the dermis, subcutaneous adipose tissue, lung, pleura and bone. In contrast to classic EHE, TFE3-rearranged EHE displayed distinctive histological features, including well-formed vascular spaces (7/9cases), solid nests and sheets of brightly eosinophilic or clear epithelioid cells (6/9 cases), spindle cell components (3/9 cases) and absence of obvious myxohyaline stroma (6/9 cases). Immunohistochemically, all 9 cases expressed CD31, ERG and TFE3, and 5 were positive for CD34 (5/7). Ki-67 proliferation index was 5%~15%. All 9 cases detected by FISH showed TFE3 translocation. Two cases tested by NGS showed YAP1-TFE3 fusion. Follow-up data (range, 3 to 38 months; mean, 21 months) were available in 7 patients. Five cases were alive with disease, and 2 cases had no evidence of disease; 2 cases developed distant or lymph node metastasis, and 1 case had local recurrence.

Table 1. Clinical characteristics of 9 cases of TFE3-rearranged epithelioid hemangioendothelioma

Case	Sex	Age(y)	Location	Size	Duration	Treatment	Metastasis/Recurrence	Outcome(mo)
1	F	35	Right metatarsals, tibia	1.5cm	3 months	Surgical resection; targeted therapy; radiotherapy	none	NED,3
2	F	56	Right groin	2.4cm	2 months	Surgical resection	none	NED,18
3	F	57	Left axilla	4cm	10 days	Surgical resection	none	NED,19
4	F	33	Right thigh	2cm	16 months	Surgical resection	none	NED,38
5	M	51	Left lower lung lobe	4cm	4 months	Surgical resection; radiotherapy; chemotherapy	Group seven lymph nodes	LR,20; NED,13
6	M	38	Left lower lung lobe	2.5cm	1 months	Surgical resection; targeted therapy	Bilateral clavicle area,left chest wall;Multiple lymph node metastases	NED,8
7	M	45	Right supraclavicular area	2.5cm	28 months	Surgical resection; radiotherapy	none	NED,26
8	M	61	Chest wall	0.8cm	/	/	/	/
9	F	34	Left neck	2cm	/	/	/	/

LR,local recurrence; NED,no evidence of disease

Figure 1 - 69

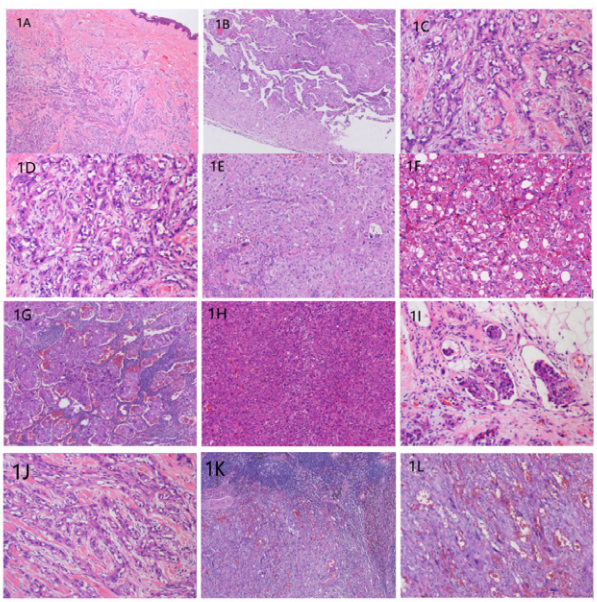

Figure 1 Histological features of TFE3-rearranged EHE: A. The tumor infiltrated the dermis and subcutaneous; B. The tumor invaded the lung pleura; C,D: Formation of obvious vascular cavities; E. Solid nests or sheets of epithelioid cells; F. Eosinophilic epithelioid cells with rich cytoplasm are distributed in solid sheets with scattered vesicular cells; G. Eosinophilic epithelioid cells are distributed in nests shapes grow along the alveolar cavity; H. Rich spindle cell components; I. Growth in the vascular cavity; J. There were at least focal areas of classic EHE in all cases (the epithelial-like cells are arranged in strips, with vesicular cells; formation of primitive vascular lumen, in which red blood cells were seen; K, L. EHE of lung developed lymph node metastasis.

Figure 2 - 69

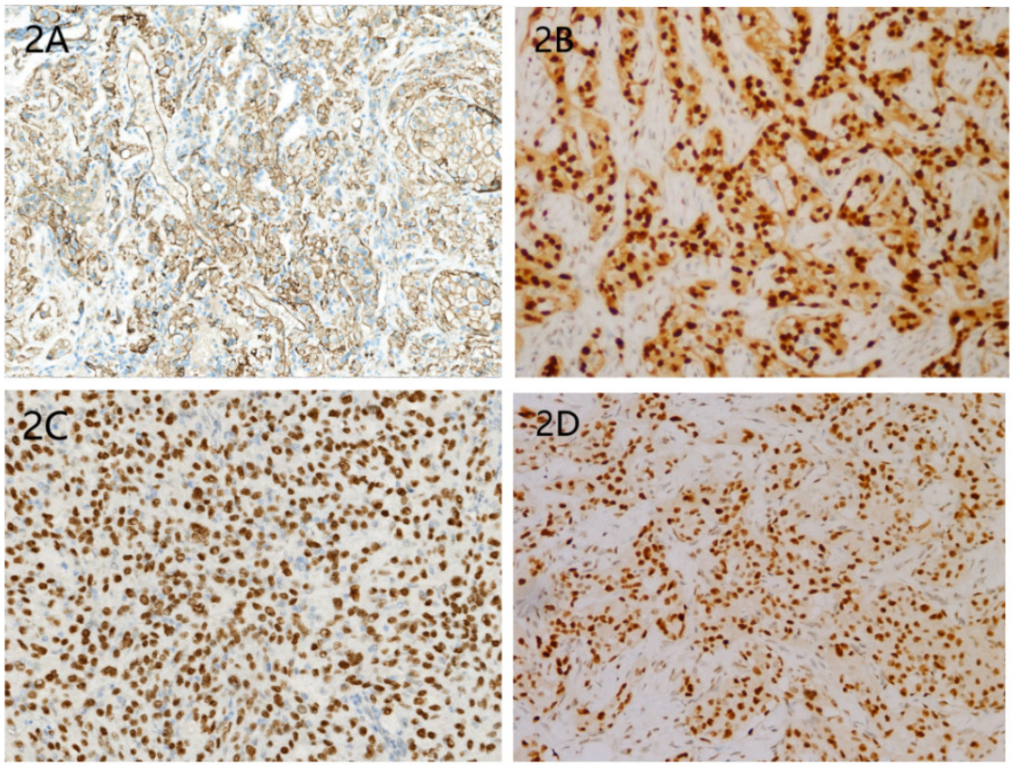

Figure 2 Immunophenotype of TFE3-rearranged EHE. The tumor cells were diffusely strongly positive for CD31(A), ERG(B), Fli-1(C) and TFE3(D).

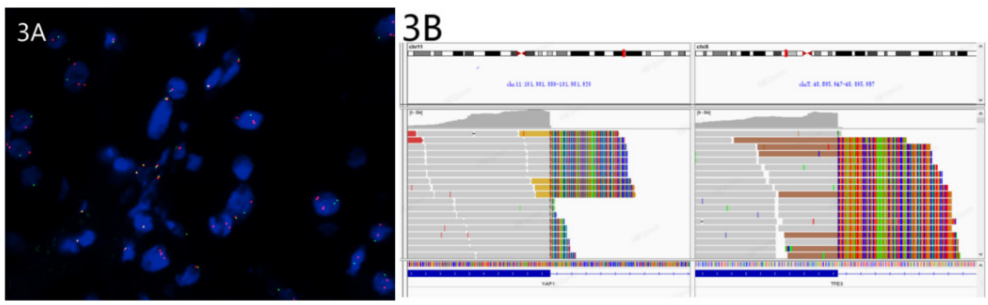

Figure 3 Molecular genetic characteristics of TFE3-rearranged EHE. A: FISH showed TFE3 gene translocation; B: NGS detection showed YAP1-TFE3 gene fusion.

Conclusions: TFE3-rearranged EHE is a rare and novel molecular subtype of vascular tumors. Compared with classic EHE, TFE3-rearranged EHE showed a broad morphological spectrum, including well-formed vascular spaces, solid nests and sheets of eosinophilic or clear epithelioid cells, spindle cell components and absence of obvious myxohyaline stroma. Familiar with the clinicopathological spectrum of TFE3-rearranged EHE and increasing of immunohistochemistry and molecular detection of TFE3 in the diagnosis of vascular tumors, will be helpful to identify this new molecular subtype.

70 Gorham-Stout Syndrome: Eleven New Cases of Idiopathic Osteolysis and Review of the Literature

Jasmine Vickery[1], Ahmed Abdelmonem[2], Aya Almashad[2], Scott Baker[3], Bahig Shehata[4]
[1]University of Chicago Medical Center, Chicago, IL, [2]Wayne State University, Detroit, MI, [3]Detroit Medical Center, Detroit, MI, [4]Detroit Medical Center/Wayne State University, Detroit, MI

Disclosures: Jasmine Vickery: None; Ahmed Abdelmonem: None; Aya Almashad: None; Scott Baker: None; Bahig Shehata: None

Background: Idiopathic isolated osteolytic bone disease, known as Gorham-Stout Syndrome (GSS) is a rare aggressive form of "vanishing bone" due to progressive mono- or polyostotic osteolysis and angiomatosis. It has an unknown etiology, most often affecting children and young adults. There is current debate on whether it is a developmental vascular malformative or true neoplastic process of capillary, venous, and/or lymphatic vasculature. No prior histologic features have been found to distinguish the true nature of the lesional vasculature. The cause of excessive bone resorption in GSS is still unclear with endothelial cells, osteoclasts and osteoblasts all having a potential role.

Design: We reviewed our medical record files including radiological and pathological findings. The clinical course and outcomes were reviewed. Histologically the following stains were performed Hematoxylin and Eosin, D2-40 (lymphatic endothelial marker), and CD-31 (pan-endothelial marker).

Results: We identified 11 patients (6 males, 5 females). They ranged in age from 1 to 18 years old. Seven patients had solitary bone involvement, and four showed multi-osseous lesions. One of the patients with multiple involved bones was 1 year old at diagnosis and succumbed to the disease a few months later. The other 10 patients were treated and are still alive. Follow up of our patient cohort ranges from 2-7 years. Biopsies revealed numerous dilated thin-walled endothelial-lined vessels with absence of cellular atypia penetrating into bone. In all cases the endothelial cells lining the vessels were strongly and diffusely positive for D2-40. The cells were moderately to strongly positive for CD-31.

Conclusions: Bones do not normally have lymphatics, our finding of strong positivity of the specific lymphatic endothelial marker D2-40 supports the notion that the underlying pathogenesis of GSS is due to extensive lymphatic proliferation. Recent mouse models using overexpression of the lymphatic growth factor vascular endothelial growth factor C (VEGFC) have demonstrated that bone lymphatics develop in a stepwise manner where regional lymphatics grow, breach the periosteum, and then invade bone. In this model, researchers also show that the development of bone lymphatics is impaired in mice that lack osteoclasts. Further investigation of the mechanisms driving osteolysis and lymphangiogenesis is needed for treatment of this insidious disease.

71 Clinicopathology and Molecule Feature in Synovial Sarcoma with ALK Immunohistochemistry Positive

Jianfeng Wu[1], Zhe Wang[2]
[1]Xijing Hospital, the Air Force Medical University, Xi'an, China, [2]Fourth Military Medical University, China

Disclosures: Jianfeng Wu: None; Zhe Wang: None

Background: Synovial Sarcoma (SS) is malignant soft tissue rumor of uncertain histogenesis with variable epithelial differentiation, accounting for approximately 5%-10% of soft tissue sarcomas. Although multidisciplinary treatment has dramatically improved prognosis, the survival rate of those affected by metastatic Synovial Sarcoma remains low. Therefore, a new treatment strategy is needed. Numerous ALK inhibitors have been developed for the treatment of patients with advanced ALK-positive cancers. For now, there is only one study that has documented ALK expression in SS, we speculated that ALK may play an oncogenic role in SS, and that it may be treatable target with ALK inhibitors.

Design: A total of 111 cases of SS were retrieved from Xijing Hospital 2006 to 2020 pathology archive. All specimens were stained by IHC with an anti-ALK monoclonal antibody(D5F3). The IHC stains were evaluated for expression of ALK by two pathologists (ZheWang and Jianfeng Wu) who were trained to identify only cytoplasmic granular staining in tumor cells, which was deemed a positive result. Intensity of staining was scored as:0(negative), 1+(faint), 2+(moderate), or 3+(strong). We have detected SS18 and ALK gene break apart by FISH(76 cases, 41 cases, respectively). Whole exon sequencing was assessed in 19 samples.

Results: ALK protein expression was detected in 40 of 111 cases(36%; 1+:10, 2+:19, 3+:11). Compared with ALK-negative SS, ALK-positive cases presented with more frequent metastasis (10 and 18 cases, respectively) and showed a lower 5-year survival rate (74% vs. 52%). The median ALK gene copy number was more in ALK-positive tumors than in ALK-negative tumors (3.7 vs.

1.4). WES and FISH results showed no ALK gene rearrangement in all tested cases. The result of WES showed some genes aberrant (see figure 2), but no ALK gene abnormality was found.

Figure 1 - 71

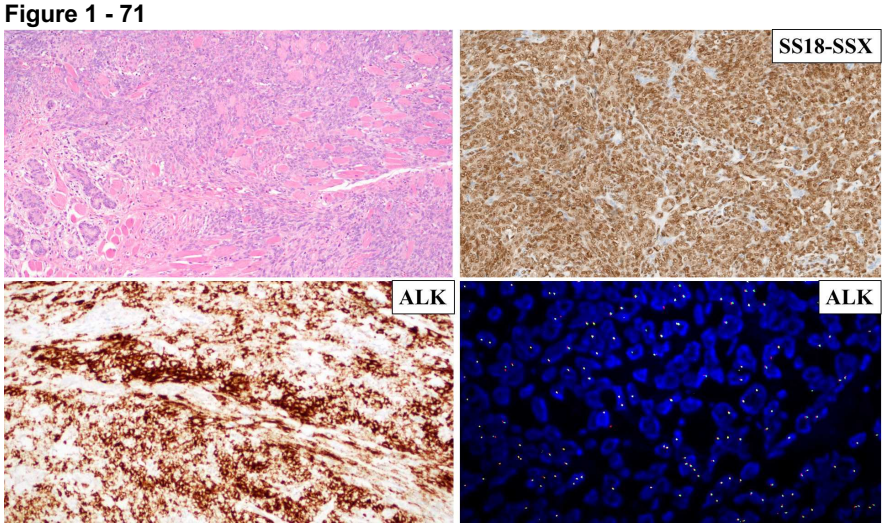

Figure 2 - 71

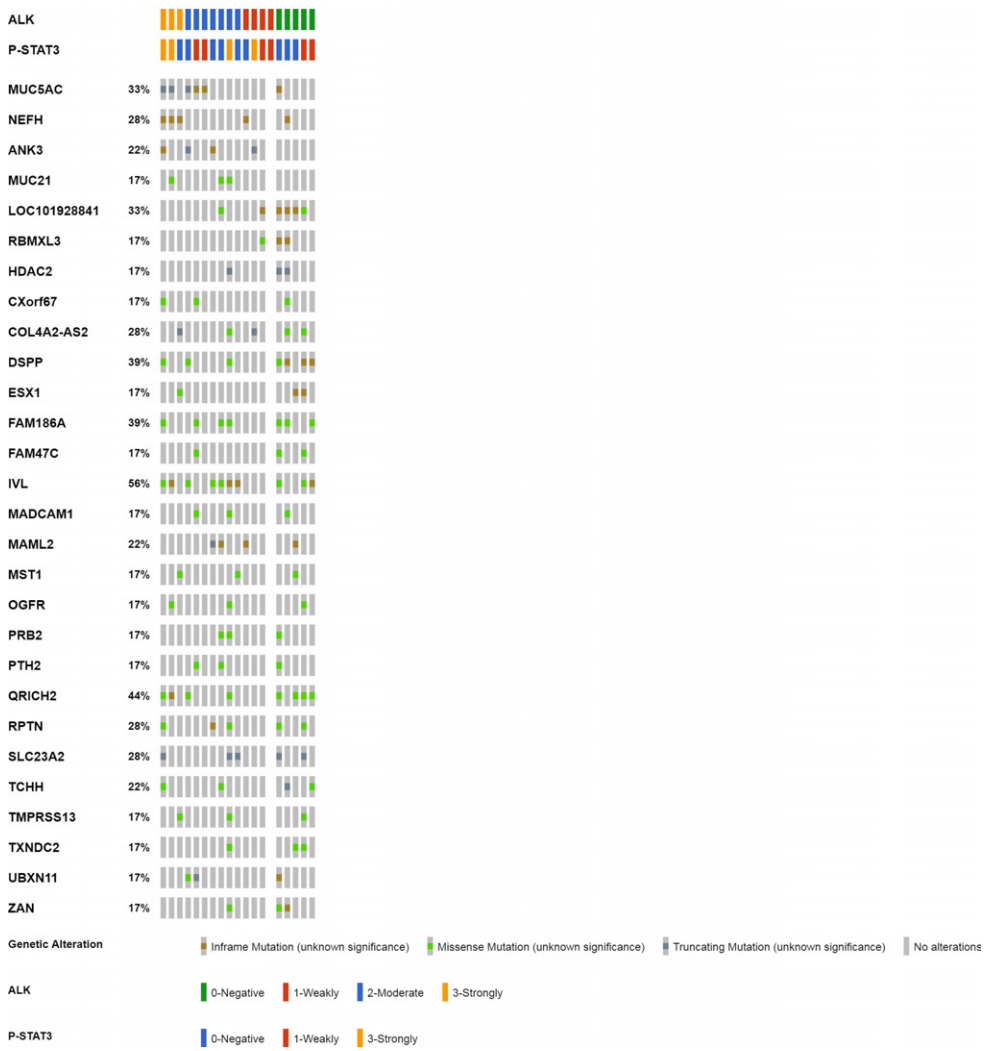

Conclusions: Although it remains controversial whether ALK expression without gene rearrangement is therapeutically relevant, this comprehensive analysis may help future studies on the utility of ALK-targeted therapy for patients with Synovial Sarcoma.

72 "Malignant Mesenchymoma" Revisited: A Clinicopathologic Study of Leiomyosarcomas with Osteosarcomatous Differentiation

Sanhong Yu[1], Jason Hornick[1]
[1]*Brigham and Women's Hospital, Harvard Medical School, Boston, MA*

Disclosures: Sanhong Yu: None; Jason Hornick: *Consultant*, Aadi Biosciences; *Consultant*, TRACON Pharmaceuticals

Background: Leiomyosarcoma (LMS) is the most common sarcoma in adults. Rarely, LMS dedifferentiates into an undifferentiated sarcoma. Very few cases of LMS with heterologous osteosarcomatous differentiation (OS) have been reported. The purpose of this study was to evaluate the clinicopathologic features of LMS with OS.

Design: LMS with OS were identified from surgical pathology and consult archives. Histologic features were reviewed. Clinical details and outcome were retrieved from the electronic medical record.

Results: Of 5124 total LMS cases diagnosed from 2006 to 2021, 13 cases (0.2%) of LMS with OS were identified, affecting 10 females and 3 males; ages ranged from 32 to 66 yrs (median 55 yrs). Eight tumors arose in the uterus, two in the retroperitoneum, and one each in the mesentery, mediastinum, and rectum. Primary tumors ranged from 7 to 20 cm (mean 13.7 cm). The LMS components showed conventional spindle cell morphology in most cases; 3 cases showed marked pleomorphism; 2 cases contained an epithelioid component; and 1 case showed myxoid features. In 7 cases OS was identified in the primary tumor, whereas in 6 cases OS was first detected in metastases, 3 of which were previously treated with systemic chemotherapy. One metastatic and two primary LMS showed both OS and chondrosarcomatous differentiation. Prominent osteoclastic giant cells were common in the OS components. Mitotic activity ranged from 17 to 61 per 10 HPF with tumor necrosis in 9 cases. Ten patients developed metastases; sites included lungs, diaphragm, kidney, adrenal glands, colon, small intestine, liver, and pancreas. At last follow-up, eight patients had died of disease, and two patients were alive with metastases. The interval between OS and death ranged from 19 days to 18 mos (median 6.5 mos).

Conclusions: Development of OS in LMS is exceptionally rare. This form of heterologous differentiation may occur in both primary tumors and metastases. LMS with OS is highly aggressive with poor outcomes. Awareness of this phenomenon is important to avoid misdiagnosis as osteosarcoma.

73 USP6-induced Soft Tissue Tumors with Bone Metaplasia: A Clinicopathologic and Genetic Study along with Identification of Novel USP6 Fusion Partners

Yahan Zhang[1], Yan Qiu[1], Xianliang Zhang[1], Xin He[1], Chen Chen[1], Min Chen[1], Hongying Zhang[1]
[1]*West China Hospital, Sichuan University, Chengdu, China*

Disclosures: Yahan Zhang: None; Yan Qiu: None; Xianliang Zhang: None; Xin He: None; Chen Chen: None; Min Chen: None; Hongying Zhang: None

Background: Among those tumors with consistent *USP6* rearrangement, some members arise from soft tissue showed bone metaplasia, including myositis ossificans (MO), fibro-osseous pseudotumor of digits (FOPD), soft tissue aneurysmal bone cyst (ST-ABC) and fasciitis ossificans (FO). Lesions of these group are easily to be confounded with malignancies in clinical diagnose-making process for showing rapidly growth rate and brisk mitosis. In this study, we aim to clarify the clinicopathologic and genetic characteristics of this entity and analyze the correlation and difference among different subtypes.

Design: 71 cases diagnosed as *USP6*-induced soft tissue tumors with bone metaplasia in 2010-2020 were enrolled into this study. Clinical and pathology data were retrospectively reviewed. 41 undecalcified samples underwent molecular detection, including fluorescence in situ hybridization (FISH), reverse transcription-polymerase chain reaction (RT-PCR) and next-generation sequencing (NGS).

Results: 39 males and 32 females with diagnosed age ranged from 2 to 80 years old (median: 31). 14 patients (14/46) had a clear history of trauma. FOPD occurred in extremal soft tissue. In the rest subgroups, lower extremities (36/56) were the most commonly

involved lesions. Histologically, hyperplastic myofibroblasts/fibroblasts with varying degrees were present. FISH was conducted and the results indicated that 20 cases (20/25) were positive for *USP6* rearrangement and 5 cases were negative. Among the 20 cases with positive FISH detection, 18 cases underwent further RT-PCR detection successfully for detecting common *USP6* fusion types. 13 cases (13/18) showed *COL1A1-USP6* fusion, one showed *MYH9-USP6* fusion, and 4 was negative for common fusion types. NGS was performed on two lesions with negative RT-PCR result, and novel fusion partners *SNHG3* and *UBE2G1* were discovered. 5 cases (5/32) showed postoperative recurrence among those with follow-up data. 2 of them demonstrated a larger tumor size and 3 underwent uncomplete resection.

Conclusions: The diagnosis of *USP6*-induced soft tissue tumors with bone metaplasia is challenging. In addition to histological morphology, detection of *USP6* rearrangement is a valuable ancillary tool in diagnose-making process. *COL1A1* is the most common fusion partner in these tumors, unlike primary aneurysmal bone cyst and nodular fasciitis. At the same time, two novel *USP6* fusion partners also have been identified in this study, which further deepens our understanding of this neoplastic spectrum.